

Phenomenological review on Quark-Gluon Plasma: concepts vs observations

Roman Pasechnik*

*Department of Astronomy and Theoretical Physics,
Lund University, 221 00 Lund, Sweden*

Michal Šumbera†

Nuclear Physics Institute ASCR, 250 68 Řez/Prague, Czech Republic

Abstract

In this review, we present an up-to-date phenomenological summary of research developments in physics of the Quark-Gluon Plasma (QGP). A short historical perspective and theoretical motivation for this rapidly developing field of contemporary Particle Physics is provided. In addition, we introduce and discuss the role of the QCD ground state, non-perturbative and lattice QCD results on the QGP properties as well as the transport models used to make a connection between theory and experiment. The experimental part presents the selected results on bulk observables, hard and penetrating probes obtained in the ultra-relativistic heavy-ion experiments carried out at BNL RHIC, CERN SPS and LHC accelerators. We also give a brief overview of new developments related to the ongoing searches of the QCD critical point and to the collectivity in small ($p+p$ and $p+A$) systems.

PACS numbers: 25.75.-q, 12.38.Mh, 25.75.Nq, 21.65.Qr

*Electronic address: Roman.Pasechnik@thep.lu.se

†Electronic address: sumbera@ujf.cas.cz

I. INTRODUCTION

Quark-Gluon Plasma (QGP) is a new state of nuclear matter existing at extremely high temperatures and densities when composite states called hadrons (protons, neutrons, pions *etc.*) lose their identity and dissolve into soup of their constituents – quarks and gluons. The existence of this novel phase of matter was proposed in mid-seventies [1, 2]. Just ten years after the birth of *Quark Model* of hadrons [3, 4] and two years after it was realised that the candidate non-Abelian field theory of inter-quark forces – *quantum chromodynamics* (QCD) [5] – predicts their weakening at short distances, the so-called *asymptotic freedom* [6, 7].

Contrary to atoms and molecules which can be ionized to reveal their constituents, quarks and gluons are never found free but are confined inside the hadrons. This situation is quite similar to decomposing the magnet into two when trying to isolate its north pole from its south pole. Even more deeper goes the analogy [8] between field lines confining quarks inside the hadrons and the magnetic field in a vicinity of superconductor which expels the magnetic flux lines (*Meissner effect*). If two magnetic poles are surrounded by a superconducting medium, the field is confined into a thin tube. A hadronic string with quark and antiquark sitting at its end points has a similar one-dimensional field confined not by a superconducting medium but by the vacuum¹.

Experimental attack on producing QGP under laboratory conditions has started in the world-leading particle physics facilities at CERN (Geneva, Switzerland) and BNL (New York, USA) in late eighties [10–12]. In the year of 2000, after finishing the main part of its heavy-ion program at the SPS accelerator, CERN has announced a circumstantial evidence for the creation of a new state of matter in Pb+Pb collisions [13]. The real discovery of QGP took place in 2005 when four international collaborations studying Au+Au collisions at the Relativistic Heavy Ion Collider (RHIC) at BNL announced the result of their first five years of measurements [14–17]. Surprisingly, the properties of new state of matter [18] differed markedly from prediction made over many years before its discovery².

This review aims at giving a short historic introduction into the vast research field of QGP physics and underlined phenomenological aspects with a comprehensive list of corresponding references. Such effects of the hot/dense medium as the nuclear suppression, initial-state interactions, in-medium energy loss, color screening and saturation are important for a proper understanding of the collective phenomena in heavy-ion collisions and are included into the scope of this review. Besides, we have qualitatively overviewed and confronted with existing observations such fundamental theoretical concepts as the QCD vacuum and phase diagram, equation of state (EoS) of deconfined QCD matter, initial-state effects, collectivity, flow, hydrodynamic properties of the QGP and associated electromagnetic effects.

The paper is organized as follows. Section II presents a short history of theoretical understanding of extreme states matter. The phase diagram of QCD is discussed in section III. Section IV gives a historical perspective on experiments operating with collisions of

¹ The string picture of hadrons makes it also possible to explain the transition from hadronic to QGP state of matter at finite temperature T as a phase transition from the ordered state to the disordered state (see Ref. [9], p. 44). With T approaching the critical temperature of deconfinement T_c the effective string tension decreases and q and \bar{q} attached to its end points lose their correlation.

² For a representative collection of papers tracing the development of theoretical ideas on the QCD deconfining phase transition before nineties, see Ref. [19].

heavy ions. Section V describes the basic signatures of QGP production while current developments in QGP research are provided in section VI. The concluding remarks are given in section VII. For further reading on fundamental concepts and latest studies of QGP dynamics, we recommend several textbooks [9, 20–24] and reviews [25–30] published in recent years.

II. MATTER UNDER EXTREME CONDITIONS

The properties of matter under extreme conditions at high values of state variables have always attracted the curiosity of scientists, owing to the possibility of advancing to new domains of the phase diagram and producing the exotic states of matter in laboratory [31, 32]. First attempts to discuss the properties of matter at densities well above the normal nuclear density $\rho_0 = 2 \times 10^{14} \text{g}\cdot\text{cm}^{-3}$ ($\approx 0.16 \text{GeV}\cdot\text{fm}^{-3}$) dates back to the seminal Oppenheimer-Volkoff paper from 1939 [33]. A study of the gravitational stability of a new phase of neutron matter suggested few years earlier by Landau [34] have led them to carry out their computations to several tens of ρ_0 before smoothly extrapolating the results to the black-hole singularity. In 1962, when discussing relativistic limitations of the equation of state (EoS) of matter made of baryons interacting via a massive vector field, Zeldovich has used the density twenty times exceeding ρ_0 [35]. In 1976, the same value of density was shown by Baym and Chin [36] to be energetically favourable for the neutron matter-quark phase transition.

In cosmology, a very dense matter with $\rho \propto 10^6 \text{g}\cdot\text{cm}^{-3}$ ($\approx 1 \text{eV}\cdot\text{fm}^{-3}$) was first studied in 1946 by Gamow [37] when discussing the relative abundances of elements in the universe. The key discovery of the cosmic microwave background radiation by Penzias and Wilson in 1965 [38] has not only provided a strong basis for the hot universe scenario which was used by Gamow but also has motivated Sakharov [39] to push it *ad extremum*. Considering the properties of hot matter at densities when gravitational interaction between photons becomes significant, he has established that the absolute maximum of the temperature of any substance in equilibrium with radiation is of the order of Planck temperature $T_P = \sqrt{\frac{hc^5}{Gk^2}} \propto 10^{32} \text{K}$ ($\approx 10^{22} \text{MeV}$). Unfortunately, the theoretical apparatus of that period was completely inadequate to deal with the thermal history of the universe from T_P downwards but even at temperatures twenty orders of magnitude lower [40].

The problem was due to two successful but mutually conflicting contemporary models of hadrons – the Bootstrap model [41, 42] based on the hypothesis that all hadrons are composite of one another and, at that time not fully developed composite model of hadrons, the Quark model [3, 4]. The Bootstrap model predicted that after reaching some limiting value of temperature, the so-called *Hagedorn temperature* $T_H=170\text{--}180 \text{MeV}$, that can be estimated from the spectrum of hadronic masses [42, 43], the subsequent heating of strongly interacting matter will lead to creation of more and more massive hadron species but not to an increase of its temperature. The quark model on the other hand has predicted relic cosmological quarks [44] roaming free through our universe. The leftover quarks were predicted to be as abundant as gold atoms [45].

The conflict was finally resolved in 1973 when Gross, Wilzek [6] and Politzer [7] discovered the asymptotic freedom in non-Abelian gauge theories of elementary particle interactions. Shortly after the idea of asymptotic freedom was introduced, two groups Collins and Perry [1], and Cabibbo and Parisi [2] have realized independently its fascinating consequence for

the properties of hot and dense matter. The first group argued that since the interaction between quarks weakens as quarks get closer at sufficiently high density, these quarks are not anymore confined inside the hadrons and become free. The superdense matter at densities higher than the nuclear one consists of a quark soup. The other group has re-interpreted the existence of the Hagedorn limiting temperature T_H as a signal of a second-order phase transition between the hadronic and quark-gluon phases of matter.

The discovery of asymptotic freedom has also paved the way to our current understanding of the evolution of the early universe. The commonly accepted scenario of subsequent cooling of the universe assumes a series of first- or second-order phase transitions associated with the various spontaneous symmetry breakings of the basic non-Abelian gauge fields [46–48]. The Standard Model (SM) of elementary particles predicts two such transitions [48]. One taking place at temperatures of a few hundred GeV is responsible for the spontaneous breaking of the electroweak (EW) symmetry providing masses to elementary particles. It is also related to the EW baryon-number violating processes, which had a major influence on the observed baryon-asymmetry of the universe [49]. The lattice simulations have shown that the EW transition in the SM is an analytic crossover [50].

The second, QGP to hadronic matter transition happens at $T < 200$ MeV and is related to the spontaneous breaking of the chiral symmetry of the non-Abelian theory of strong interactions which is based on the $SU(3)_c$ color group – the QCD. Nature of this phase transition affects to a great extent our understanding of the evolution of the early universe [48]. For instance, in a strong first-order phase transition the QGP supercools before bubbles of hadron gas are formed. Since the hadronic phase is the initial condition for nucleosynthesis, the inhomogeneities in this phase could have a strong effect on the nucleosynthesis epoch [48]. Here, the lattice non-perturbative QCD calculations developed since late seventies [51] (for a recent review, see Ref. [52]) can be of great help. Knowing that the typical baryon chemical potentials μ_B are much smaller than the typical hadron masses ($\mu_B \approx 45$ MeV at $\sqrt{s_{NN}} = 200$ GeV [16] and negligible in the early universe) we can use the lattice QCD calculations performed at $\mu_B = 0$. The results [53] not only confirm the previous finding [51] that confinement of quarks into hadrons is strictly a low-temperature phenomenon but provide the strong evidence that the QCD transition is also a crossover, and thus the above mentioned scenarios – and many others – are ruled out. The same conclusion was made in Ref. [54] where the first lattice analysis of the QCD phase transition in a model with chiral quarks having physical masses was performed. Numerical simulations on the lattice also indicate that at vanishing $\mu_B \approx 0$ MeV the two phase transitions which are possible in the QCD – de-confining and chiral symmetry restoring – occur at essentially the same point [55].

The situation at large μ_B and T is more complicated (see the left panel of Fig. 1). Here, the wealth of novel QCD phases is predicted to exist [56] including the so-called quarkyonic phase [57]. At $T \approx 0$ MeV and $\mu_B \geq 1$ GeV, a variety of color superconducting phases occur [56, 58]. Somewhere on the phase boundary at $\mu_B \approx 400$ MeV, a critical point separating the first- and second-order phase transitions is predicted [56]. Search for this point is now underway at RHIC [59] and some of the recent results will be discussed in section VI.

III. PHASES OF QCD MATTER

Although the quark matter was mentioned as early as 1970 by Itoh [60] in the context of neutron stars, the term “hadronic plasma” was first introduced in 1977 by Shuryak [61]

in order to describe a new state of matter existing at temperatures above 1 GeV. This makes a good analogy with a classical gaseous plasma case when electrically neutral gas at high enough temperatures turns into statistical plasma system of mobile charged particles [62]. While in the later case their interactions obey the $U(1)_{em}$ gauge symmetry of Quantum Electrodynamics (QED), in the QCD case the interactions between plasma constituents is driven by their $SU(3)_c$ color charges. For this reason, the $SU(3)_c$ plasma is now called the quark-gluon plasma (QGP). For exhaustive collection of papers tracing development of theoretical ideas on the topic of QGP up to 1990, see e.g. Ref. [19]. For summary of later developments, see recent reviews [26, 63].

Let us note that contrary to the first oversimplified expectations [19] strongly interacting multi-particle systems feature numerous emergent phenomena that are difficult to predict from the underlying QCD theory, just like in condensed matter and atomic systems where the interactions are controlled by the QED theory. In addition to the hot QGP phase, several additional phases of QCD matter were predicted to exist [64, 65]. In particular, the long-range attraction between quarks in the color anti-triplet ($\bar{\mathbf{3}}$) channel was predicted to lead to the color superconductivity (CSC) with the condensation of 1S_0 Cooper pairs [66]. The analysis of CSC two-flavor deconfined quark matter at moderate densities [67] has revealed quite spectacular properties of this novel phase of matter like the spontaneous breakdown of rotation invariance manifested in the form of the quasi-fermion dispersion law. At high baryon density an interesting symmetry breaking pattern $SU(3)_c \times SU(3)_R \times SU(3)_L \times U(1)_B \rightarrow SU(3)_{c+L+R} \times Z(2)$ leading to the formation of quark Cooper pairs was found in QCD with three massless quark flavours (i.e. $m_u=m_d=m_s=0$) [65, 68]. This breaking of color and flavor symmetries down to the diagonal subgroup $SU(3)_{c+L+R}$ implies a simultaneous rotation of color and flavor degrees of freedom called the color-flavor locking (CFL). Let us note that the CSC and CFL phases of deconfined QCD matter might play an important role when studying the EoS of neutron stars [69]. Another interesting phase is the matter-pion condensate studied by Migdal [70].

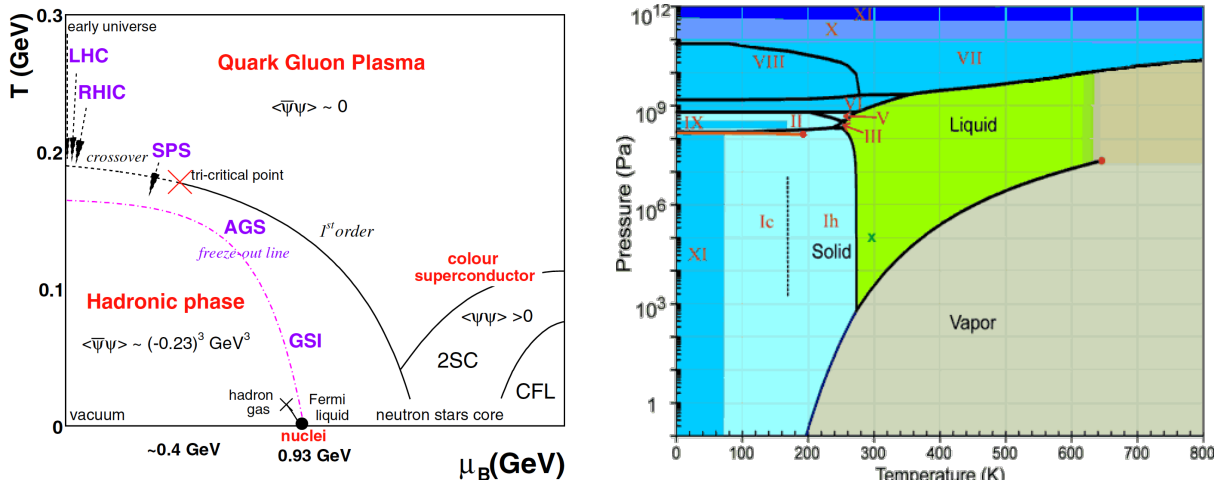


FIG. 1: Left: The schematic phase diagram of QCD in terms of T and μ_B state variables adapted from Ref. [71]. Right: The phase diagram of water illustrates a similar complexity and is taken from Ref. [72].

Current knowledge on the QCD phase diagram is summarized on the left panel of Fig. 1. The arrows indicate the expected crossing through the deconfinement transition during the

expansion phase in heavy-ion collisions at different accelerators. The red and black full circles denote the critical endpoints of the chiral and nuclear liquid-gas phase transitions, respectively. The (dashed) freeze-out curve indicates where hadro-chemical equilibrium is attained at the final stage of the collision. The nuclear matter ground-state at $T=0$ and $\mu_B = 0.93$ GeV and the approximate position of the QCD critical point at $\mu_B \sim 0.4$ GeV are also indicated. The dashed line is the chiral pseudo-critical line associated with the crossover transition at low temperatures. Comparing this diagram to the phase diagram of water shown on the right panel, one notices that at least theoretically the complexity of the former approaches the later.

A. The role of the QCD ground state

The quantum ground state of QCD plays an immensely important role in both Particle Physics and Cosmology. In particular, the quark-gluon condensate is responsible for spontaneous chiral symmetry breaking, color confinement and hadron mass generation (for a comprehensive review on the QCD vacuum, see e.g. Refs. [73–76] and references therein). It determines, in particular, the properties and, possibly, the generation mechanism of the quark-gluon plasma, dynamics of the phase transitions and hadronisation. The latter phenomena are the most critical QCD phenomena taking place beyond the Perturbation Theory (PT) and thus are very difficult to explore by means of the well-known approaches. This strongly motivates further even deeper studies in this direction.

Let us start with the classical Yang-Mills (YM) gauge theory in the $SU(N_c)$ ($N_c=3$ for QCD) determined by the gauge-invariant Lagrangian

$$\mathcal{L}_{\text{cl}} = -\frac{1}{4} F_{\mu\nu}^a F_a^{\mu\nu}, \quad (3.1)$$

where

$$F_{\mu\nu}^a = \partial_\mu A_\nu^a - \partial_\nu A_\mu^a + g_s e^{abc} A_\mu^b A_\nu^c$$

is the gluon field stress tensor with $SU(N_c)$ adjoint $a, b, c = 1, \dots, N_c^2 - 1$ and Lorentz $\mu, \nu = 0, 1, 2, 3$ indices, and with the strong coupling constant g_s . The generating functional of such a classical theory is given by the Euclidean functional integral

$$Z \propto \int [DA] e^{-S_{\text{cl}}[A] + \int J_\mu^a A_\mu^a d^4x}, \quad S_{\text{cl}}[A] = \int \mathcal{L}_{\text{cl}} d^4x, \quad (3.2)$$

which is dominated by minima of the classical action $S_{\text{cl}}[A]$ corresponding to the classical vacuum state with $F_{\mu\nu}^a = 0$ unaltered by quantum corrections. The field excitations about the classical YM vacuum are referred to as instantons [77, 78].

In fact, the classical YM equations of motion corresponding to Eq. (3.1) are form-noninvariant with respect to small quantum fluctuations which break the conformal invariance of the gauge theory [79] – the effect known as *the conformal (or trace) anomaly*. Indeed, there is no any threshold for the vacuum polarisation of a massless quantum gluon field by its classical component such that the solutions of the classical YM equations are unstable w.r.t the radiative corrections and cannot be used in physical applications. The conformal anomaly in QCD has notable implications, for example, in Cosmology leading to an appearance of the Lorentz-invariant negative-valued contribution to the cosmological

constant,

$$\epsilon^{\text{QCD}} = \frac{\beta(g_s^2)}{8} \langle 0 | :F_{\mu\nu}^a F_a^{\mu\nu} : | 0 \rangle + \frac{1}{4} \sum_{q=u,d,s} \langle 0 | :m_q \bar{q} q : | 0 \rangle \simeq -(5 \pm 1) \times 10^{-3} \text{ GeV}^4, \quad (3.3)$$

where the one-loop expression for the QCD β -function $\beta = -b\alpha_s/(4\pi)$, $b = b_{\text{eff}} = 9$ accounting for three light flavours u, d, s (for pure gluodynamics, $b = b_g = 11$) is typically used. Besides the wrong sign, the QCD vacuum density ϵ^{QCD} is over forty orders of magnitude larger in absolute value than the positive cosmological constant observed in astrophysical measurements,

$$\epsilon_{\text{CC}} > 0, \quad \left| \frac{\epsilon_{\text{CC}}}{\epsilon^{\text{QCD}}} \right| \simeq 10^{-44}, \quad (3.4)$$

The nonperturbative QCD vacuum effect is expected to be dynamically cancelled at macroscopically large distances in the course of cosmological expansion (see Ref. [80] and references therein). A dynamical mechanism of such a cancellation of vacua terms is yet unknown (for the existing scenarios discussed in the literature, see Refs. [80–83]).

Consider a consistent effective Lagrangian formulation of the YM theory incorporating the conformal anomaly. In the corresponding variational technique the strong coupling g_s is treated as an operator depending on operators of quantum gluon fields by means of the RG equations in the operator form. Namely, the gauge field operator \mathcal{A}_μ^a , is considered as a variational variable which together with the corresponding stress tensor operator are related to those in the standard normalisation as follows

$$\mathcal{A}_\mu^a \equiv g_s A_\mu^a, \quad \mathcal{F}_{\mu\nu}^a \equiv g_s F_{\mu\nu}^a = \partial_\mu \mathcal{A}_\nu^a - \partial_\nu \mathcal{A}_\mu^a + f^{abc} \mathcal{A}_\mu^b \mathcal{A}_\nu^c. \quad (3.5)$$

The effective action and Lagrangian operators of the quantum gauge theory is given in terms of the gauge-invariant operator of the least dimension J by [84]

$$S_{\text{eff}}[\mathcal{A}] = \int \mathcal{L}_{\text{eff}} d^4 x, \quad \mathcal{L}_{\text{eff}} = -\frac{J}{4g_s^2(J)}, \quad J = \mathcal{F}^2 \equiv \mathcal{F}_{\mu\nu}^a \mathcal{F}_a^{\mu\nu} = 2g_{s,*}^2 (B^2 - E^2), \quad (3.6)$$

respectively, whose variation w.r.t \mathcal{A}_μ^a leads to the energy-momentum tensor of the gauge theory

$$T_\mu^{\nu,g} = \frac{1}{g_s^2} \left[1 - \frac{1}{2} \beta(g_s^2) \right] \left(-\mathcal{F}_{\mu\lambda}^a \mathcal{F}_a^{\nu\lambda} - \frac{1}{4} \delta_\mu^\nu J \right) - \frac{\delta_\mu^\nu \beta(g_s^2)}{8g_s^2} J, \quad g_s^2 = g_s^2(J). \quad (3.7)$$

In Eq. (3.6), as a normalisation point, one can choose e.g. the strong coupling in the minimum of the effective action $g_{s,*}^2 = g_s^2(J=J^*)$. One distinguishes chromomagnetic $\langle B^2 \rangle > \langle E^2 \rangle$ and chromoelectric $\langle B^2 \rangle < \langle E^2 \rangle$ condensates, such that one or both of the corresponding ground-state solutions (minima of the effective action) should be stable in order to contribute to the physical QCD vacuum. The strong coupling dependence on J is determined by the RG evolution equation

$$2J \frac{dg_s^2}{dJ} = g_s^2 \beta(g_s^2), \quad g_s^2 = g_s^2(J), \quad (3.8)$$

The effective action (3.6) can be considered as an effective classical model [84] which possesses well-known properties of the full quantum theory such as (i) local gauge invariance, (ii) RG evolution and asymptotic freedom, (iii) correct quantum vacuum configurations, and (iv) trace anomaly.

In Ref. [83] it was noticed that the effective YM equation of motion in expanding universe with the conformal metric $g_{\mu\nu}=a^2\text{diag}(1,-1,-1,-1)$ ($g\equiv\det(g_{\mu\nu})$)

$$\left(\frac{\delta^{ab}}{\sqrt{-g}}\partial_\nu\sqrt{-g}-f^{abc}\mathcal{A}_\nu^c\right)\left[\frac{\mathcal{F}_b^{\mu\nu}}{g_s^2\sqrt{-g}}\left(1-\frac{1}{2}\beta(g_s^2)\right)\right]=0, \quad (3.9)$$

has a partial nonperturbative solution $\beta(g_{s,*}^2)=2$, where $g_{s,*}^2=g_s^2(J^*)$ is the solution of the RG equation (3.8) evaluated in the minimum of the effective action (3.6) $J^*=\langle J\rangle$. The corresponding value of the ground state density

$$T_0^{0,g}=-\frac{J^*}{4g_{s,*}^2}\equiv\mathcal{L}_{\text{eff}}\Big|_{J=J^*} \quad (3.10)$$

indicates that the QCD vacuum $\epsilon^{\text{QCD}}<0$ has indeed a chromomagnetic nature $\langle B^2\rangle>\langle E^2\rangle$ for $g_{s,*}^2>0$ in the deeply non-perturbative domain. This means that the corresponding solution is stable, namely, any small perturbation around the vacuum state effectively vanishes at the typical QCD time scale $\Delta t\sim 1/\Lambda_{\text{QCD}}$.

In asymptotically free gauge theories like QCD the quantum vacuum configurations are controlled by the strong coupling regime. Performing an analysis in Euclidean spacetime, in Ref. [84] it was shown that the vacuum value of the gauge invariant $\langle J\rangle$ in a strongly-coupled quantum gauge theory does not vanish as it does in the classical gauge theory and the corresponding functional integral is not dominated by the minima of the classical action (3.2). Moreover, it was shown that there are no instanton solutions to the effective action (3.6) such that the ground state of the quantum YM theory does not contain the classical instanton configurations. Instead, the quantum vacuum can be understood as a state with ferromagnetic properties which undergoes the spontaneous magnetisation providing a consistent description of the nonperturbative QCD vacuum and confinement alternative to the conventional instanton model.

How to understand the smallness of the observed cosmological constant within the effective QCD action approach? One way elaborated in Ref. [83] is to assume that such a compensation happens due to the presence of an additional QCD-like dynamics – Mirror QCD – with a confinement scale $\Lambda_{\text{mQCD}}\gg\Lambda_{\text{QCD}}$. The corresponding nonperturbative Mirror QCD vacuum contribution may have an opposite sign to that in QCD and can, therefore, compensate the QCD one at a certain time scale in the course of cosmological expansion. Another interesting possibility explored in Ref. [81] is to assume that the QCD vacuum is degenerate itself and at a given time scale consists two opposite-sign (quantum-topological and quantum-wave) contributions. Then, as soon as such a compensation occurs, the observable small cosmological constant can then be generated by means of weak gravitational interactions in the QCD vacuum. Both possibilities, however, require a fine tuning of vacuum parameters in order to provide an exact compensation of bare (zeroth-order in gravitational interactions) QCD contributions to the ground state density.

Can one avoid such a major fine tuning problem? The stable ground-state solution $J^*>0$ can actually be both chromomagnetic, when $g_{s,*}^2>0$, $\langle B^2\rangle>\langle E^2\rangle$ and $\epsilon^-<0$, and chromoelectric one corresponding to $g_{s,*}^2<0$, $\langle B^2\rangle<\langle E^2\rangle$ and $\epsilon^+>0$. Indeed, the standard argument in favor of positive definiteness of g_s^2 is given in a classical YM theory where

$$\mathcal{F}^2\propto-\frac{\partial}{\partial t}A_i^a\frac{\partial}{\partial t}A_i^a, \quad (3.11)$$

in Minkowski space such that $g_s^2 < 0$ would lead to infinitely fast growth of the field A_i^a and action $S_{cl} = \int \mathcal{L}_{cl} d^4x$ would not have a minimum. In the quantum case, however, g_s^2 is a function of J and can take negative values as long as the effective action S_{eff} has a minimum for $g_s^2 < 0$. Besides, in a close vicinity of the ground-state solution $\beta(g_{s,*}^2) = 2$ the corresponding solution of the RG equation (3.8) takes a linear behaviour

$$\frac{d \ln g_s^2}{d \ln J} \approx 1, \quad g_s^2 = \pm |g_{s,*}^2| \frac{J}{J^*}, \quad J, J^* > 0, \quad (3.12)$$

Adopting that the stable attractor solution $J \rightarrow J^* > 0$ is realised at macroscopically large time scales, the net QCD ground-state density would then asymptotically vanish [80]

$$\epsilon^\pm \rightarrow \pm \frac{J^*}{4|g_{s,*}^2|}, \quad \epsilon^-(T) + \epsilon^+(T) \rightarrow 0, \quad T \ll T_{QCD} = \Lambda_{QCD} \sim 100 \text{ MeV}, \quad (3.13)$$

if both contributions coexist in the QCD vacuum, thus, canceling each other beyond the confinement radius or after the QCD phase transition epoch in the cosmological history of the universe. The latter is an important example of conformal anomalies' cancelation in the classical limit of a YM theory without any fine tuning. In the deconfined (QGP) phase i.e. at temperatures $T \gtrsim T_{QCD}$ the chromoelectric contribution $\epsilon^+(T)$ should quickly vanish such that $\epsilon^{QCD} \simeq \epsilon^-(T = T_{QCD})$ providing a consistency with hadron physics phenomenology. This effect becomes plausible as long as $\epsilon^+(T)$ is attributed to the ground state of hadronic degrees of freedom which indeed becomes relevant only as soon as QGP is hadronised [81].

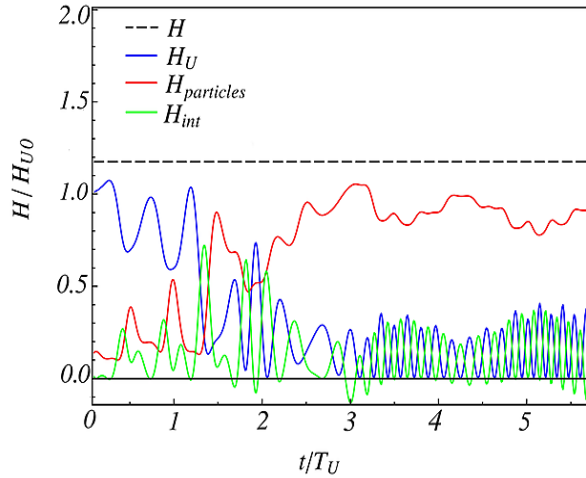


FIG. 2: Real time evolution of the energy density components of the interacting YM system – homogeneous gluon condensate H_U and inhomogeneous waves $H_{particles}$ versus the interactions' contribution H_{int} and the total Hamiltonian $H = H_U + H_{particles} + H_{int}$. Source: reproduced from Ref. [85].

What is the possible role of the QCD vacuum in the generation of QGP? As was demonstrated in Ref. [85] within a semi-classical analysis, an interacting YM system of homogeneous gluon condensate and inhomogeneous wave modes evolves in real time in such a way that the amplitude of waves parametrically grows at expense of decaying gluon condensate. The corresponding effect of the energy “swap” from the condensate to the gluon plasma

waves is illustrated in Fig. 2. Together with the growth of the plasma wave amplitudes, a vacuum average of their bi-linear products do not vanish and grow as well inducing the positive-valued component $\epsilon^+(T)$ of the ground-state density. This effect, if holds in the full quantum formulation, can then be the basis for the QGP generation and reheating mechanism, both in heavy ion collisions and in Cosmology. A similar mechanism may be responsible for reheating of the cosmological plasma and particle production in the end of Cosmic Inflation due to decay of the dominant spatially-homogeneous chromoelectric condensate (inflaton) driving the inflationary epoch.

Can such parametric growth of plasma modes due to a decay of the gluon condensate be studied in particle (e.g. heavy-ion) collisions? Can this effect be detectable and, if yes, be used as a tool for investigation of dynamical evolution of the quantum ground state in QCD? Answers to these and other related questions are big unknowns, and very little has been done so far in this direction. An interesting insight into the problem of QCD ground state can be offered by the low- p_\perp (<200 MeV) spectra of pions measured at the LHC which show up to $\sim 30\text{--}50\%$ enhancement compared to the hydrodynamic models (see e.g. Refs. [86–88]). A possible interpretation could be found in the framework of hypothesis about hadronization and freeze-out processes in chemical non-equilibrium [89]. Among the possible reasons for the non-equilibrium dynamics are the QGP supercooling [90, 91] and the gluon condensation [92] phenomena. A particularly interesting possibility has been proposed in Refs. [93–95] where it was shown that the Bose-Einstein pion condensate at the level of 5 % can account for the missing low- p_\perp charged pion yields coming from a coherent source in Pb+Pb collisions ($\sqrt{s} = 2.76$ TeV) at various centralities. Moreover, if there is such a condensate, there must be large fluctuations of pions, which should be seen starting from the fourth moment of the multiplicity distribution [96]. Further studies of the non-equilibrium QCD dynamics accounting for the ground state are certainly required from both theoretical and experimental standpoints.

B. Strongly interacting Quark Gluon Plasma

A surprising fact that the deconfined matter found at RHIC [14–17] does not behave as a gas of almost free quarks and gluons but as a strongly interacting liquid [18, 26] was anticipated only by a few [97–99]. The fact that QGP close to the critical temperature T_c is a strongly interacting system was used in Ref. [100, 101] to exploit its analogy with strongly coupled, classical, non-relativistic plasmas [62] in order to understand experimental observations as well as to interpret the lattice QCD results.

By definition, plasma is a state of matter in which charged particles interact via long-range (massless) gauge fields [26]. This distinguishes it from neutral gases, liquids or solids in which the inter-particle interaction is of short range. So plasmas themselves can be gases, liquids or solids depending on the value of the plasma parameter Γ which is the ratio of interaction energy to kinetic energy of the particles forming the plasma [62].

A non-relativistic electromagnetic plasma is called strongly coupled if the interaction energy (Coulomb energy) between the particles is larger than the thermal energy of the plasma particles, i.e. if the Coulomb coupling parameter $\Gamma_{\text{EM}}=q^2/(aT^2) > 1$, where q is the particle charge, a is the interparticle distance and T is the plasma temperature (in the system of units where $\hbar=c=k_B=1$). Let us note that the strongly-coupled classical electromagnetic plasmas are not exotic objects at all [62]. For example, table salt NaCl can be considered as a crystalline plasma made of permanently charged ions Na^+ and Cl^- [26].

At $T \approx 10^3$ K (still too small to ionize non-valence electrons) it transforms into a molten salt, which is a liquid plasma with $\Gamma \approx 60$. An estimate of the plasma parameter for QGP was considered in Ref. [100] where it was found that $\Gamma_{\text{QGP}} = 2C\alpha_s/(aT^2)$, where, depending on the type of plasma, $C = 4/3$ or $C = 3$ is the Casimir invariant for quarks or gluons and a is the interparton distance $a = 0.5$ fm. For QGP at temperature only slightly above the critical de-confining temperature, i.e. $T = 200$ MeV, the corresponding coupling constant $\alpha_s = 0.3\text{--}0.5$ and $\Gamma_{\text{QGP}} = 1.5\text{--}6$ the plasma can be considered as a strongly interacting one.

fluid	p [Pa]	T [K]	η [Pa·s]	η/n [\hbar]	η/s [\hbar/k_B]
H ₂ O	$0.1 \cdot 10^6$	370	$2.9 \cdot 10^{-4}$	85	8.2
⁴ He	$0.1 \cdot 10^6$	2.0	$1.2 \cdot 10^{-6}$	0.5	1.9
H ₂ O	$22.6 \cdot 10^6$	650	$6.0 \cdot 10^{-5}$	32	2.0
⁴ He	$0.22 \cdot 10^6$	5.1	$1.7 \cdot 10^{-6}$	1.7	0.7
⁶ Li ($a = \infty$)	$12 \cdot 10^{-9}$	$23 \cdot 10^{-6}$	$\leq 1.7 \cdot 10^{-15}$	≤ 1	≤ 0.5
QGP	$88 \cdot 10^{33}$	$2 \cdot 10^{12}$	$\leq 5 \cdot 10^{11}$		≤ 0.4

TABLE I: The viscosity η , the viscosity over density η/n ratio and the viscosity over entropy density η/s ratio for several fluids at particular values of pressure p and temperature T (from Ref. [102]).

The strongly interacting plasmas $\Gamma \geq 1$ are also a special case of strongly correlated systems where *correlated behavior* means a deviation from the trivial ideal gas behavior [103]. Prominent properties of all strongly correlated systems (see Fig. 3) can be quantified by a few dimensionless parameters: the coupling parameter Γ , the degeneracy parameter $\chi = n\lambda_{th}^3$ and the Brueckner parameter $r_s = a/a_B$, where n is the number density of the particles, $\lambda_{th} = \sqrt{2\pi/(mT)}$ is the thermal de Broglie wavelength, a is the average interparticle distance, m is the particle mass, and $a_B = 1/(me^2)$ is the Bohr radius.

Strongly interacting plasmas which can be studied in laboratory are ultracold atomic Fermi gases [104], in particular, strongly coupled ⁶Li atoms [105, 106]. A distinctive property of these plasmas is that, similarly to the strongly coupled QGP (sQGP), their shear viscosity to entropy density ratio η/s (see Ref. IV C 1 for definition), characterizing how close the fluid is to a perfect liquid [107], is effectively negligible [26, 102, 105]. Cold atomic gases are produced in optical or magneto-optical traps containing typically $10^5\text{--}10^6$ atoms [108]. The hydrodynamic behaviour is observed when the trapping potential is modified, or if the local density or energy density is modified using laser beams [105]. In this way, the scattering length a (and hence the interaction strength between the atoms) can be made almost infinite [26]. This is also the case of data point ⁶Li ($a = \infty$) shown in Table I where the thermodynamical parameters for several other substances of interest are summarized. For H₂O and ⁴He two points are displayed. First are the data at atmospheric pressure and temperatures just below the boiling point and the λ transition, respectively. These data points roughly correspond to the minimum of η/n at atmospheric pressure. Second are the data near the critical point which roughly corresponds to the global minimum of η/s .

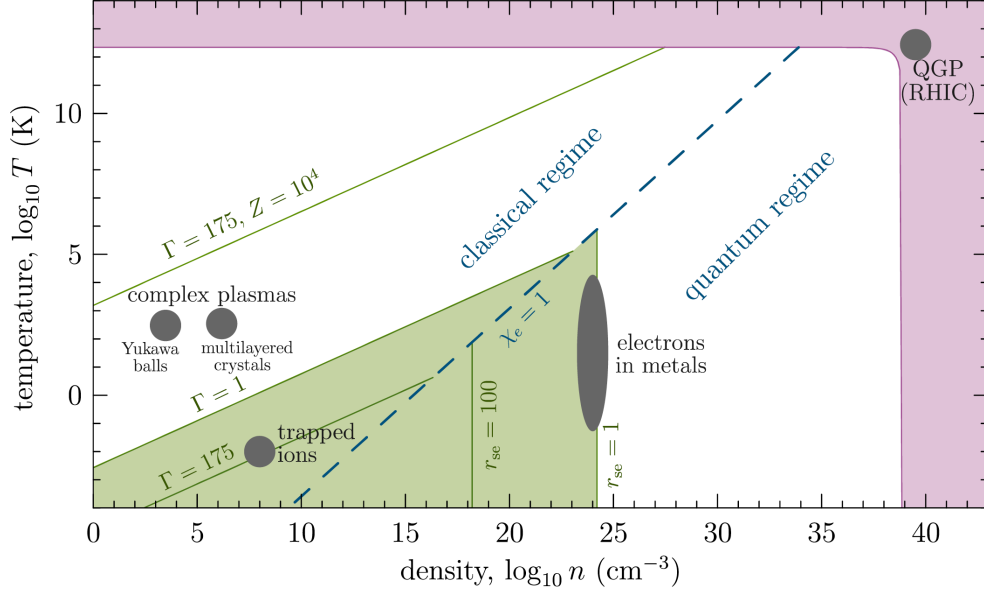


FIG. 3: Examples of strongly correlated systems in thermodynamic equilibrium include complex plasmas, trapped ions and the QGP extending along the outer (pink) area while dot shows the conditions at RHIC. The figure has been reproduced from Ref. [103].

C. QCD at high temperatures and vanishing chemical potentials

The grand canonical partition function in $SU(N_c)$ gauge theory (such as QCD) with N_f fermion flavours having a common chemical potential μ reads

$$Z(T, \mu) = \int DU e^{-S_g(T)} \prod_{f=1}^{N_f} \text{Det } M(m_f, \mu, T), \quad (3.14)$$

where M is the Dirac operator, S_g is the gauge part of the QCD action which depends on temperature T through boundary conditions. In the Hamiltonian formulation,

$$Z(T, \mu) = \text{Tr} \exp \left[-\frac{\hat{H}}{T} - \frac{\mu \hat{N}}{T} \right], \quad (3.15)$$

where \hat{N} is the number operator, and \hat{H} is the Hamiltonian. Needless to mention, the analytic properties of the free energy $F(T, \mu)$

$$F(T, \mu) = -T \ln Z(T, \mu) \quad (3.16)$$

as a function of general complex μ are known to be useful for studying the phase structure of QCD on the lattice [109].

Let us consider QCD thermodynamics at high temperatures and zero chemical potentials, the region relevant for the LHC and partly also for RHIC, by recalling how the basic bulk thermodynamic observables can be obtained from the grand canonical partition function with vanishing quark chemical potentials, $Z(T, V) \equiv Z(T, \mu)|_{\mu \rightarrow 0}$ [55]. The grand canonical potential, $\Omega(T, V)$, normalized in such a way that it vanishes at zero temperature,

$$\Omega(T, V) = T \ln Z(T, V) - \Omega_0, \quad \Omega_0 = \lim_{T \rightarrow 0} T \ln Z(T, V), \quad (3.17)$$

can be used to obtain the thermal part of the pressure (p) and energy density (ϵ)

$$p = \frac{1}{V} \Omega(T, V), \quad \epsilon = \frac{T^2}{V} \frac{\partial \Omega(T, V) / T}{\partial T}, \quad (3.18)$$

both vanishing at small temperature, by construction. Using these relations one can express the difference between ϵ and $3p$, i.e. the thermal contribution to the trace of the energy-momentum tensor $\Theta^{\mu\mu}(T)$ (also called the trace anomaly or the interaction measure), in terms of a derivative of the pressure with respect to temperature:

$$\frac{\Theta^{\mu\mu}(T)}{T^4} \equiv \frac{\epsilon - 3p}{T^4} = T \frac{\partial}{\partial T} (p/T^4). \quad (3.19)$$

In fact, it is $\Theta^{\mu\mu}(T)$ which is the basic thermodynamic quantity conveniently calculated on the lattice as the total derivative of $\ln Z$ with respect to the lattice spacing a [110]:

$$\Theta^{\mu\mu} = \epsilon - 3p = -\frac{T}{V} \frac{d \ln Z}{d \ln a}. \quad (3.20)$$

Before moving to the results of lattice calculations, it is useful, for comparison, to recall a description of the strongly interacting matter below deconfinement temperature T_c . Here, all thermodynamic quantities are expected to be well-described by the hadron resonance gas (HRG) model consisting of non-interacting hadrons as proposed by Hagedorn in mid sixties [41] (see also Ref. [42]). The trace anomaly in the HRG model is given by

$$\left(\frac{\epsilon - 3p}{T^4} \right)^{HRG} = \sum_{m_i \leq m_{max}} \frac{d_i}{2\pi^2} \sum_{k=1}^{\infty} \frac{(-\eta_i)^{k+1}}{k} \left(\frac{m_i}{T} \right)^3 K_1 \left(\frac{km_i}{T} \right), \quad (3.21)$$

where $K_1(\frac{km_i}{T})$ is a modified Bessel function, the different particle species of mass m_i have degeneracy factors d_i and $\eta_i = -1(+1)$ for bosons (fermions), and the sum runs over all known hadrons up to the resonance mass of $m_{max} = 2.5$ GeV.

The results on temperature dependence of the trace anomaly and suitably normalized pressure, energy density, and entropy density from lattice calculations together with the HRG predictions are shown on the left and right panels of Fig. 4, respectively. The vertical band in the right panel marks the crossover region, $T_c = (154 \pm 9)$ MeV. The horizontal line at $95\pi^2/60 \approx 15.6$ corresponds to the ideal Stefan-Boltzmann (SB) gas limit for the energy density of relativistic massless gas consisting of $N_f = 3$ quark flavours and gluons with $N_c = 3$ colors having altogether g degrees of freedom:

$$\frac{3p_{SB}}{T^4} = \frac{\epsilon_{SB}}{T^4} = g \frac{\pi^2}{30}, \quad g = 2(N_c^2 - 1) + \frac{7}{2} N_c N_f = \frac{95}{2}. \quad (3.22)$$

The fact that even at $T \propto 400$ MeV the pressure, energy density, and entropy density of the QGP are far from their ideal gas values indicates substantial remaining interactions among the quarks and gluons in the deconfined phase. It is interesting to compare, at least qualitatively, this behaviour with the gaseous two-component plasma of particles with charge $q = \pm ze$. The pressure normalized to that of the ideal gas can be deduced from the standard textbook formula (see e.g. Ref. [111])

$$\frac{p}{p_{id}} = 1 - \frac{\sqrt{\pi}}{3} \sqrt{\frac{nq^6}{T^3}}, \quad (3.23)$$

which is valid for $n \ll T^3/q^6$. The non-ideal behaviour of gaseous two-component plasma thus increases very fast with charge q of the plasma particles but much slower with their density n and decreases rather quickly with the plasma temperature T .

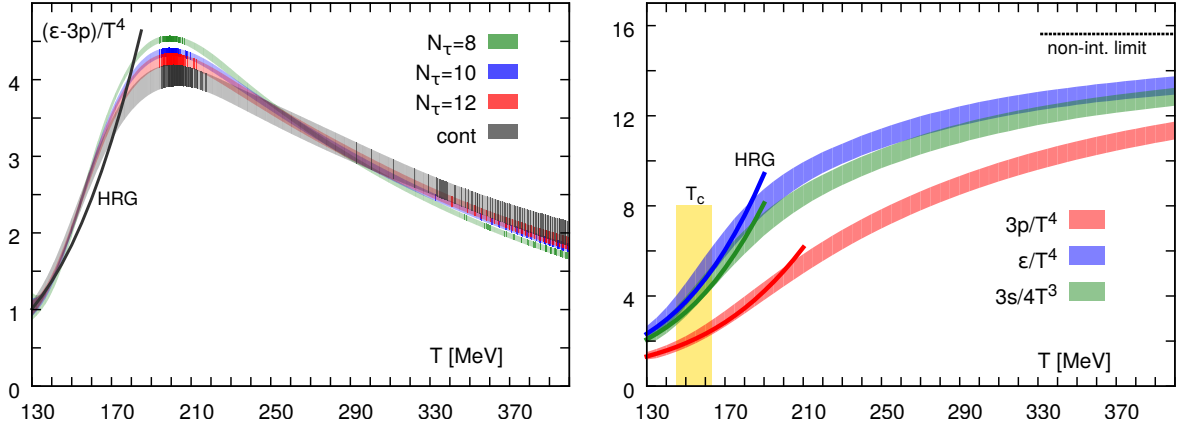


FIG. 4: Left: The continuum-extrapolated trace anomaly for several values of the lattice spacing $aT=1/N_\tau$ and its continuum extrapolation. Right: The continuum-extrapolated values of suitably normalized pressure, energy density, and entropy density as functions of the temperature. Both figures have been reproduced from Ref. [110]. The darker lines in both figures show the corresponding predictions of the HRG model.

1. Softest point in the EoS of deconfined QCD matter

An important property of the QGP phase transition is the presence of a local minimum in the ratio of pressure to energy density p/ϵ as a function ϵ [112, 113]. Possible existence of this *softest point* in the QCD EoS is distinguishable by a very small sound velocity of the deconfined medium and has thus been suggested as a signal of the first-order phase transition. This also becomes evident in second order derivatives of the QCD partition function with respect to temperature. The speed of sound, c_s , is related to the inverse of the specific heat, $C_V=d\epsilon/dT$,

$$c_s^2 = \frac{\partial p}{\partial \epsilon} = \frac{dp/dT}{d\epsilon/dT} = \frac{s}{C_V}, \quad \frac{C_V}{T^3} = \frac{\partial \epsilon}{\partial T} \Big|_V \equiv \left(4 \frac{\epsilon}{T^4} + T \frac{\partial(\epsilon/T^4)}{\partial T} \Big|_V \right). \quad (3.24)$$

The quantity $Td(\epsilon/T^4)/dT$ can be calculated directly from the trace anomaly and its derivative with respect to temperature,

$$T \frac{d\epsilon/T^4}{dT} = 3 \frac{\Theta^{\mu\mu}}{T^4} + T \frac{d\Theta^{\mu\mu}/T^4}{dT}. \quad (3.25)$$

In Fig. 5 (left panel), we show the speed of sound as a function of temperature. The softest point of the EoS predicted in Ref. [113] at $T \simeq (145-150)$ MeV, *i.e.*, at the minimum of the speed of sound, lies on the low temperature side of the crossover region. At this point, the speed of sound is only slightly below the corresponding HRG value. Furthermore, the value $c_s^2 \simeq 0.15$ is roughly half way between zero, the value expected at a second order phase transition with a divergent specific heat, and the value for an ideal massless gas, $c_s^2=1/3$ [110]. At the high temperature end, $T \sim 350$ MeV, it reaches within 10% of the ideal gas value.

The softest point of the EoS is of interest for phenomenology of heavy ion collisions as it characterizes the temperature and energy density range in which the expansion and cooling of matter slows down. The system spends a longer time in this temperature range, and one

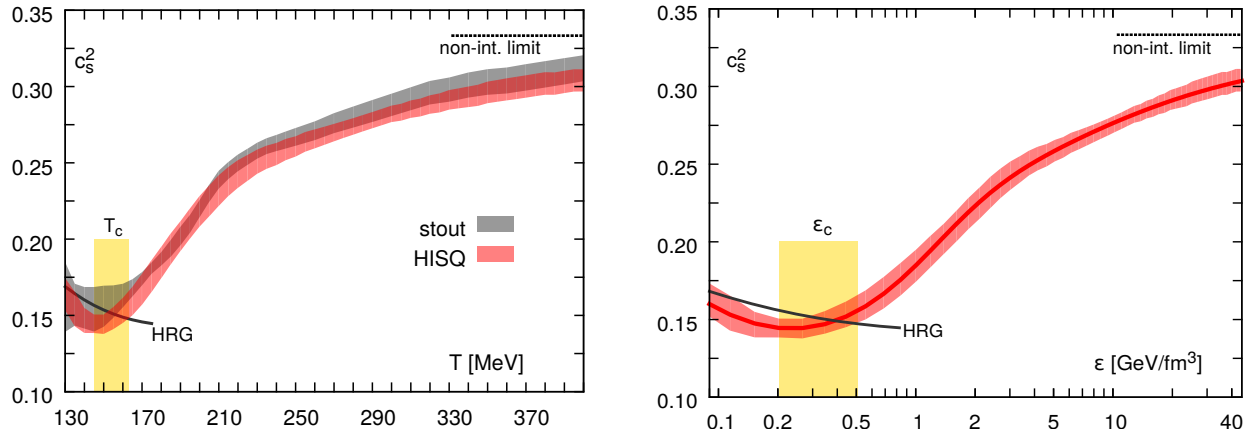


FIG. 5: The speed of sound squared c_s^2 from lattice QCD and the HRG model versus temperature T (left) and energy density ϵ (right). The figure has been reproduced from Ref. [110]. The vertical yellow bands marks the location of the crossover region $T_c=(154\pm 9)$ MeV and the corresponding range in energy density, $\epsilon_c=(0.18-0.5)$ GeV/fm³, respectively.

expects to observe characteristic signatures from this regime. The quantity c_s^2 as a function of the energy density is shown in Fig. 5 (left). At the softest point, the energy density is only slightly above that of normal nuclear matter, $\rho_0=160$ MeV/fm³. In the crossover region, $T_c=(154\pm 9)$ MeV, the energy density varies from 180 MeV/fm³ at the lower edge to 500 MeV/fm³ at the upper edge, slightly above the energy density inside the proton $\epsilon_{\text{proton}}=450$ MeV/fm³.

The QCD crossover region, thus, starts at or close to the softest point of the EoS and the entire crossover region corresponds to relatively small values of the energy density, $(1.2-3.1)\epsilon_{\text{nuclear}}$. This value is about a factor of four smaller than that of an ideal quark-gluon gas in this temperature range.

2. Testing the properties of the medium with infinitely heavy, static test charges

An important property of the QGP medium is the color screening: the range of interaction between heavy quarks becomes inversely proportional to the temperature. This effect also forms a basis of the most common description of dynamics of quarkonia, mesons consisting of heavy $Q\bar{Q}$, produced in heavy ion collisions – the potential between the heavy quarks $c\bar{c}$ or $b\bar{b}$ becomes screened by deconfined quarks and gluons, and the heavy quarks separate from each other leading to a suppression of quarkonia yields [114].

On the lattice this phenomenon is studied using (infinitely) heavy, static test charges [115, 116]. The color screening effect is estimated from the spatial correlation function $G(r,T)$ of a static quark and anti-quark, which propagate in Euclidean time from $\tau=r=0$ to $\tau=r=1/T$, where T is the temperature. The free energy of static quark pair $Q\bar{Q}$ is then calculated as the logarithm of the correlator $F(r,T)=-T\ln G(r,T)$ [115, 117]. In the zero temperature limit the singlet free energy coincides with the zero temperature potential calculated on the lattice [118]. However, as argued in Ref. [116] using the free energies instead of potentials is preferable since the later are not gauge invariant. On the other hand, the gauge-invariant static quark-antiquark pair free energy is a non-perturbatively well-defined quantity that carries information about the deconfinement properties of the QGP.

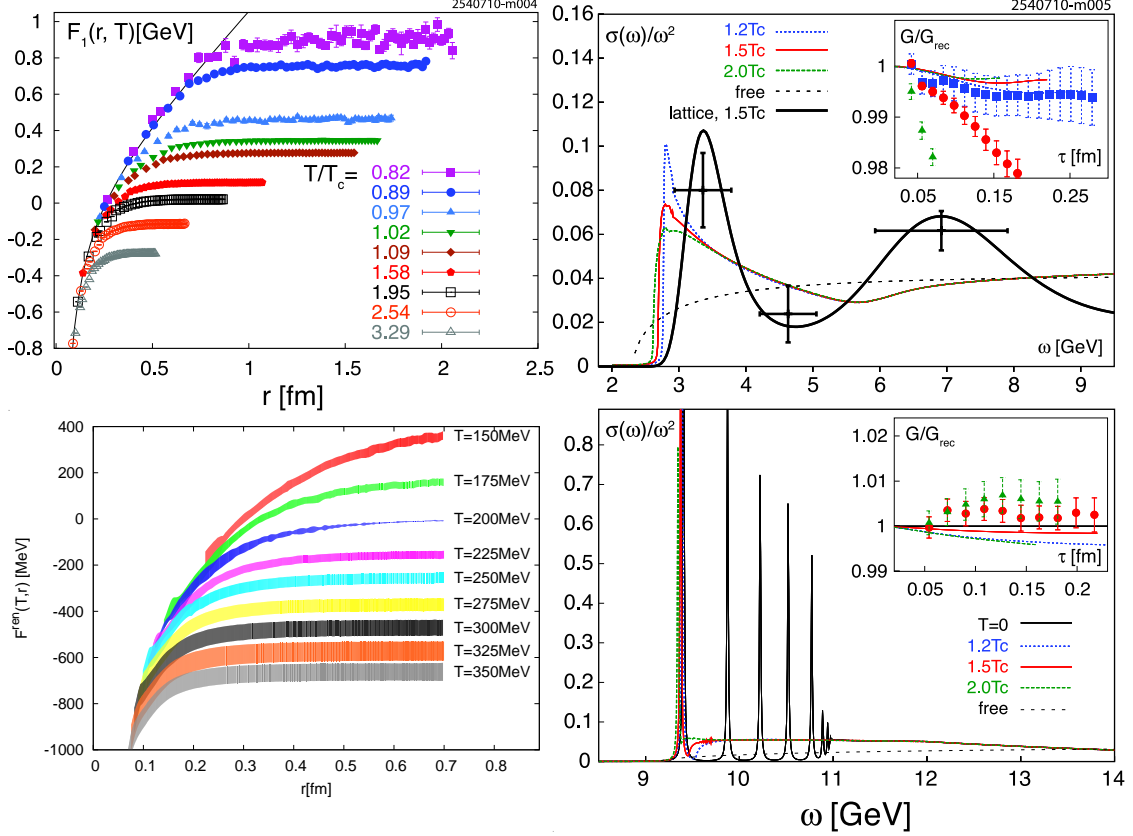


FIG. 6: Left: Heavy-quark-singlet free energy versus quark separation calculated in 2+1 flavor QCD for different values of T/T_c (top) [115] and continuum-extrapolated values of the static $Q\bar{Q}$ free energy for different temperatures (bottom) [116]. The solid black line on the right top plot is a parameterisation of the zero temperature potential. Right: The S-wave charmonium (upper) and bottomonium (lower) spectral functions calculated in potential models. Insets: correlators compared to lattice data. The dotted curves are the free spectral functions. Source: reproduced from Ref. [115].

The heavy-quark free energies for different temperatures T of the medium from two different lattice calculations are presented on Fig. 6 (left). The solid black line on the upper plot is a parameterisation of the zero temperature potential. One can see that with increasing temperature the free energy and, hence, the spatial correlations between Q and \bar{Q} get more and more diluted.

The correlation functions in time variable are related to the spectral functions $\sigma(\omega, T)$ by

$$G(\tau, T) = \int_0^\infty d\omega \sigma(\omega, T) \frac{\cosh(\omega(\tau - 1/(2T)))}{\sinh(\omega/2T)}. \quad (3.26)$$

While a stable $Q\bar{Q}$ quarkonium state in the vacuum contributes to the spectral function a δ -function-like peak at the value of its mass m_H , in the medium it gives a quasi-particle-like smeared peak with the width being the thermal width. As one increases the temperature, the width increases and at sufficiently high temperatures, the contribution from the meson state in the spectral function becomes sufficiently broad so that it is no longer meaningful to speak of it as a well-defined state, Fig. 6 (right). The effect is more prominent for the

lighter mesons like charmonia consisting of $c\bar{c}$ pairs and much weaker for the bottomonia – $b\bar{b}$ mesons.

D. QCD at high temperatures and non-zero chemical potentials

As direct lattice QCD calculations at non-zero μ_B are not yet possible one has to analyze the EoS using Taylor expansion in quark chemical potentials μ_u , μ_d and μ_s [52, 119]

$$\frac{p}{T^4} = \frac{1}{VT^3} \ln Z(T, \mu_u, \mu_d, \mu_s) = \sum_{ijk} \frac{1}{i!j!k!} \chi_{ijk}^{uds} \left(\frac{\mu_u}{T}\right)^i \left(\frac{\mu_d}{T}\right)^j \left(\frac{\mu_s}{T}\right)^k \quad (3.27)$$

$$\chi_{ijk}^{uds} = \frac{\partial^{i+j+k} p/T^4}{\partial(\mu_u/T)^i \partial(\mu_d/T)^j \partial(\mu_s/T)^k}, \quad (3.28)$$

where μ_u , μ_d and μ_s are related to the chemical potentials corresponding to the baryon number B , electric charge Q and strangeness S of hadrons as follows

$$\mu_u = \frac{1}{3}\mu_B + \frac{2}{3}\mu_Q, \quad \mu_d = \frac{1}{3}\mu_B - \frac{1}{3}\mu_Q, \quad \mu_s = \frac{1}{3}\mu_B - \frac{1}{3}\mu_Q - \mu_S. \quad (3.29)$$

The EoS at non-zero $\mu_{B,Q,S}$ can thus be obtained from the coefficients χ_{ijk}^{BQS} of the Taylor expansion in hadronic chemical potentials expressed via χ_{ijk}^{uds} [52]. Here, we report the result [119] for $\mu_Q = \mu_S = 0$ which sufficiently illustrates the relative importance of higher-order corrections in different temperature and μ_B regions. The Taylor series for the pressure is given by

$$\frac{p(T, \mu_B) - p(T, 0)}{T^4} = \frac{1}{2} \chi_2^B(T) \left(\frac{\mu_B}{T}\right)^2 \left[1 + \frac{1}{12} \frac{\chi_4^B(T)}{\chi_2^B(T)} \left(\frac{\mu_B}{T}\right)^2 \right] + \mathcal{O}(\mu_B^6). \quad (3.30)$$

The leading-order correction to the pressure at non-vanishing μ_B is proportional to the quadratic fluctuations of the net baryon number. The next-to-leading order corrections are proportional to the quartic fluctuations. In Fig. 7 we show $\chi_2^B(T)$ (left) and $\chi_4^B(T)/\chi_2^B(T)$ (right). With increasing temperature the $\mathcal{O}(\mu_B^4)$ correction rapidly loses importance relative to the leading $\mathcal{O}(\mu_B^2)$ term. Moreover, the results for the μ_B -dependent contribution to the total pressure evaluated for different values of μ_B/T [119] suggest that the EoS given by Eq. 3.30 works well for all values of the chemical potential below $\mu_B/T = 2$ corresponding to the region of nuclear collisions at energies $\sqrt{s_{NN}} \geq 20$ GeV.

Let us note that χ_{ijk}^{BQS} are interesting on their own right as they are related to the fluctuations and correlations of conserved charges. The later are sensitive to the underlying degrees of freedom which could be hadronic or partonic and so they are used as sensitive probes of deconfinement. While the off-diagonal expansion coefficients are related to correlations among conserved charges, e.g. $\chi_{11}^{XY} = \frac{1}{VT^3} \langle N_X N_Y \rangle$, the diagonal ones describe their second and higher order fluctuations

$$\chi_2^X = \frac{1}{VT^3} \langle N_X^2 \rangle, \quad \chi_4^X = \frac{1}{VT^3} (\langle N_X^4 \rangle - 3\langle N_X^2 \rangle^2), \quad \text{etc.} \quad (3.31)$$

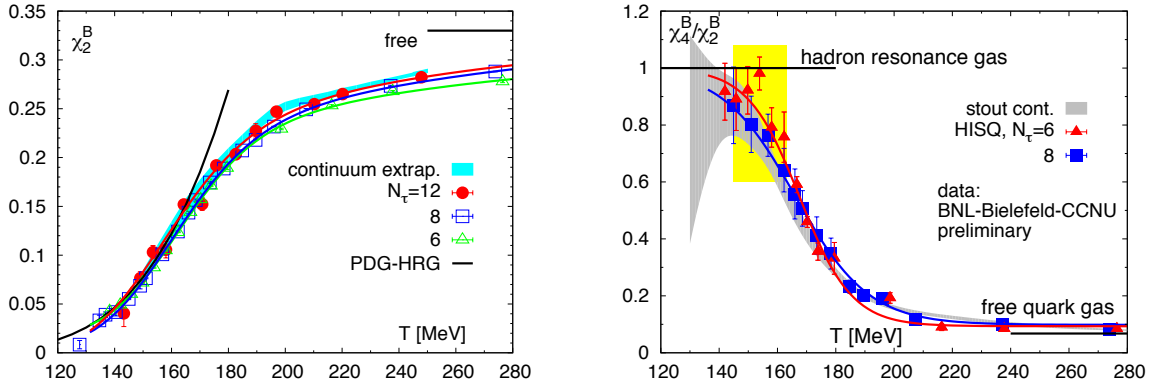


FIG. 7: The expansion coefficients of the pressure at the non-zero baryon chemical potential adopted from Ref. [119]. Left: The leading-order correction. Right: The relative contribution of the next-to-leading order correction.

IV. STUDY OF HOT AND DENSE NUCLEAR MATTER USING NUCLEAR COLLISIONS

A. Heavy ion accelerators

The basic hopes and goals associated with investigations of very hot and dense nuclear matter in laboratory were first formulated in mid-seventies [120–122]. It was the experience with astrophysical objects like supernovae and neutron stars, and with thermonuclear ignition which led the authors to an idea that the nuclear matter shock compression [31] of about five-fold normal nuclear density should be accomplished in violent head-on collisions of heavy nuclei [11]. The goal was to find out the response of the nuclear medium under compression by pressure resisting that compression, i.e. to study the nuclear matter EoS. The original question was: is such a bulk nuclear matter EoS accessible within the dynamics of relativistic heavy ion collisions? [123, 124]. The prospect to observe a phase transition in highly compressed nuclear matter [125] was lurking behind.

The interest in collisions of high-energy nuclei as a possible route to a new state of nuclear matter was substantially strengthened with arrival of QCD as the microscopic theory of strong interactions. Since mid-seventies the particle physics community has begun to adapt existing high-energy proton accelerators to provide heavy-ion nuclear beams. The Berkeley Bevalac and JINR Synchrophasotron started to accelerate nuclei to kinetic energies from few hundreds of MeV to several GeV per nucleon [11, 124]. By the mid-1980s, the first ultra-relativistic nuclear beams became available. Silicon and gold ions were accelerated to 10 GeV/nucleon at Brookhaven’s Alternating Gradient Synchrotron (AGS) [10]. The first nuclear collisions took place at CERN in early eighties when alpha particles were accelerated to *center-of-mass energy per nucleon-nucleon pair* $\sqrt{s_{NN}}=64$ GeV at the ISR collider. The new era of research begun at CERN in fall 1986 when oxygen and later on (in summer 1990) sulphur ions were injected into the SPS and accelerated up to energy of 200 GeV/nucleon ($\sqrt{s_{NN}} = 19.6$ GeV) [10–12]. However, the genuine heavy ion program has started only in 1994, after the CERN accelerator complex has been upgraded with a new lead ion source which was linked to pre-existing, interconnected accelerators, the Proton Synchrotron (PS) and the SPS. Seven large experiments involved (NA44, NA45/CERES, NA49, NA50, NA52,

WA97/NA57 and WA98) have studied different aspects of Pb+Pb and Pb+Au collisions at $\sqrt{s_{NN}} = 17.3$ GeV and $\sqrt{s_{NN}} = 8.6$ GeV [11, 12].

In the meantime, at the Brookhaven National Laboratory (BNL) the Relativistic Heavy Ion Collider (RHIC) [126] rose up from the ashes of ISABELLE/CBA $\bar{p}p$ collider project abandoned in 1983 by particle physicists. In 1984 the first proposal for a dedicated nucleus-nucleus machine accelerating gold nuclei up to $\sqrt{s_{NN}} = 200$ GeV was submitted. Funding to proceed with the construction was received in 1991 and on June 12th, 2000 the first Au+Au collisions at $\sqrt{s_{NN}} = 130$ GeV were recorded by the BRAHMS, PHENIX, PHOBOS and STAR experiments [14–17].

The idea of the Large Hadron Collider (LHC) [127] dates even further back – to the early 1980s. Although CERN’s Large Electron Positron Collider (LEP), which ran from 1989 to 2000, was not built yet, scientists considered re-using the 27-kilometer LEP ring for an even more powerful pp machine running at highest possible collision energies $\sqrt{s} = 14$ TeV and intensities. The ion option ($\sqrt{s_{NN}} = 5.4$ TeV per nucleon-nucleon pair for Pb+Pb collisions) was considered since the beginning. The LHC was approved in December 1994, its official inauguration took place on 21st October 2008. First proton-proton collisions occurred on 23rd November 2009, first Pb+Pb collisions on November 7th 2010. The ALICE, ATLAS and CMS experiments are currently involved in the heavy-ion program at the LHC [25, 29].

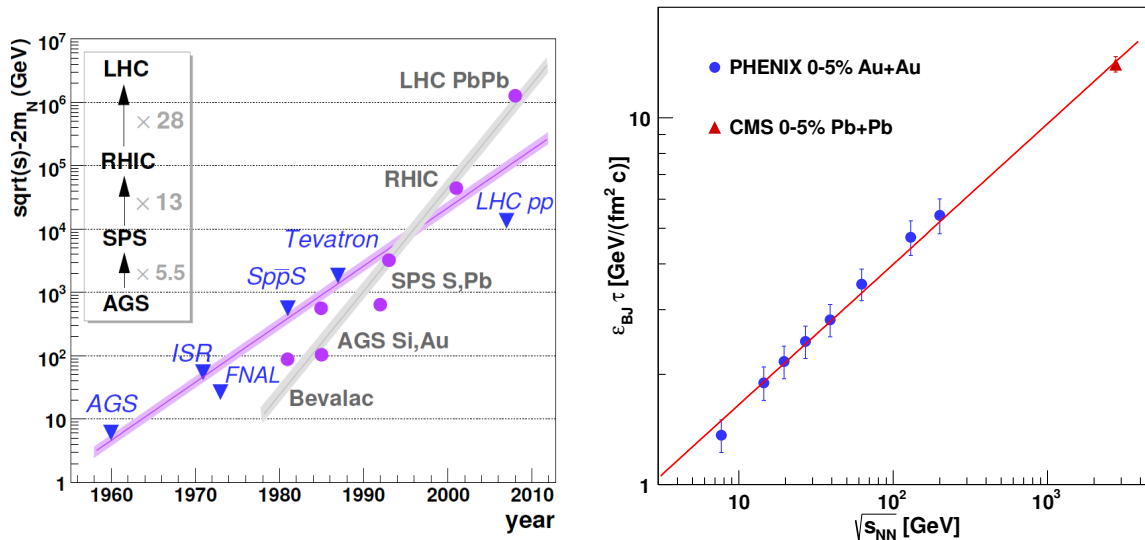


FIG. 8: Left: Available center-of-mass energy $\sqrt{s}-2m_N$ versus time for (anti)proton (blue triangles) and ion (magenta circles) accelerators, adapted from Ref. [71]. Right: The Bjorken estimate of the initial energy density ϵ_{BJ} (Eq. (4.1)) multiplied by τ calculated from the data on transverse energy distributions in 5% most central Au+Au [128] and Pb+Pb [129] collisions as a function of c.m.s. energy per one nucleon-nucleon pair $\sqrt{s_{NN}}$. The red line corresponds to a power law fit. From Ref. [130].

Many years ago, American accelerator physicist M. Stanley Livingston noted that advances in accelerator technology increase the energy records achieved by new machines by a factor of ten every six years. This trend is illustrated on the left panel of Fig. 8 summarising

the worldwide advances in high-energy accelerators in the period of 1960 – 2008. One can see that for the ion accelerators the increase in the energy is even faster than for the proton accelerators. However, even in the most central nucleus-nucleus collisions not all that energy could be converted into a thermalised form of energy needed for the phase transition from hadronic into QGP state of matter to occur. The experimentally accessible quantity measuring this transformation is the density of transverse energy E_T per unit of pseudorapidity η . The later can be used to estimate the initial energy density using the Bjorken formula [131]:

$$\epsilon_{BJ} = \frac{1}{S_{\perp}\tau} \left. \frac{dE_T}{d\eta} \right|_{\eta=0}, \quad (4.1)$$

where S_{\perp} is the transverse overlap area of the nuclei and τ is the time scale for the evolution of the initial non-equilibrium state of matter into a (locally) thermalized system. The dependence of $\epsilon_{BJ\tau}$ on $\sqrt{s_{NN}}$ for most central Au+Au and Pb+Pb collisions is presented on the right panel of Fig. 8. Even for a rather pessimistic value of the equilibration time $\tau=1$ fm/c [17] the achieved energy density increases from 1.4 to 14 GeV/fm³. It is thus not only much higher than than the normal nuclear density but 3 – 30 times bigger than the energy density inside the nucleon $\epsilon_N=0.45$ GeV/fm³ and is definitely higher then 1 GeV/fm³ scale required for the QCD deconfining transition from the lattice calculations which were discussed in section III C.

B. Heavy ion collisions as a source of strong electromagnetic fields

The important quantity determining the lifetime of heavy ion beams inside the accelerator tube (and hence their potential to produce an adequate number of nuclear collisions) is loss of ions in the bunch. Its decay rate λ_T is given by the formula:

$$\lambda_T = -\frac{1}{N} \frac{dN}{dt} = \frac{N_{IR}L\sigma_T}{kN}, \quad (4.2)$$

in which k is the number of bunches, N is the number of particles per bunch, N_{IR} is the number of interaction regions, σ_T is the total cross section and L is the available luminosity:

$$L = f\gamma \frac{N^2k}{4\pi\epsilon\beta^*} F, \quad (4.3)$$

which besides k and N depends also on the revolution frequency f , the Lorentz factor of the beam γ , the emittance ϵ , the beta function at the collision point β^* and the geometric luminosity reduction factor F due to the crossing angle at the interaction point [127]. Since the event rate for a certain process is given by its cross section times the luminosity $N_{evt} = L\sigma_{evt}$, the possibility of studying rare phenomena depends on the maximum luminosity accessible. At the same time the rate of background processes, which in general have large cross sections, will increase L , reaching at some point the maximum event rate that the experiment can handle. Secondary beams created by these background processes can limit the collider heavy ion luminosity since they have a different charge-to-mass ratio than the primary beam and can be lost in cryogenically cooled magnets.

At RHIC and the LHC, quite surprisingly, these background processes are not part of the strong nuclear interaction cross section σ_R determined primarily by the nuclear geometry $\sigma_R \approx \pi r_0^2 (A_I^{1/3} + A_{II}^{1/3})^2$ but are solely accounted for by the coherent action of all electric charges

in colliding nuclei. The cross section of electromagnetic processes, primarily due to creation of e^+e^- pairs with subsequent e^- atomic shell capture and electro-magnetic dissociation, becomes important for ions with $Z>30$. It is as large as hundreds of barns, i.e. about 30 (60) times larger than σ_R for Au+Au collisions at RHIC (Pb+Pb collisions at the LHC) [132].

A classical description of electromagnetic action of fast moving charged particle on another one based on the equivalence between the perturbative action of its field and the flux of electromagnetic radiation dates back to Fermi [133], Weizsäcker [134] and Williams [135]. This equivalence is true as far as the effects caused by different spectral components add up incoherently, i.e. a perturbation caused by the fields is small enough. The solution for the time-dependent electromagnetic fields mutually seen by the two incident ions can be found, for example, in the textbook on ‘‘Classical Electrodynamics’’ [136]. The longitudinal (\parallel) and transversal (\perp) field components induced by a heavy ion I passing a target II at distance b and with velocity β are given by the following formulas:

$$E_{\parallel}(t)=\frac{-Z_I e \gamma \beta t}{(b^2+\gamma^2 \beta^2 t^2)^{3/2}}, \quad \vec{E}_{\perp}(t)=\frac{Z_I e \gamma \vec{b}}{(b^2+\gamma^2 \beta^2 t^2)^{3/2}}, \quad B_{\parallel}(t)=0, \quad \vec{B}_{\perp}(t)=\vec{\beta} \times \vec{E}_{\perp}(t). \quad (4.4)$$

Let us note that for $\gamma \gg 1$ these fields act on a very short time scale of order $\Delta t \propto b/\gamma$. During this time fields $\vec{E}_{\perp}(t)$ and $\vec{B}_{\perp}(t)$ are *equivalent* to a linearly polarized pulse of radiation incident on a target in the beam direction. Thus, according to the equivalent photon method, the strong and rapidly time varying field of the point charge Z_I is seen by a passing charge as a flux of virtual (nearly real) photons with intensity

$$I(\omega, b) = \frac{1}{4\pi} |\vec{E}(\omega) \times \vec{B}(\omega)| \approx \frac{1}{2\pi} |E_{\perp}(\omega)|^2 \sim Z_I^2, \quad (4.5)$$

where $\vec{E}(\omega)$, $\vec{B}(\omega)$ and $E_{\perp}(\omega)$ are the Fourier components of the fields \vec{E} , \vec{B} and E_{\perp} . The energy spectrum of these photons falls as $\propto 1/E_{\gamma}$ up to a maximum energy $E_{\gamma}^{max} = \gamma/b_{min}$. The interaction between the colliding nuclei becomes dominantly electromagnetic for impact parameters b exceeding the size of the radii of colliding nuclei $b > b_{min} = R_I + R_{II} = \sqrt{\sigma_R/\pi}$.

Interactions between ultra-relativistic nuclei taking place at $b > b_{min}$ are called the ultra-peripheral collisions. By taking advantage of the photon fields carried by relativistic nuclei they are used to study photoproduction and two-photon physics at hadron colliders. This field of ultra-relativistic heavy ion collisions is sometimes called ‘‘*non-QGP*’’ physics and is thus outside the scope of this article. We refer the interested reader to reviews [137–140] where more detailed information on these aspects can be found.

1. Quark-gluon plasma in a strong magnetic field

More important from the point of view of QGP physics are the strong magnetic fields accompanying ultra-relativistic heavy ion collisions [141]. Consider collision of two identical nuclei of radius R with electric charge Ze and use the Biot–Savart law to estimate the magnitude of perpendicular magnetic field they create in the center-of-mass frame

$$B_{\perp} \sim \gamma Z e \frac{b}{R^3}. \quad (4.6)$$

Here, $\gamma = \sqrt{s_{NN}}/2m_N$ is the Lorentz factor. At RHIC heavy ions are collided at $\sqrt{s_{NN}} = 200$ GeV per nucleon, hence $\gamma = 100$. Using $Z = 79$ for Gold and $b \sim R_A \approx 7$ fm we estimate $eB \approx m_\pi^2 \sim 10^{18}$ G. At the LHC at $\sqrt{s_{NN}} = 5.02$ TeV and $Z = 82$ this value is even 30 times bigger. To appreciate how strong is this field, compare it with the magnetic field of a neutron star $10^{10} - 10^{13}$ G [69] or that of its slowly rotating magnetic variant, the magnetar, 10^{15} G [142]. It is very likely the strongest magnetic field in nature though existing only for a minute period of time.

Calculation with the realistic distribution of protons in a nucleus shows that magnetic field rapidly decreases as a power of time and after first 3 fm/c drops from its maximal value (4.6) by more than three orders of magnitude [143]. However, different estimates to be discussed in the next sections indicate that a strongly interacting thermalised medium is formed as early as 0.5 fm/c. Therefore, a more realistic calculation going beyond the above field in the vacuum calculation has to include response of the medium determined by its electrical conductivity. It has been found by lattice calculations [144] that the gluon contribution to the electrical conductivity of static quark-gluon plasma is

$$\sigma = (5.8 \pm 2.9) \frac{T}{T_c} \text{ MeV}. \quad (4.7)$$

This result was confirmed and further extended by more elaborate lattice simulations with 2+1 dynamical flavours for temperatures $T = (120 - 350)$ MeV [145, 146]. The calculations have shown that σT starts to deviate from zero already for $T < T_c$, i.e. in the confined phase and increases towards the QGP value (4.7) and further on. The non-zero electrical conductivity in the QGP and (probably also) in the hadronic phase when taken at its face value would inevitably lead to a substantially prolonged lifetime of the magnetic field inside the medium and might thus even influence the hadron decay widths [147].

A plethora of novel non-dissipative transport phenomena related to the interplay of quantum anomalies with the magnetic field and vorticity in systems with chiral fermions, including the QGP is reviewed in Ref. [148]. The most direct effect of magnetic field \vec{B} on the QGP is induction of electric currents carried by the charged quarks and antiquarks in the plasma and, later, by the charged hadrons. In Ref. [149] it was suggested that it may leave its imprint on the azimuthal distributions and correlations of the produced charged hadrons. Charged particles moving along the magnetic field direction y are not influenced by the magnetic Lorentz force while those moving in the xz -plane (i.e. in the reaction plane) are affected the most. The result is azimuthally anisotropic flow of expanding plasma in the xy -plane even when the initial plasma geometry is completely spherically symmetric.

Another effect is related to the chiral symmetry restoration. In such a state, within a localized region of space-time, gluon fields can generate nontrivial topological charge configurations that lead to parity violation in strong interactions [125]. In ultra-relativistic heavy-ion collisions, interactions between quarks and these gluonic states can lead to an imbalance in left- and right-handed quarks which violates parity symmetry [150]. The presence of a strong magnetic field induced by the spectator protons transforms this chirality imbalance into an electromagnetic current perpendicular to the reaction plane. This interesting phenomenon stemming from the interplay of chirality, magnetic field and the chiral anomaly is called the Chiral Magnetic Effect (CME) [148].

Several manifestations of the phenomena related to strong magnetic fields produced in Au+Au or Pb+Pb collisions have been reported by RHIC [151–153] and the LHC [154] experiments. Some doubts on prevailing interpretation were cast by the recent observation of charge-dependent azimuthal correlations also in p +Pb collisions at the LHC [155].

Moreover in the presence of elliptic flow (for its definition, see Ref. V A), practically all conventional two-particle correlations like the local charge conservation [156] may contribute to the reaction-plane dependent correlation function used to quantify the CME [157]. Obviously, more investigations are needed. The program of varying the magnetic field by a controlled amount while keeping all else fixed by using nuclear isobars (pairs of nuclei with the same mass number A but different charge Z) is now under consideration at RHIC. Most attractive isobars are Zr+Zr and Ru+Ru or some other combinations having charge differences of four like Sn¹²⁴/Xe¹²⁴, Te¹³⁰/Ba¹³⁰ and Xe¹³⁶/Ce¹³⁶ [157].

An interesting suggestion addressing the simultaneous effects of huge vorticity of nearly-perfect fluid and strong magnetic field generated in non-central heavy-ion collisions was made in Ref. [158]. The authors suggest to measure a global polarization of the final hadrons in order to estimate the thermal vorticity due to the large orbital momentum of colliding nuclei as well as the electromagnetic field developed in the plasma stage of the collision.

C. Transport models

One of the main tasks of the theory is to link experimental observables to different phases and manifestations of the QCD matter. To achieve this goal, a detailed understanding of dynamics of heavy-ion reactions is essential. This is facilitated by transport theory which helps to interpret or predict the quantitative features of heavy-ion reactions. It is particularly well suited for a non-equilibrium situation, finite size effects, non-homogeneity, N-body phase space, particle/resonance production and freeze-out as well as for collective dynamics. Microscopic [159–166], macroscopic (hydrodynamical) [167–170] or hybrid [171–173] transport models attempt to describe the full time evolution from the initial state of a heavy-ion reaction up to the freeze-out of all initial and produced particles after the reaction. This is illustrated in Fig. 9 where a comparison of the data from heavy-ion collisions to the microscopic and hydrodynamical models is presented.

The hadronic cascade models, some with mean-field interactions, have succeeded in reproducing the gross and many detailed features of the nuclear reactions measured at SIS, AGS and SPS [159, 160, 162, 163]. They have become indispensable for experimentalists who wish to identify interesting features in their data or to make predictions to plan new experiments. The main strength of the models based on superposition of pp collisions, relativistic geometry and final-state hadronic rescattering is not that it gives a precise agreement with experiment for individual observables in particular kinematic regions, but in its ability to give an overall qualitative description of a range of observables in a wide kinematic region. The price to be paid for this simplicity is to assume that either hadrons or hadron-like objects can exist at the earliest stage of the heavy-ion collision just after the two nuclei pass through each other, i.e. that the hadronization time in the frame of the particle is short and insensitive to the environment in which it finds itself. The general success of these models at lower energies can nonetheless easily lead to misconceptions at higher energies. The main concern is the relevance of these models at high particle densities which are so characteristic for collisions of heavy systems. Here, all the models based on hadronic dynamics are fundamentally inconsistent [177]. Studying how big is the fraction of the energy contained in known hadrons and that one temporarily stored in a more elusive objects, such as pre-hadronized strings, it was found [162] that up to a time of 8 fm/ c most of the energy density resides in strings and other high-mass continuum states that have not fully decayed. The physical properties of these objects are poorly known even when they occur in isolation

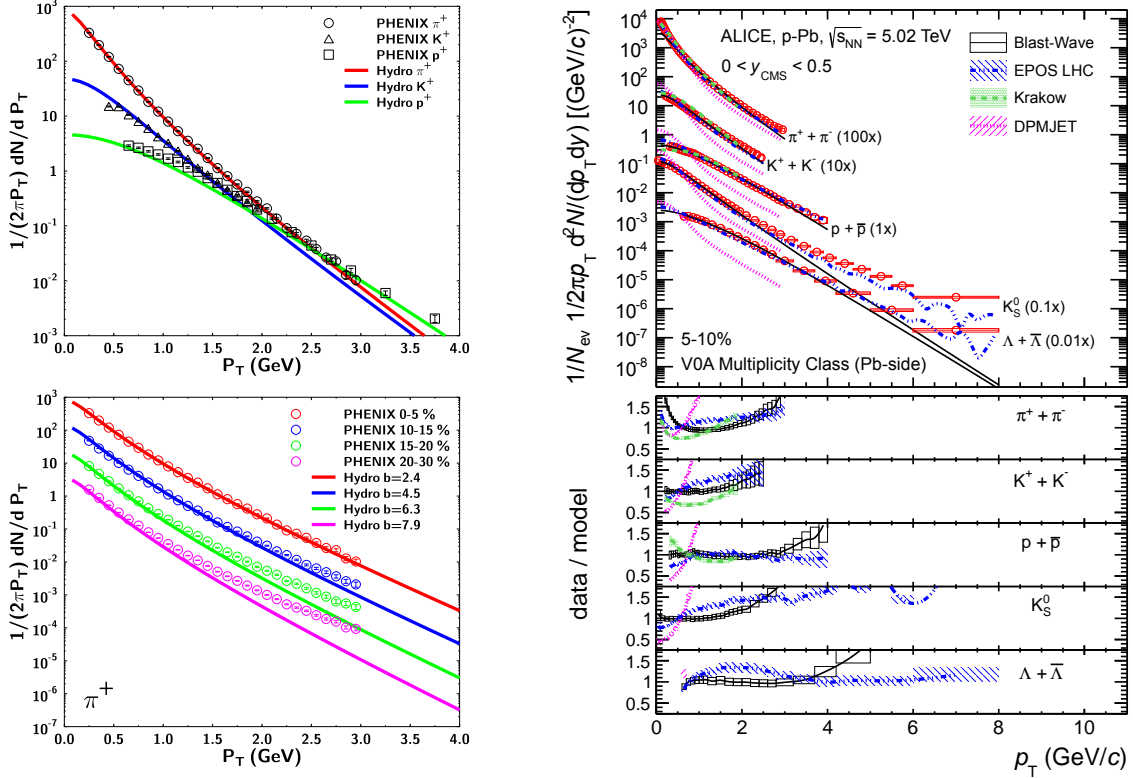


FIG. 9: Left: Transverse momentum spectra of pions, kaons, and protons emitted into the incident lead nucleus hemisphere ($0 < y_{cms} < 0.5$) in 5-10% most central p +Pb collisions at $\sqrt{s_{NN}} = 5.02$ TeV. Data (red circles) are compared to two microscopic models: EPOS LHC [166], DPMJET [165], to the hydrodynamics calculation [168] and to the Blast-Wave fit with formula Eq. (4.22). Source: reproduced from Ref. [174]. Right: Comparison of the experimental p_T -spectra of π^+ , K^+ and p^+ from Au+Au collisions at $\sqrt{s_{NN}} = 200$ GeV (top) and (for the case of π^+) of their centrality dependence (bottom) [175] with the hydrodynamical model calculations. Source: reproduced from Ref. [176].

[178], not to speak about their interactions (or even their existence) in a dense environment. The application of these models to the early phase of collision of two ultra-relativistic heavy nuclei is therefore ill-founded [177].

A complementarity between the microscopic and macroscopic descriptions becomes obvious for the case of strongly interacting plasmas. The fact that for liquids neither Boltzmann equation nor cascades can be used stems from the fact that particles are strongly correlated with several neighbours at all times. The very idea of “scattering” and cross section involves particles coming from and going to infinity: it is appropriate for dilute gases but not for condensed matter where interparticle distances do not exceed the range of the forces at any time [26].

The idea to use the laws of ideal hydrodynamics to describe the expansion of the strongly interacting matter formed in high energy hadronic collisions was first formulated by Landau in 1953 [179]. Later on, Bjorken [131] discovered a simple scaling solution that provides a natural starting point for more elaborate solutions in the ultra-relativistic domain. The phenomenological success of the Landau model was for decades a big challenge for high energy physics [180]. First, because hydrodynamics is a classical theory, second that it assumes

local equilibrium. Both these assumptions imply a large number of degrees of freedom and it is by no means clear that the highly excited, but still small systems produced in violent nuclear collisions satisfy the criteria justifying treatment in terms of a macroscopic theory [181]. Therefore, the Landau model (and other statistical models of strong interactions) were considered up to the mid-seventies as exotic approaches, outside mainstream physics [180]. Then the authors of Refs. [120, 121] realized that exploitation of hydrodynamics in an interpretation of data is the only chance of proving in laboratory the existence of a new state of matter. This is a trivial corollary of the well-known fact that a state of matter is defined by its EoS, and there is no other way to get information about the EoS than by using hydrodynamics [180–182].

1. Elements of relativistic hydrodynamics

Let us now briefly recall some of the basic results from relativistic hydrodynamics [9, 20, 22, 183] on which the contemporary models are based upon. The basic hydrodynamical equations describe the energy-momentum and the current conservation

$$\partial_\mu T^{\mu\nu}=0, \quad \partial_\mu j_i^\mu=0, \quad (4.8)$$

where $j_i^\mu, i=B,S,Q$ is the conserved current. Both quantities can be decomposed into time-like and space-like components using natural projection operators, the local flow four-velocity u^μ and the second-rank tensor perpendicular to it $\Delta^{\mu\nu}=g^{\mu\nu}-u^\mu u^\nu$:

$$T^{\mu\nu} = \epsilon u^\mu u^\nu - p \Delta^{\mu\nu} + W^\mu u^\nu + W^\nu u^\mu + \pi^{\mu\nu}, \quad (4.9)$$

$$j_i^\mu = n_i u^\mu + V_i^\mu, \quad (4.10)$$

where $\epsilon=u_\mu T^{\mu\nu} u_\nu$ is the energy density, $p=p_s+\Pi=-\frac{1}{3}\Delta_{\mu\nu}T^{\mu\nu}$ is the hydrostatic + bulk pressure, $W^\mu=\Delta^\mu_\alpha T^{\alpha\beta}u_\beta$ is the energy (or heat) current, $n_i=u_\mu j_i^\mu$ is the charge density, $V_i^\mu=\Delta^\mu_\nu j_i^\nu$ is the charge current and $\pi^{\mu\nu}=\langle T^{\mu\nu} \rangle$ is the shear stress tensor. The angular brackets in the definition of the shear stress tensor $\pi^{\mu\nu}$ stand for the following operation,

$$\langle A^{\mu\nu} \rangle = \left[\frac{1}{2}(\Delta^\mu_\alpha \Delta^\nu_\beta + \Delta^\mu_\beta \Delta^\nu_\alpha) - \frac{1}{3} \Delta^{\mu\nu} \Delta_{\alpha\beta} \right] A^{\alpha\beta}. \quad (4.11)$$

To further simplify our discussion we restrict ourselves in the following to the one conserved charge only and denote the corresponding baryon current as $j^\mu=j_B^\mu$. The various terms appearing in the decompositions (4.9) and (4.10) can then be grouped into ideal and dissipative parts

$$T^{\mu\nu} = T_{id}^{\mu\nu} + T_{dis}^{\mu\nu} = [\epsilon u^\mu u^\nu - p_s \Delta^{\mu\nu}]_{id} + [-\Pi \Delta^{\mu\nu} + W^\mu u^\nu + W^\nu u^\mu + \pi^{\mu\nu}]_{dis} \quad (4.12)$$

$$j^\mu = j_{id}^\mu + N_{dis}^\mu = [n u^\mu]_{id} + [V^\mu]_{dis}. \quad (4.13)$$

Neglecting the dissipative parts, the energy-momentum conservation and the current conservation (4.8) define *ideal hydrodynamics*. In this case (and for a single conserved charge) a solution of the hydrodynamical equations (4.8) for a given initial condition describes the space-time evolution of the six variables – three state variables $\epsilon(x)$, $p(x)$, $n(x)$ and three space components of the flow velocity u^μ . However, since (4.8) constitute only five independent equations the sixth equation relating p and ϵ , the EoS, has to be added by hand to solve

them. For this one can either use the relativistic non-interacting massless gas EoS or its generalization to the case of a non-zero interacting measure $\Theta^{\mu\mu}(T)=\epsilon-3p$. In addition to many different phenomenological parametrizations of $\Theta^{\mu\mu}$ one can exploit the relation (3.20) to obtain the EoS directly from the lattice QCD simulations. The examples of this approach were given in section III C 1, see particularly Eqs. (3.24) and (3.25) and are illustrated on Fig. 5.

Two definitions of flow can be found in the literature [9, 20, 183], one related to the flow of energy (Landau) [179] reads

$$u_L^\mu = \frac{T^\mu{}_\nu u_L^\nu}{\sqrt{u_L^\alpha T_\alpha{}^\beta T_{\beta\gamma} u_L^\gamma}} = \frac{1}{e} T^\mu{}_\nu u_L^\nu, \quad (4.14)$$

while the other – to the flow of conserved charge (Eckart) [184] as follows

$$u_E^\mu = \frac{j^\mu}{\sqrt{j_\nu j^\nu}}. \quad (4.15)$$

Let us note that, $W^\mu=0$ ($V^\mu=0$) in the Landau (Eckart) frame. In the case of vanishing dissipative currents, both definitions represent a common flow. In ultra-relativistic heavy-ion collisions the Landau definition is more suitable when describing the evolution of matter in the region with a small baryon number deposition (i.e. when $j=j_B=0$) like the mid-rapidity region at the LHC and RHIC, see Fig. 1.

In order to solve the hydrodynamic equations with the dissipative terms it is customary to introduce the following two phenomenological definitions, so-called *constitutive equations*, for the shear stress tensor $\pi^{\mu\nu}$ and the bulk pressure Π [183],

$$\pi^{\mu\nu} = 2\eta \langle \nabla^\mu u^\nu \rangle, \quad \Pi = -\zeta \partial_\mu u^\mu = -\zeta \nabla_\mu u^\mu, \quad (4.16)$$

where the coefficients η and ζ are called the *shear viscosity* and *bulk viscosity*, respectively.

For the boost-invariant Bjorken flow [131] which is also called the one-dimensional Hubble flow since velocity in the z direction, v_z , is proportional to z

$$u_{\text{BJ}}^\mu = \frac{x^\mu}{\tau} = \frac{t}{\tau} \left(1, 0, 0, \frac{z}{t} \right), \quad (4.17)$$

where $\tau = \sqrt{t^2 - z^2}$ is the proper time, one obtains the following equation of motion [183]:

$$\frac{d\epsilon}{d\tau} = -\frac{\epsilon + p_s}{\tau} \left(1 - \frac{4}{3\tau T} \frac{\eta}{s} - \frac{1}{\tau T} \frac{\zeta}{s} \right). \quad (4.18)$$

Neglecting the last two terms in Eq. (4.18) one obtains the famous Bjorken solution of ideal hydrodynamics [131]. The last two terms on the r.h.s. in Eq. (4.18) describe a compression of the energy density due to viscous corrections. The first one is due to the shear viscosity in compressible fluids, while the second one comes from the bulk viscosity. Two dimensionless coefficients in the viscous correction, η/s and ζ/s , reflect the intrinsic properties of the fluids, see Table I and Fig. 15 (left panel). The value $\eta/s=1/4\pi$ has been obtained in the framework of $\mathcal{N}=4$ SUSY Yang-Mills theory [107]. The conformal nature of this theory gives $\zeta/s=0$ automatically. Moreover, $\eta/s=\mathcal{O}(0.1-1)$ for gluonic matter is obtained from the lattice calculations of pure $SU(3)$ gauge theory [185] while the bulk viscosity ζ has a prominent peak around T_c resulting from the trace anomaly of QCD [186].

2. Blast wave parametrization

Interpretation of the results of hydrodynamical calculations or of the experimental data in terms of the collective flow of matter [86, 187] is greatly facilitated by the use of the analytical, so called *Blast wave* (BW) parametrization [188–190]. Within the boost-invariant scenario of Bjorken [131] and for the full azimuthal symmetry which is valid in central collisions of two nuclei, the velocity field of expanding matter is given by

$$u^\mu(\rho,\eta)=(\cosh\rho \cosh\eta, \vec{e}_r \sinh\rho, \cosh\rho \sinh\eta), \quad (4.19)$$

where $\rho=\tanh^{-1}\beta_T$ and η are transverse and longitudinal rapidities, respectively, and \vec{e}_r is the unit vector in the transverse plane. The transverse velocity distribution $\beta_T(r)$ of the thermalized matter in the region $0\leq r\leq R$ is described by a self-similar profile

$$\beta_T(r)=\beta_s\left(\frac{r}{R}\right)^k, \quad (4.20)$$

where β_s is the surface velocity and parameter k is usually given the value $k=2$ to resemble the solutions of hydrodynamics [189]. The spectrum of locally thermalized matter is constructed as a superposition of the individual thermal components [191]:

$$E\frac{d^3N}{d^3p}=\frac{g}{(2\pi)^3}\int e^{-(u^\nu p_\nu-\mu)/T_{kin}}p^\lambda d\sigma_\lambda, \quad (4.21)$$

where σ is the hypersurface defining a borderline between the hydrodynamical behaviour and free-streaming particles, the so-called *freeze-out hypersurface* and T_{kin} is the *temperature of the kinetic freeze-out*. Boosting each component with the transverse rapidity $\rho=\tanh^{-1}\beta_T$ one obtains the transverse momentum spectra of particles from the collective radial flow of expanding matter:

$$\frac{dN}{p_T dp_T}\propto\int_0^R r dr m_T I_0\left(\frac{p_T \sinh\rho}{T}\right) K_1\left(\frac{m_T \cosh\rho}{T}\right), \quad (4.22)$$

where $m_T=\sqrt{(m^2+p_T^2)}$ and $I_0(x)$ and $K_1(x)$ are the Bessel functions.

Formulas for the case of non-central collisions when the transverse shape (4.20) is controlled not by the one but the two parameters R_x and R_y can be found in Ref. [190]. In full generality there are eight parameters describing the blast wave parametrization: $T, \rho_0, \rho_2, R_x, R_y, a_s, \tau_0$ and $\Delta\tau$. Here, T is the temperature, ρ_0 and ρ_2 describe the strength of the zero- and second-order oscillation of the transverse rapidity, the parameter a_s corresponds to a surface diffuseness of the emission source and τ_0 and $\Delta\tau$ are the mean and width of a Gaussian longitudinal proper time $\tau=\sqrt{t^2-z^2}$ freeze-out distribution.

On Figs. 9 and 10 the examples of the BW fit analysis are presented. As can be seen from Fig. 10 the kinetic freeze-out temperature T_{kin} which determines the shape of the p_T -spectra of particles is strongly anti-correlated with the radial flow velocity $\langle\beta\rangle$: higher is the T_{kin} lower is the $\langle\beta\rangle$ and vice versa. Nevertheless, the radial flow reveals itself as a shoulder structure at small transverse momenta in the p_T -spectra of Λ s, protons and kaons, see Figs. 9. For the pions, there is almost no sensitivity to distinguish between the two cases – a reduction of temperature is almost compensated by the radial flow.

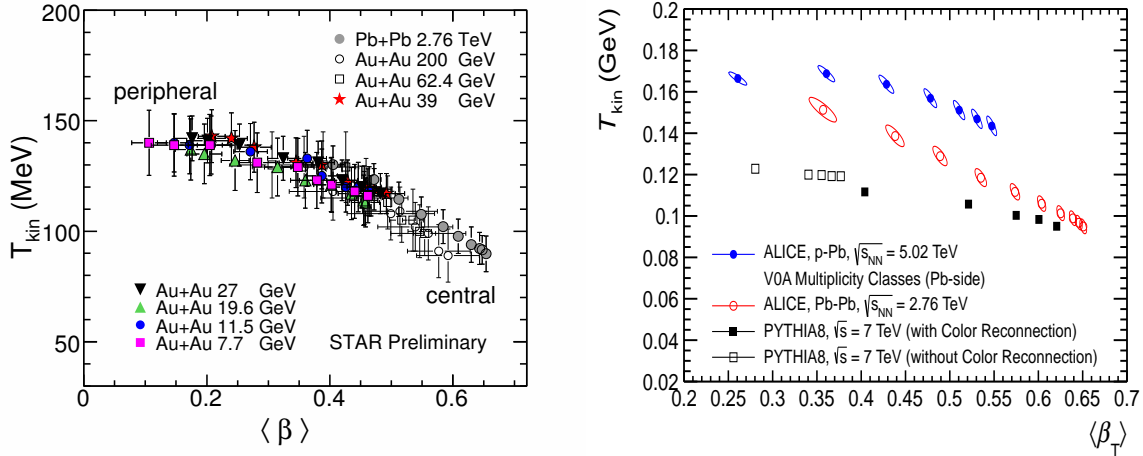


FIG. 10: Left: Variation of the blast wave parameters T_{kin} and $\langle\beta\rangle$ obtained from the fits to the spectra of pions, kaons, protons and their anti-particles produced in Au+Au and Pb+Pb collisions at energies $\sqrt{s_{NN}} = 7.7$ GeV – 2.76 TeV and different collision centralities. The centrality increases from left to right for a given energy. Source: reproduced from Ref. [192]. Right: The same but for Pb+Pb at $\sqrt{s_{NN}} = 2.76$ TeV and p+Pb at $\sqrt{s_{NN}} = 5.02$ TeV. MC simulations of p+p collisions at $\sqrt{s} = 7$ TeV using the PYTHIA8 event generator [193] with and without color reconnection are shown as open and filled squares, respectively. Source: reproduced from Ref. [174].

D. Initial state description of nuclear and hadronic interactions

An indispensable part of the full description of the experimental data from heavy-ion collisions comes not only from the understanding of its dynamics starting from the moment of thermalization but also at earlier times. In particular, the question of where the observed (local) thermalization of deconfined matter comes from is still quite open [194–197]. The importance of event-by-event initial state fluctuations on anisotropic collective flow and other final state observables is also worth mentioning [198–201]. Since these topics currently remain a significant source of uncertainty in predicting the final state observables we will in the next two paragraphs provide two alternative ways how to describe the initial state of the collision.

1. Glauber model

In high-energy nucleus-nucleus (A+B) interactions the de Broglie wavelength of the nucleons (N) of the incoming nucleus is much smaller than the inter-nucleon distances inside the partner nucleus. To each incoming nucleon the positions of the nucleons within the partner nucleus appear to be frozen. After a single elementary NN (elastic or inelastic) collision both participating nucleons acquire a transverse momentum which is in the majority of cases very small compared to their longitudinal one and so the longitudinal momenta before and after the collision are very close to each other $p_z \approx p_{z'}$. High incident energies and small scattering angles mean that the scattering is dominated by a large orbital momentum ℓ and so it is convenient to replace the partial-wave expansion of the scattering amplitude by

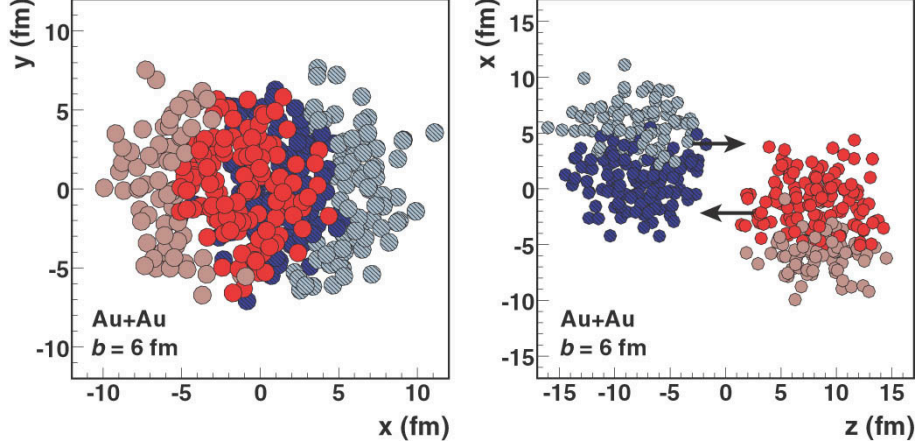


FIG. 11: A Glauber Monte-Carlo event (Au+Au at $\sqrt{s_{NN}} = 200$ GeV) viewed in the transverse plane (left panel) and along the beam axis (right panel). The nucleons are drawn with diameter $\sqrt{\sigma_{NN}^{in}}/\pi$. Darker disks represent the participants, lighter disks – the spectators. Source: reproduced from Ref. [202].

an impact parameter $b=(1+\ell)/p$ representation. The A+B collision can thus be described using a semi-classical approach due to Glauber [203–206] which treats the nuclear collision as multiple NN interactions [207, 208]. The nucleons which have suffered at least one NN collision are called the *participants*, those who have avoided it are called the *spectators*, see Fig. 11. The total number of spectators and participants thus adds up to $N_{\text{spec}}+N_{\text{part}}=A+B$. On the other hand, the total number of collisions suffered by all participants fulfils inequality $N_{\text{coll}} \geq N_{\text{part}}/2$.

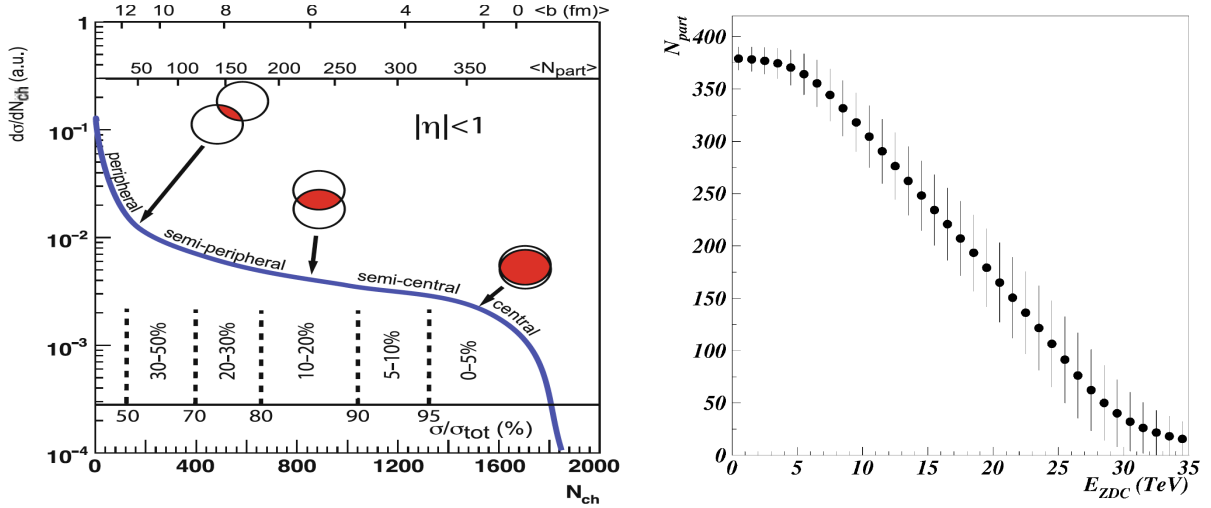


FIG. 12: Left: A cartoon showing the centrality definition from the final-state charged particle multiplicity N_{ch} and its correlation with the average impact parameter $\langle b \rangle$ and the mean number of nucleons participating in the collision $\langle N_{\text{part}} \rangle$. Source: reproduced from Ref. [27]. Right: The number of participants N_{part} as a function E_{ZDC} in Pb+Pb collision at incident momentum per nucleon 158 GeV/c ($\sqrt{s_{NN}} = 17.3$ GeV) calculated in the Glauber approach. Source: reproduced from Ref. [209]. The error bars represent the r.m.s. of the N_{part} distribution at fixed E_{ZDC} .

Using the nuclear mass number density $\int dz d^2\mathbf{s} \rho_{A,B}(z,\mathbf{s}) = A,B$ and the inelastic NN cross section σ_{NN}^{in} , we can express N_{part} and N_{coll} analytically [9, 22, 28, 202]:

$$N_{\text{part}}(b) = \int d^2\mathbf{s} T_A(\mathbf{s}) \left(1 - e^{-\sigma_{NN}^{in} T_B(\mathbf{s})}\right) + \int d^2\mathbf{s} T_B(\mathbf{s}-\mathbf{b}) \left(1 - e^{-\sigma_{NN}^{in} T_A(\mathbf{s})}\right) \quad (4.23)$$

$$N_{\text{coll}}(b) = \int d^2\mathbf{s} \sigma_{NN}^{in} T_A(\mathbf{s}) T_B(\mathbf{b}-\mathbf{s}) \equiv \sigma_{NN}^{in} T_{AB}(\mathbf{b}), \quad (4.24)$$

where $T_A(\mathbf{b})$ and $T_{AB}(\mathbf{b})$ are the nuclear thickness and the nuclear overlap functions, respectively:

$$T_A(\mathbf{b}) \equiv \int dz \rho_A(z,\mathbf{s}), \quad T_{AB}(\mathbf{b}) \equiv \int d^2\mathbf{s} T_A(\mathbf{s}) T_B(\mathbf{b}-\mathbf{s}). \quad (4.25)$$

The Glauber model calculations are also often carried out via Monte Carlo [202, 210, 211]. Nucleons inside the colliding nuclei are distributed randomly according to a nuclear density profile. At a given impact parameter, \mathbf{b} the impact parameter \mathbf{s} of all the pairs of nucleons is calculated. Interaction occurs when $\pi s^2 < \sigma_{NN}^{in}$, see Fig. 11. The calculated $N_{\text{part}}(b)$ and $N_{\text{coll}}(b)$ are then used to make a contact with the measured bulk observables like the multiplicity of charged particles N_{ch} measured by the tracking detectors at midrapidity, Fig. 12 (left panel), or the energy left by the spectator nucleons in the Zero Degree Calorimeter E_{ZDC} , Fig. 12 (right panel). The left panel also explains how different bins in multiplicity of charged particles N_{ch} can be transformed into the bins in collision centrality. The left panel of Fig. 13 illustrates that even for quite different nuclear systems (Au+Au, Cu+Au, Cu+Cu) the number of participants N_{part} selects the collisions with almost the same energy density ε_{BJ} . The right panel of Fig. 13 shows that centrality dependence of the yields of EW-interacting particles (like direct photons, W^\pm or Z -bosons) is completely determined by the N_{coll} .

A generalisation of the Glauber model beyond its original non-relativistic potential description of the scattering process was first formulated by Gribov [213, 214] who used the effective field theory to describe multiple interactions proceeding via the Pomeron exchange. The interference terms appearing naturally in this treatment of multiple scattering assure automatically the unitarity of the theory [215]. With the advent of the QCD the parton-based multiple scattering models became popular [216–220]. Such models allow to treat A+B and NN collisions on more equal footing. Their participants could thus be not only nucleons but also the pQCD partons, the valence quarks [216, 221] or any effective sub-nucleon degrees of freedom [222].

2. Color Glass Condensate

In addition to the sQGP matter, another instance where quarks and gluons can not be treated as independent degrees of freedom is a case of parton coherence. A generalization of pQCD to hard collisions of small- x ($x \ll 1$) partons (called also a *semi-hard regime*) was first discussed by Gribov, Levin and Ryskin [223]. The basic failure of the standard DGLAP approach [224–226] is that it predicts too fast increase of small- x parton density with the scale Q^2 . Consequently, the growth of hadronic cross sections proceeds at rate which would sooner or later violate unitarity. The proposed solution – parton recombination and saturation – is at variance with the standard assumption that the partons themselves can be considered

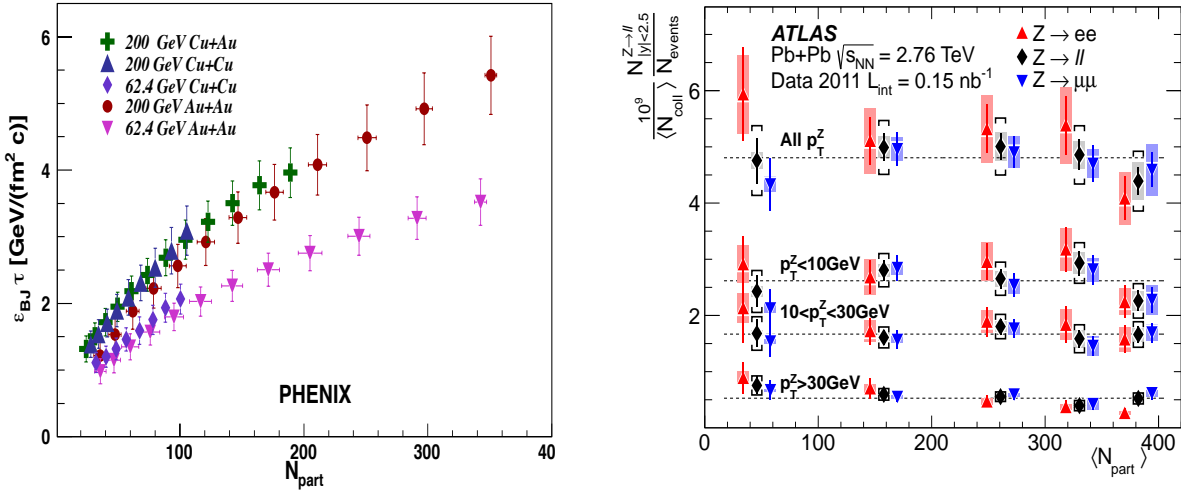


FIG. 13: Left: The Bjorken estimate of the initial energy density ε_{BJ} (Eq. (4.1)) multiplied by the thermalization time τ as a function of N_{part} for different colliding systems (Au+Au, Cu+Au, Cu+Cu) at two energies ($\sqrt{s_{NN}} = 62.4$ and 200 GeV). Source: reproduced from Ref. [128]. Right: The dependence of Z boson yields divided by average number of collisions $\langle N_{\text{coll}} \rangle$ on the average number of participants $\langle N_{\text{part}} \rangle$ for Pb+Pb collisions at $\sqrt{s_{NN}} = 2.76$ TeV. Source: reproduced from Ref. [212].

as independent free particles. The parameter determining the probability of parton-parton recombination is the ratio of the parton-parton cross section to the square of the average distance between partons. The fact that the cross section of such semi-hard process (which now complies with the unitarity) increases rapidly with incident energy gives rise to expectations that (at least, asymptotically) bulk particle production in hadron-hadron collisions can be described via pQCD [18].

The modern implementation of the above ideas is the Color Glass Condensate (CGC) formalism [227–230] – a natural generalization of pQCD to dense partonic systems. When applied to heavy nuclei it predicts strong color fields in the initial stage of the collision. The strength of the fields is due to condensation of low- x gluons into single macroscopic (i.e. classical) field state called the CGC. Since characteristic scale of the parton saturation grows as $Q_s \propto A^{1/3}$ [18, 228] it is enhanced on nuclear targets. According to the CGC motivated phenomenology the saturation phenomena are expected to show up, if not already, in $p(d)+\text{Au}$ collisions at RHIC and, for sure, in nuclear collisions at the LHC. For example, due to the gluon saturation, the growth of the inelastic nucleon-nucleon cross section σ_{NN}^{in} with increasing collision energy \sqrt{s} may result in a broadening of the nucleon density distribution in position space. This in turn leads to a natural smoothing of the initial energy density distribution in the transverse plane of the matter created near midrapidity in heavy-ion collisions [200].

The CGC is described by an effective field theory that separates two kinds of degrees of freedom – fast frozen color sources and slow dynamical color fields. The basic evolution equation of such an effective field theory is a RG equation known as the Jalilian-Marian–Iancu–McLerran–Weigert–Leonidov–Kovner (JIMWLK) equation [231–236] which reflects the independence of physical quantities with respect to variations of the cutoff separating

these degrees of freedom (for more details, see Ref. [229] and references therein).

A supporting argument for the CGC as a possible state of QCD matter comes from successful analysis of HERA data in terms of Geometrical Scaling (GS) [237]. The GS is the statement that the total γ^*p cross section depending a priori on two independent variables – the photon virtuality Q^2 and the Bjorken variable x – is a function of a single variable $\tau=Q^2/Q_s^2$, where the so-called saturation scale Q_s^2 depends nontrivially on x , with dimensions given by a fixed reference scale Q_0^2 . However, calculations of Ref. [238] shows that the standard linear leading-order DGLAP perturbative evolution is able to explain the geometric scaling. The situation with CGC applicability at current energies is thus unsettled (see also Refs. [239, 240]). The experimental data from RHIC and the LHC as well as exploitation of non-CGC based models [221] are needed to resolve this problem.

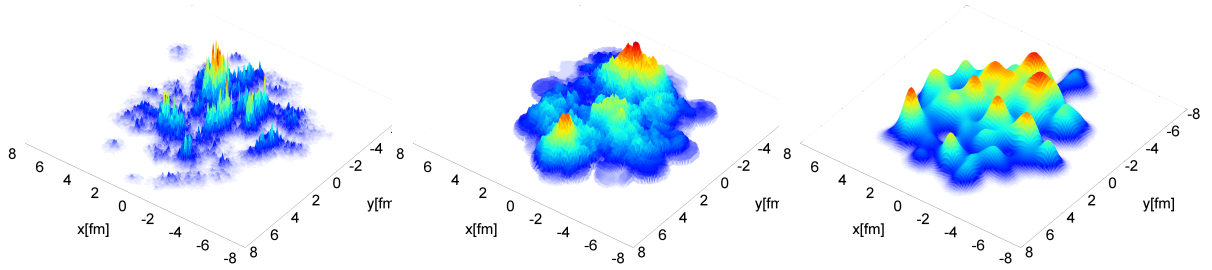


FIG. 14: Examples of the initial energy density distribution from the IP-Glasma model at $\tau=0$ fm (left), the MC-KLN model (middle) and the MC-Glauber model (right). Source: reproduced from Ref. [241].

There are two popular representative models of the initial state which are based on the CGC – the KLN model [242] and the IP Glasma model [241]. A Monte Carlo implementation of KLN CGC initial state [172, 200, 243] is based on the number distribution of gluons produced in transverse plane given by the k_T -factorisation formula [242] :

$$\begin{aligned} \frac{dN_g}{d^2r_\perp dy} &= \kappa \frac{4N_c}{N_c^2-1} \int \frac{d^2p_\perp}{p_\perp^2} \int \frac{d^2k_\perp}{4} \alpha_s(Q^2) \\ &\times \phi_A(x_1, (\mathbf{p}_\perp + \mathbf{k}_\perp)^2/4) \phi_B(x_2, (\mathbf{p}_\perp - \mathbf{k}_\perp)^2/4) . \end{aligned} \quad (4.26)$$

Here, p_\perp and y denote the transverse momentum and rapidity of the produced gluons and $x_{1,2}=p_\perp \exp(\pm y)/\sqrt{s_{NN}}$ are the light-cone momentum fractions of the colliding gluons. The running coupling $\alpha_s(Q^2)$ is evaluated at the scale $Q^2=\max((\mathbf{p}_\perp - \mathbf{k}_\perp)^2/4, (\mathbf{p}_\perp + \mathbf{k}_\perp)^2/4)$. The gluon distribution function is given by

$$\phi_A(x, k_\perp^2; \mathbf{r}_\perp) \sim \frac{1}{\alpha_s(Q_{s,A}^2)} \frac{Q_{s,A}^2}{\max(Q_{s,A}^2, k_\perp^2)} . \quad (4.27)$$

An overall normalisation factor κ is chosen to fit the multiplicity data in most central Au+Au collisions at RHIC. In the MC-KLN model [242], the saturation momentum is parameterised by assuming that the saturation momentum squared is 2 GeV² at $x=0.01$ in Au+Au collisions at $b=0$ fm at RHIC where $\rho_{\text{part}}=3.06$ fm⁻², i.e.

$$Q_{s,A}^2(x; \mathbf{r}_\perp) = 2 \text{ GeV}^2 \frac{\rho_A(\mathbf{r}_\perp)}{1.53 \text{ fm}^{-2}} \left(\frac{0.01}{x} \right)^\lambda . \quad (4.28)$$

Here, λ is a free parameter which is expected to be in the range of $0.2 < \lambda < 0.3$ from the global analysis of $e+p$ scattering for $x < 0.01$ [237, 244].

The IP-Glasma model [241] solves the classical Yang-Mills equations in which initial charge distributions of two colliding nuclei are sampled from a Gaussian distribution with the impact parameter and Bjorken x dependent color charge distributions. A parameterisation of x and impact parameter dependence of the saturation scale is taken from the IP-Sat (Impact Parameter Saturation) model [245, 246]. Fluctuations in the IP-Glasma model have a length scale of the order of the inverse of the saturation scale $Q_s^{-1}(\mathbf{x}_\perp) \sim 0.1-0.2$ fm. A comparison of the initial energy density distribution among the IP-Glasma, MC-KLN and MC-Glauber models is shown in Fig. 14.

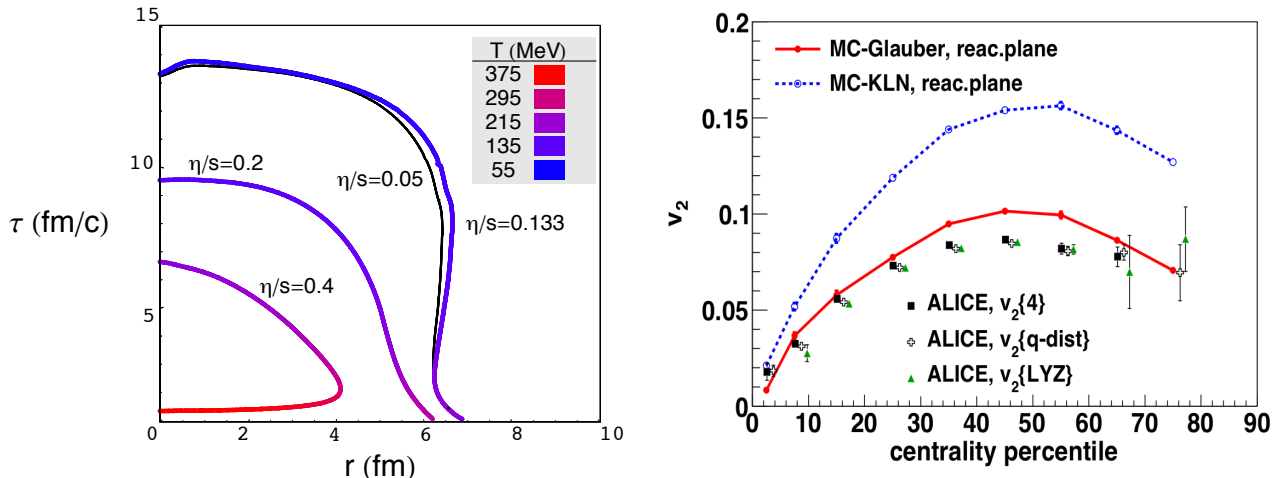


FIG. 15: Left: Location of freeze-out surfaces for central Au+Au collisions [102]. Right: The centrality dependence of the elliptic flow of charged hadrons from Pb-Pb collisions at $\sqrt{s_{NN}} = 2.76$ TeV [247]. The ALICE data are from Ref. [248].

Fig. 15 provides two examples of transport model calculations. The left panel shows location of freeze-out surfaces for central Au+Au collisions at several fixed values of the shear viscosity to entropy density ratio η/s obtained from a numerical solution of viscous hydrodynamics [102]. The shading corresponds to the freeze-out temperature. The freeze-out occurs when the viscous terms become large compared to the ideal terms. Note that hydrodynamics breaks down not only at late but also at early times (see the curve $\eta/s=0.4$ in Fig. 15). The right panel displays the centrality dependence of the elliptic flow coefficient v_2 (Eq. (5.1)) for two models for the initial density in the transverse plane – the one is motivated by the parton saturation (CGC) and the other exploits nucleons only (Glauber). The calculations [247] were done within a hybrid model where the expansion of the QGP starting at $\tau_0=0.6$ fm/c is described by ideal hydrodynamics with a state-of-the-art lattice QCD EoS, and the subsequent evolution of hadronic matter below switching temperature $T_{sw} = 155$ MeV is described using a hadronic cascade model. This nicely illustrates the strength of hydrodynamics – either the viscosity of QGP from RHIC to the LHC increases or the CGC initial condition is ruled out [247].

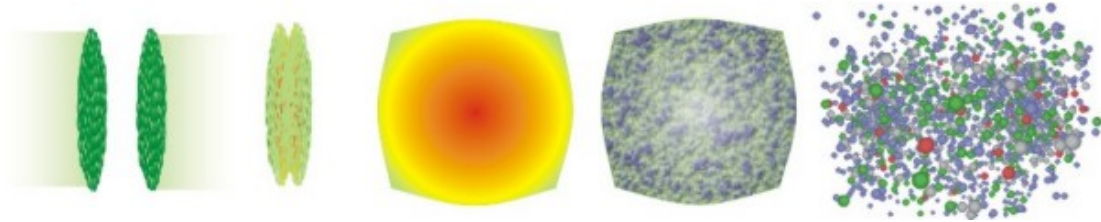


FIG. 16: Cartoon of a collision of two ultra-relativistic nuclei. Left to right: the two nuclei approach, collide, form a hot and dense equilibrated system, QGP expands and hadronizes, finally hadrons rescatter and freeze out. The figure is taken from Ref. [249].

V. EXPERIMENTAL SIGNATURES OF DECONFINED QCD MATTER

Evolution of the high energy nucleus-nucleus collision is schematically depicted on Fig. 16. Two Lorentz-contracted pancakes of nuclear matter collide, thermalize and form a deconfined QGP medium which expands, cools down and hadronise to final state hadrons. Experimentally we do not observe each stage separately but only through the time integrated final state quantities – the momentum spectra of hadrons, photons or leptons, particle multiplicities, energy flow *etc.* Nevertheless some time ordering of different processes giving rise to the final state observables exists. At very early collision times when colliding matter thermalizes the entropy is produced which later, after (almost) isotropic expansion transforms into particle multiplicities [28, 179, 198]. Early collision times also favour production of high p_T partons [29, 250] or heavy quarks (c , b) [251]. The formation of QGP reveals itself in many ways including radiation of low momentum direct or virtual photons serving as a thermometers, enhanced production of hadrons containing strange (s) quarks [21, 252, 253] and melting of $c\bar{c}$ or $b\bar{b}$ mesons [114, 115, 251] called quarkonia. The subsequent rapid expansion of deconfined matter having more than ten times degrees of freedom than the hadronic matter (see Eq. (3.22)), and therefore also much higher internal pressure, produces a strong radial flow which leaves its imprint on the spectra of final state particles and their yields [28, 181, 198, 254, 255].

In the following we present several examples of observables related to different stages of dynamics of nucleus-nucleus collisions at high-energies.

A. Bulk observables

Traditionally, the very first measurements of heavy-ion collisions at a new energy regime comprise the charged-particle density at midrapidity $dN_{\text{ch}}/d\eta|_{\eta=0}$, including also its centrality dependence. Its collision-energy dependence for the 5% (6%) most central heavy-ion collisions, normalized per participant pair (i.e. $\langle N_{\text{part}} \rangle / 2$), is presented in Fig. 17 (left panel). The right panel of Fig. 17 shows that the normalized charged-particle density is rising with centrality which means that the particle multiplicity at mid-rapidity increases faster than N_{part} , presumably due to the contribution of hard processes to the particle production [29]. However, this increase is very similar to that observed at the top RHIC energy.

One of the most celebrated prediction of collective behaviour of matter created in non-central collisions of ultra-relativistic nuclei concerns its evolution in the transverse plane which results from the pressure gradients due to spatial anisotropy of the initial density

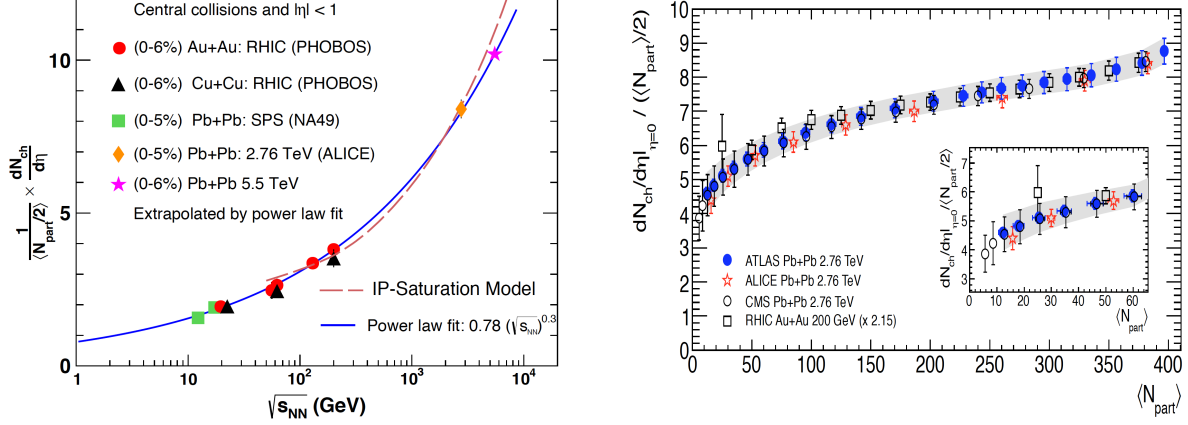


FIG. 17: Left: The charged particle rapidity density per participating pair, $dN_{\text{ch}}/d\eta/(0.5N_{\text{part}})$, in central Au+Au, Cu+Cu and Pb+Pb collisions from SPS to LHC energies. The star denotes an extrapolation to Pb+Pb collisions at 5.5 TeV. The IP-saturation model calculation [256] is illustrated by a dashed curve. Source: adapted from Ref. [30]. Right: $dN_{\text{ch}}/d\eta/(0.5N_{\text{part}})$ vs. $\langle N_{\text{part}} \rangle$ in Pb+Pb and Au+Au collisions at the LHC and RHIC, respectively. The RHIC data are multiplied by 2.15. The inset shows the $\langle N_{\text{part}} \rangle < 60$ region in more detail. Source: reproduced from Ref. [257].

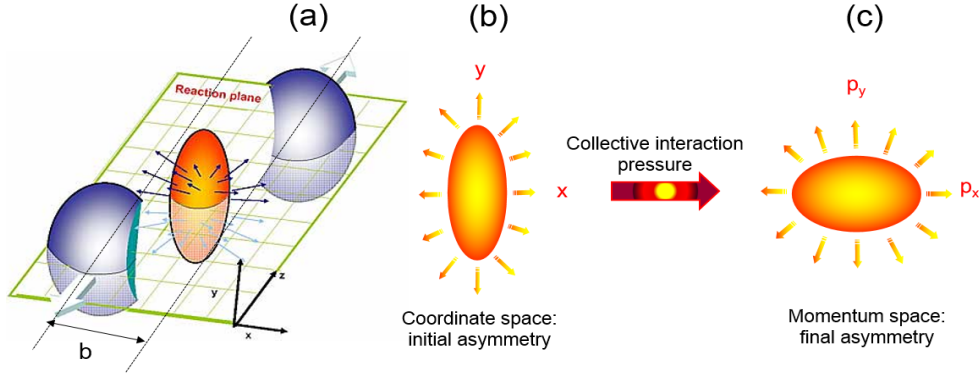


FIG. 18: A non-central collision of two nuclei leads to an almond shaped interaction volume (a). This initial spatial anisotropy with respect to the reaction plane (b) translates via pressure gradients into a momentum anisotropy (c) of the produced particles. Source: reproduced from Ref. [30].

profile [181, 258], see Fig. 18. The azimuthal anisotropy is usually quantified by the Fourier coefficients [259]:

$$v_n = \langle \cos[n(\phi - \Psi_n)] \rangle, \quad (5.1)$$

where ϕ is the azimuthal angle of the particle, Ψ_n is the angle of the initial state spatial plane of symmetry, and n is the order of the harmonic. In a non-central heavy ion collision the beam axis and the impact parameter define the reaction plane azimuth Ψ_{RP} . For a smooth matter distribution in the colliding nuclei, the plane of symmetry is the reaction plane $\Psi_n = \Psi_{\text{RP}}$ and the odd Fourier coefficients are zero by symmetry. However due to fluctuations in the matter distribution, including contributions from fluctuations in the positions of the participating nucleons in the nuclei (see Fig. 11), the plane of symmetry

fluctuates event-by-event around the reaction plane. This plane of symmetry is determined by the participating nucleons and is therefore called the participant plane Ψ_{PP} [260]. Since the planes of symmetry Ψ_n are not known experimentally, the anisotropic flow coefficients are estimated from measured correlations between the observed particles [248, 261].

In the following we shall restrict ourselves to the properties of the Fourier coefficients v_n with $n = 2$ and $n = 3$ which provide the dominant contributions to the observed azimuthal *elliptic* and *triangular* asymmetry, respectively. The sensitivity of v_2 to initial condition is illustrated on Fig. 15 (right panel) where the centrality dependence of the elliptic flow in Pb+Pb collisions at $\sqrt{s_{NN}} = 2.76$ TeV is shown. For more details on the corresponding initial state models, see section IV D 2.

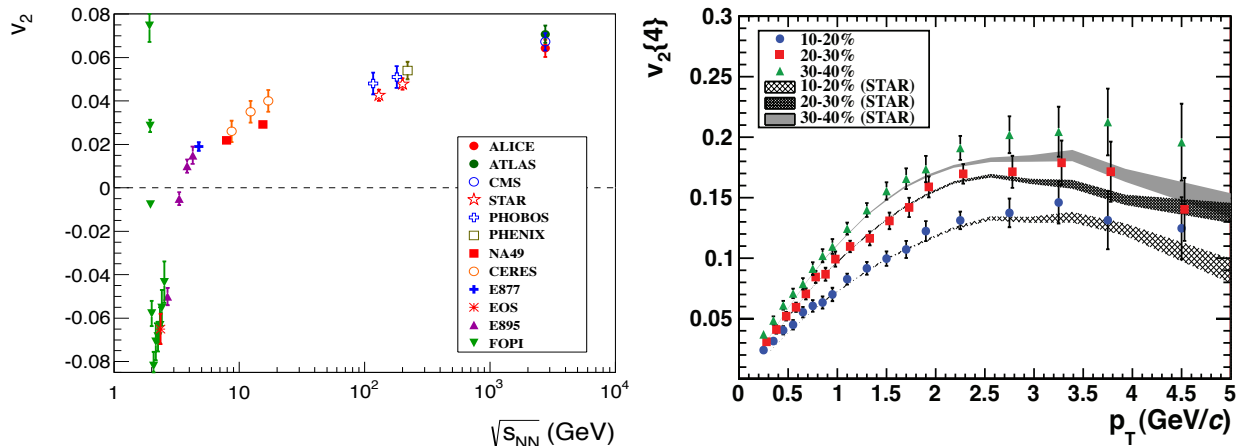


FIG. 19: Left: A compilation of data on the dependence of the integrated elliptic flow, v_2 , on the beam energy. The data correspond to (~ 20 – 30%) Au+Au or Pb+Pb most central collisions. Source: reproduced from Ref. [262]. Right: The differential elliptic flow of charged particles. The Pb+Pb collisions at $\sqrt{s_{NN}} = 2.76$ TeV (colored symbols) are compared to Au+Au collisions at $\sqrt{s_{NN}} = 200$ GeV (grey lines). Source: reproduced from Ref. [248].

Left panel of Fig. 19 shows the measured energy dependence of the integrated elliptic flow coefficient v_2 in one centrality bin. Starting from $\sqrt{s_{NN}} \approx 5$ GeV there is a continuous increase of v_2 . Below this energy two phenomena occur. At very low energies, due to the rotation of the compound system generated in the collision, the emission is in-plane ($v_2 > 0$). At the laboratory kinetic energy around 100 MeV/nucleon, the preferred emission turns into out-of-plane and v_2 becomes negative. The slowly moving spectator matter prevents the in-plane emission of participating nucleons or produced pions which appear to be squeezed-out of the reaction zone [263]. As the spectators move faster their shadowing disappears changing the pattern back to the in-plane emission.

Let us note that at RHIC for the first time the magnitude of the elliptic flow (Fig. 19) was found to be consistent with the EoS expected from the QGP [16, 181]. The integrated value of v_2 for the produced particles increases by 70% from the top SPS energy to the top RHIC energy (see left panel of Fig. 19), and it appears to do so smoothly. In comparison to the elliptic flow measurements in Au+Au collisions at $\sqrt{s_{NN}} = 200$ GeV, at the LHC v_2 increases by about 30% at $\sqrt{s_{NN}} = 2.76$ TeV. This increase is however not seen in the differential elliptic flow of charged particles shown on the right panel of Fig. 19. Thus the bulk medium produced at RHIC and LHC has similar properties and the 30% increase of v_2 between the

two energies is due to an enlarged available phase space resulting in the same increase of the average transverse momentum of particles $\langle p_T \rangle$ between the RHIC and LHC energies.

As was first noted in Ref. [258] at high energies only the interactions among the constituents of matter formed in the initially spatially deformed overlap can produce $v_2 > 0$. A transfer of this spatial deformation into momentum space provides a unique signature for re-interactions in the fireball and proves that the matter has undergone significant nontrivial dynamics between its creation and its freeze-out [181]. The rapid degradation of the initial spatial deformation due to re-scattering causes the “self-quenching” of elliptic flow: if the elliptic flow does not develop early, when the collision fireball was still spatially deformed, it does not develop at all [181]. In particular, the transformation of fast expanding ideal gas of non-interacting quarks and gluons into strongly interacting hadrons is unable to produce a sufficient elliptic flow. The elliptic flow thus reflects the pressure due to re-scattering – the induced expansion and stiffness of the EoS during the earliest collision stages. Its continuous rise with the energy up to its highest value at the LHC indicates that the early pressure increases too.

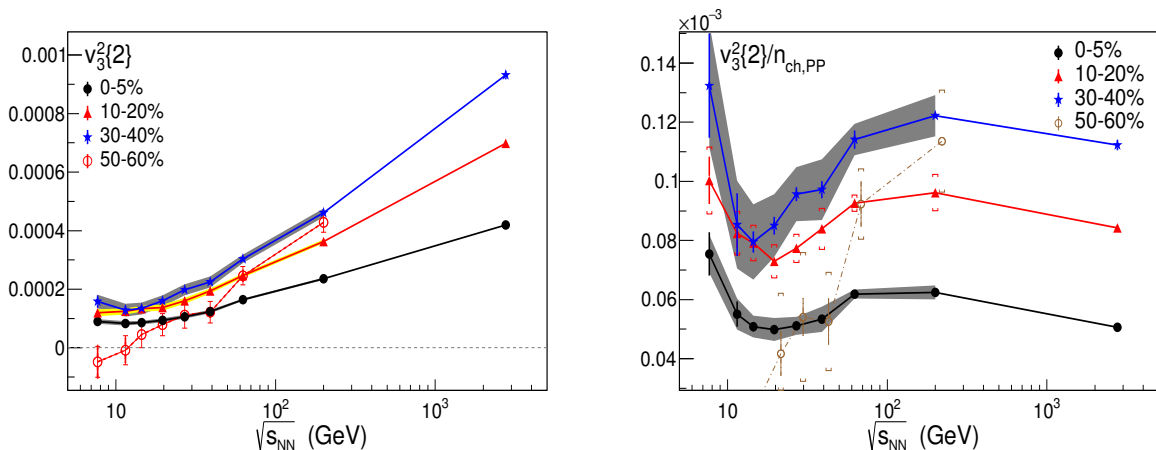


FIG. 20: Left: The energy dependence of $v_3^2\{2\}$ for four centrality bins. Points at 2.76 TeV corresponding to Pb+Pb [261]. Right: $v_3^2\{2\}$ divided by $n_{ch,PP}$ pair. Source: reproduced from Ref. [264].

The energy dependence of the integrated triangular flow coefficient $v_3^2\{2\}$ of charged hadrons is shown on the left panel of Fig. 20 in four bins of centrality, 0-5%, 10-20%, 30-40% and 50-60%. As $v_3^2\{2\}$ is sensitive to the fluctuations in the initial matter distribution it is interesting to observe that at $\sqrt{s_{NN}} = 7.7$ and 11.5 GeV values of $v_3^2\{2\}$ for 50%-60% centrality become consistent with zero. For more central collisions, however, $v_3^2\{2\}$ is finite even at the lowest energies and changes very little from 7.7 GeV to 19.6 GeV. Above that, it begins to increase more quickly and roughly linearly with $\log(\sqrt{s_{NN}})$. Generally one would expect that higher energy collisions producing more particles should be more effective at converting the initial state geometry fluctuations into $v_3^2\{2\}$. Deviations from that expectation could indicate interesting physics like a softening of the EoS [112, 113] discussed already in section III C. This can be investigated by scaling $v_3^2\{2\}$ by the charged particle rapidity density per participating NN pair, $n_{ch,PP} = dN_{ch}/d\eta/(0.5N_{part})$, see the right panel of Fig. 20. A local minimum of $v_3^2\{2\}/n_{ch,PP}$ in the region near 15-20 GeV observed in the centrality range 0-50% and absent in the more peripheral events could indicate an interesting trend in the pressure developed inside the system.

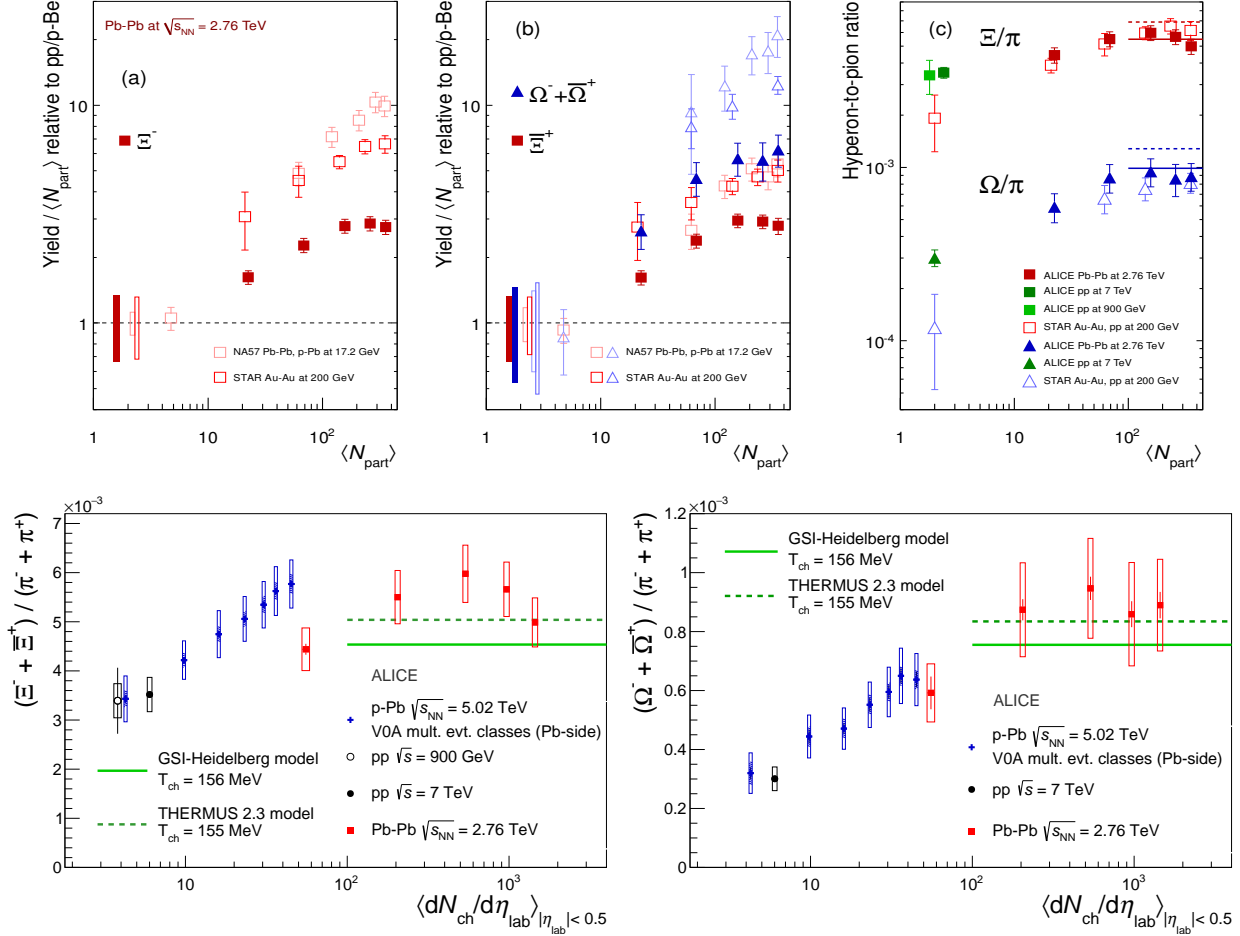


FIG. 21: Top: (a,b) Normalized (to $p+p$ or $p+Be$) yields of multistrange baryons per participants at midrapidity as a function of $\langle N_{\text{part}} \rangle$ for the LHC (full symbols), RHIC and SPS (open symbols) data. Boxes on the dashed line at unity indicate the statistical and systematic uncertainties on the $p+p$ or $p+Be$ reference. (c) Hyperon-to-pion ratios as a function of $\langle N_{\text{part}} \rangle$, for Pb+Pb, Au+Au and $p+p$ collisions at LHC and RHIC energies. The lines are the thermal model [254] (full line) and [265] (dashed line) predictions. Source: reproduced from Ref. [266]. Bottom: $(\Xi^- + \bar{\Xi}^+)/(\pi^+ + \pi^-)$ (left) and $(\Omega^- + \bar{\Omega}^+)/(\pi^+ + \pi^-)$ (right) ratios as functions of $\langle dN_{\text{ch}}/d\eta \rangle_{|\eta_{\text{lab}}| < 0.5}$ for $p+p$, $p+Pb$ and Pb+Pb collisions at the LHC. The Pb+Pb data points [266] represent, from left to right, the 60-80%, 40-60%, 20-40% and 10-20% and 0-10% centrality classes. The chemical equilibrium predictions by the GSI-Heidelberg [254] and the THERMUS 2.3 [265] models are represented by the horizontal lines. Source: reproduced from Fig. [267].

Enhanced production of hadrons with the quantum numbers not present in colliding matter is one of the oldest signals of the deconfined QGP medium [252, 253]. Measurements of the yields of multistrange baryons have been carried out at CERN SPS by WA85 and later on by WA97/NA57 collaborations since the mid-eighties. After 2000 more data came from RHIC and starting from 2010 also from the LHC. Current status is summarized on the five panels of Fig. 21. On top left and middle panels ((a) and (b)) a compilation of the results from SPS, RHIC and the LHC in terms of *strangeness enhancement* defined as normalized (to $p+p$ or $p+Be$) yield per participants is presented. On top right (c) the hyperon-to-pion ratios as functions of $\langle N_{\text{part}} \rangle$, for Pb+Pb, Au+Au and $p+p$ collisions at the LHC and RHIC

energies are displayed. The normalized yields are larger than unity for all the particles and increase with their strangeness content. This behaviour is consistent with the picture of enhanced $s\bar{s}$ pair production in a hot and dense QGP medium [252, 253].

Two bottom plots represent a comparison between the hyperon to pion ratios from $p+p$, $p+Pb$ and $Pb+Pb$ collisions. Interestingly, the ratios in $p+Pb$ collisions increase with multiplicity from the values measured in $p+p$ to those observed in $Pb+Pb$. The rate of increase is more pronounced for particles with higher strangeness content. Let us note that the Grand canonical statistical description of $Pb+Pb$ data shown as a full and dashed lines in Fig. 21 may not be appropriate in small multiplicity environments such as those produced in the $p+Pb$ case. It appears that for the later case the evolution of hyperon-to-pion ratios with the event multiplicity is qualitatively well described by the Strangeness Canonical model implemented in THERMUS 2.3 [265]. In this case a local conservation law is applied to the strangeness quantum number within a correlation volume V_c while treating the baryon and charge quantum numbers grand-canonically within the whole fireball volume V [267].

B. Hard probes

Heavy quarks, quarkonia and jets, commonly referred to as *hard probes*, are created in the first moments after the collision and are therefore considered as key probes of the deconfined QCD medium. Production of these high transverse momentum ($p_T \gg \Lambda_{QCD}$) objects occurs over very short time scales, $\tau \approx 1/p_T \approx 0.1 fm/c$, and can thus probe the evolution of the medium. Since the production cross sections of these energetic particles are calculable using pQCD, they have been long recognised as particularly useful “tomographic” probes of the QGP [268–270].

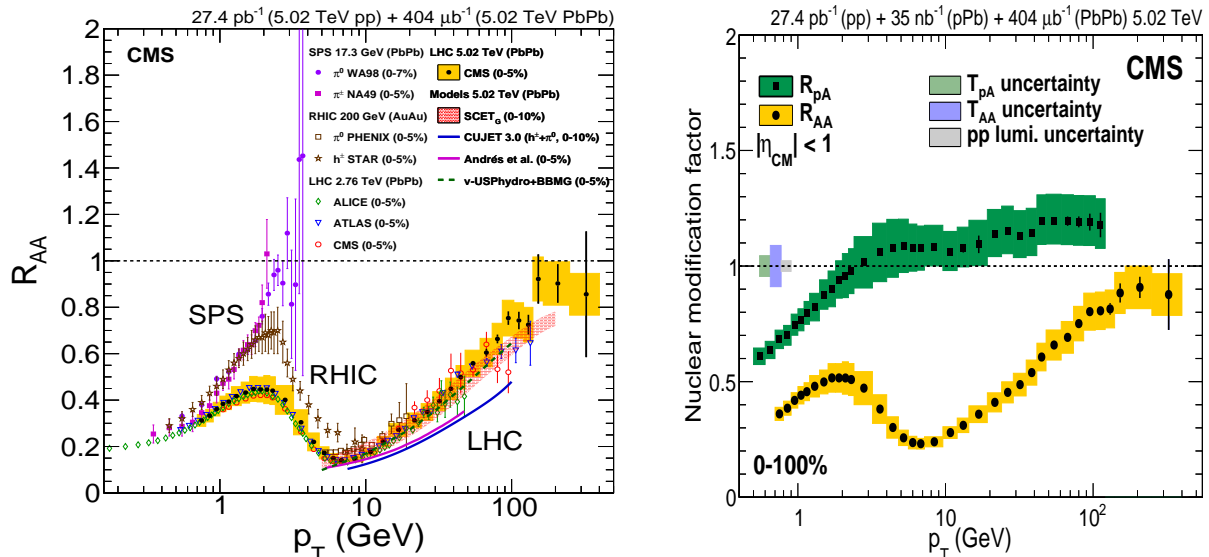


FIG. 22: Left: A compilation of the measurements of $R_{AA}(p_T)$ for neutral pions (π^0), charged hadrons (h^\pm), and charged particles in central heavy-ion collisions at SPS, RHIC and the LHC. Source: reproduced from Ref. [271]. Right: The nuclear modification factor $R_{pPb}(p_T)$ in $p+Pb$ compared to R_{AA} from $Pb+Pb$ collisions at $\sqrt{s_{NN}} = 5.02$ TeV at the LHC. Source: reproduced from Ref. [271].

1. High- p_T hadrons and jets

Let us start our discussion with the results on inclusive production of high- p_T hadrons. The later are interesting on their own because it was there where for the first time the suppression pattern was observed [14–17]. In an inclusive regime the comparison between $d^2N/dp_T d\eta$, the differential yield of high- p_T hadrons or jets per event in A+B collisions, to that in $p+p$ collisions is usually quantified by introducing the nuclear modification factor

$$R_{AB}(p_T, \eta) = \frac{dN_{AB}^2(p_T)/dp_T d\eta}{\langle N_{\text{coll}} \rangle dN_{pp}^2(p_T)/dp_T d\eta}. \quad (5.2)$$

For collisions of two nuclei behaving as a simple superposition of N_{coll} nucleon-nucleon collisions, the nuclear modification factor would be $R_{AB} = 1$. The data of Fig. 22 reveal a very different behaviour. The left panel shows a compilation of R_{AA} from Au+Au and Pb+Pb collisions, the right panel result on R_{pPb} from three LHC experiments at the same energy $\sqrt{s_{NN}} = 5.02$ TeV. In the R_{AA} case the suppression pattern of high- p_T ($> 2\text{--}3$ GeV/c) hadrons in the deconfined medium, predicted many years ago [268–270] as a *jet quenching effect*, is clearly visible at RHIC and the LHC. However, for proton-nucleus collisions, Fig. 22 (right panel), no suppression is seen even at the highest LHC energy. Moreover, R_{AA} in the 5% most central Pb+Pb collisions at the LHC shows a maximal suppression by a factor of 7–8 in the p_T region of 6–9 GeV. This dip is followed by an increase, which continues up to the highest p_T measured at $\sqrt{s_{NN}} = 5.02$ TeV, and approaches unity in the vicinity of $p_T = 200$ GeV [271].

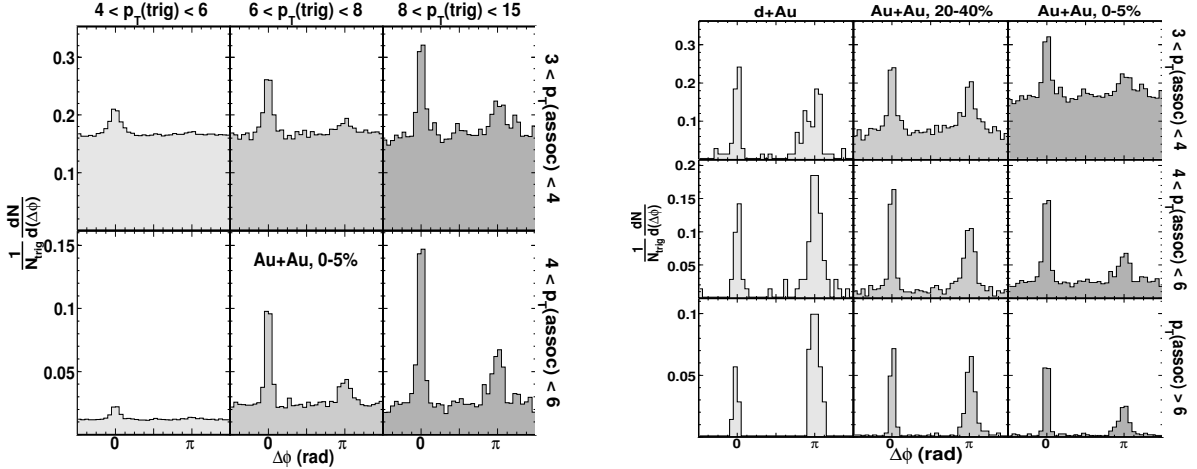


FIG. 23: Left: Azimuthal correlation histograms of high- p_T charged hadron pairs normalized per trigger particle for 0-5% Au+Au events for various p_T^{trig} and p_T^{assoc} ranges. The yield in the lower left panel is suppressed due to the constraint $p_T^{\text{assoc}} < p_T^{\text{trig}}$. Right: The same but for $8 < p_T^{\text{trig}} < 15$ GeV/c, for $d+\text{Au}$, 20-40% Au+Au and 0-5% Au+Au events. Source: reproduced from Ref. [272].

The suppression of high- p_T hadrons in the deconfined medium was thoroughly studied at RHIC using azimuthal correlations between the trigger particle and associated particle, see Fig. 23. Near-side peaks in central (0-5%) Au+Au collisions present in all panels of Fig. 23 (left) indicate that the correlation is dominated by jet fragmentation. An away-side peak emerges as p_T^{trig} is increased. The narrow, back-to-back peaks are indicative of the

azimuthally back-to-back nature of dijets observed in an elementary parton-parton collision. Contrary to the later the transverse-momentum imbalance of particles from the jet fragmentation due to different path lengths of two hard partons in the medium is apparent. The azimuthal angle difference $\Delta\phi$ for the highest p_T^{trig} range ($8 < p_T^{\text{trig}} < 15$ GeV/c) for mid-central (20-40%) and central Au+Au collisions, as well as for d+Au collisions, is presented in Fig. 23 (right panel). We observe narrow correlation peaks in all three p_T^{assoc} ranges. For each p_T^{assoc} , the nearside peak shows a similar correlation strength above background for the three systems, while the away-side correlation strength decreases from d+Au to central Au+Au. For d+Au case the yield of particles on the opposite side $\Delta\phi=\pi$ prevails over the same side. Moreover, for Au+Au collisions the nearside yields obtained after subtraction of the background contribution due to the elliptic flow show a little centrality dependence, while the away-side yields decrease with increasing centrality [272].

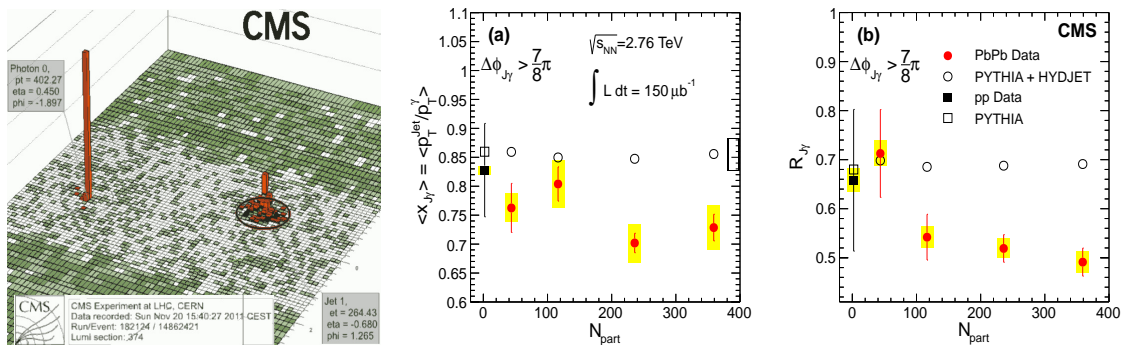


FIG. 24: Left: The energy distribution in $\eta \times \phi$ plane in a single Pb+Pb event recorder by the CMS detector at LHC (reproduced from Ref. [273]). Middle and right: The average ratio of jet transverse momentum to photon transverse momentum, $\langle x_{J\gamma} \rangle$, and the average fraction $R_{J\gamma}$ of isolated photons with an associated jet with energy above 30 GeV as functions of number of participants N_{part} . Photons and jets are emitted almost back-to-back in azimuth $\phi_{J\gamma}$. Source: reproduced from Ref. [274].

Unfortunately, the advantage of the large yield of dijets is offset by a loss of information about the initial properties of the probes, i.e. prior to their interactions with the medium. Correlating two probes that both undergo an energy loss also induces a selection bias towards scatterings occurring at, and oriented tangential to, the surface of the medium. It is thus interesting to study correlations when one of the particles does not interact strongly with the medium. Triggering on the high- p_T isolated photon (i.e. not from $\pi^0 \rightarrow 2\gamma$ decays) would do the job. While in $p+p$ collisions an emerging quark jet should balance its transverse momentum with the photon, in the heavy-ion collisions much of its momentum is thermalized while the quark traverses the plasma. This is illustrated in Fig. 24 (left panel) where a single hard photon with $p_T = 402$ GeV emerges unhindered from the de-confined medium produced in Pb+Pb collisions at the LHC. The accompanying quark jet produced via the QCD Compton scattering $qg \rightarrow q\gamma$ loses 1/3 of its energy (≈ 140 GeV!) inside the hot and dense matter.

The measurement presented on the middle and right panels of Fig. 24 shows that for more central Pb+Pb collisions, a significant decrease in the ratio of jet transverse momentum to photon transverse momentum, $\langle x_{J\gamma} \rangle$, relative to the PYTHIA reference [193] is observed. Furthermore, significantly more photons with $p_T > 60$ GeV/c in Pb+Pb are observed not

to have an associated jet with $p_T > 30$ GeV/c jet, compared to the reference. However, no significant broadening of the photon + jet azimuthal correlation has been observed.

An important progress in theoretical understanding of suppression of energetic partons traversing a deconfined matter was the introduction of the diffusion coefficient \hat{q} relevant for the transverse momentum broadening and collisional energy loss of partons (jets) [275]. This quantity, which is commonly referred to as the jet quenching parameter can be determined either via weak coupling techniques [276–278], a combination of lattice simulations and dimensionally reduced effective theory [279], or from the gauge/gravity duality [280]. Typical estimates for this quantity at RHIC and LHC energies range between 5 and 10 GeV²/fm, demonstrating the currently still sizable uncertainties in these calculations.

2. Quarkonia

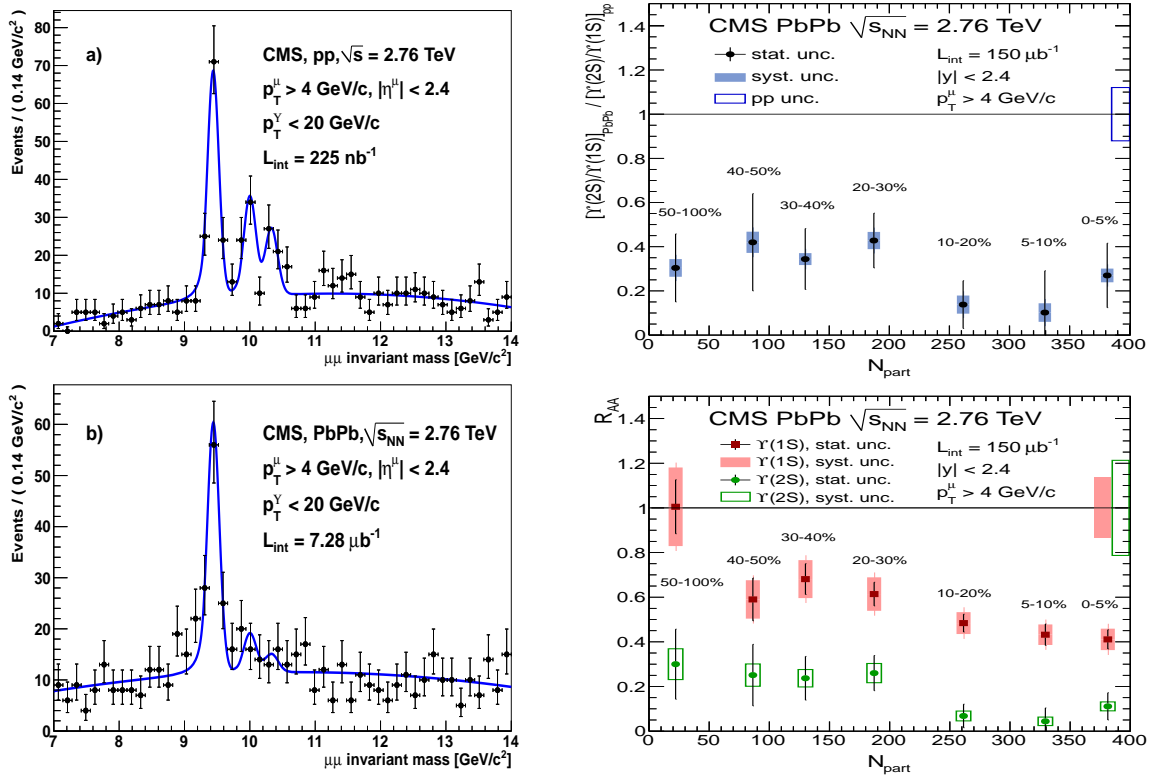


FIG. 25: Left: The di-muon invariant-mass distributions from the $p+p$ (a) and Pb+Pb (b) data at $\sqrt{s_{NN}} = 2.76$ TeV. Right: The centrality dependence of the double ratio (top) and of the nuclear modification factors R_{AA} (bottom) for the $\Upsilon(1S)$ and $\Upsilon(2S)$ states. The event centrality bins are indicated by percentage intervals. Source: reproduced from Ref. [281].

Melting of the quarkonia, bound states of heavy quark and anti-quark $q\bar{q}$ where $q=c,b$, due to a colour screening in the deconfined hot and dense medium has been proposed thirty years ago as a clear and unambiguous signature of the deconfinement [114]. However, shortly after that it was noticed that not only diffusion of the heavy quarks from melted quarkonium but also the drag which charm quarks experience when propagating through the plasma is

important [282]. The later might lead to an enhancement instead of suppression. This is in variance with the original proposal that the heavy quarks, once screened, simply fly apart. With the advent of the strongly interacting QGP the Langevin equation model of quarkonium production was formulated where the charm quark-antiquark pairs evolve on top of a hydrodynamically expanding fireball [283]. A heavy quark and anti-quark interact with each other according to the screened Cornell potential and interact, independently, with the surrounding medium, experiencing both drag and rapidly decorrelating random forces. An extension of this approach to bottomonium production [284] shows that a large fraction of $b\bar{b}$ pairs that were located sufficiently close together during the initial hard production will remain correlated in the hot medium for a typical lifetime of the system created in heavy-ion collisions. The distribution of the correlated $b\bar{b}$ pair in relative distance is such, that it will dominantly form 1S bottomonium. A study of quarkonia production in heavy-ion collisions thus provides an interesting window not only into static but also into dynamical properties of the hot, dense and rapidly expanding medium [115, 251].

On left panels of Fig. 25 the invariant-mass distributions of $\mu^+\mu^-$ pairs (di-muons) produced in the $p+p$ (a) and Pb+Pb (b) collisions at the LHC are presented. A prominent peak due to production of the heavy quarkonium state, the bottomonium $\Upsilon(1S)$, can be clearly seen in both $p+p$ and Pb+Pb data. Peaks from the higher excited states of Υ , $\Upsilon(2S)$ and $\Upsilon(3S)$, although discernible in the $p+p$ case are barely visible in the Pb+Pb data. More quantitative information on this effect can be found on the right panels of Fig. 25 where the centrality dependence of the double ratio $[\Upsilon(2S)/\Upsilon(1S)]_{\text{PbPb}}/[\Upsilon(2S)/\Upsilon(1S)]_{\text{pp}}$ (top) and of the nuclear modification factors R_{AA} of $\Upsilon(1S)$ and $\Upsilon(2S)$ (bottom) are displayed. Let us note that the observed suppression of the relative yield is in agreement with the expectations that different quarkonium states will dissociate at different temperatures with a suppression pattern ordered sequentially with the binding energy, i.e. the difference between the mass of a given quarkonium and twice the mass of the lightest meson containing the corresponding heavy quark [285]. Moreover, the observed pattern is now confirmed also in Pb+Pb collisions at $\sqrt{s_{NN}}=5.02$ TeV [286]. The double ratio is significantly below unity at all centralities and no variation with kinematics is observed confirming a strong Υ suppression in heavy-ion collisions at the LHC.

C. Penetrating probes

The electromagnetic probes like photons [289, 290] and di-leptons [291] (for recent developments, see Refs. [239, 240, 292]) were since a long time expected to provide a crucial information on the properties of QGP. The absence of strong final-state interactions makes them an ideal *penetrating probe* of strongly-interacting matter [293]. In collisions of ultra-relativistic nuclei the photons and leptons can be produced either in the initial hard collisions between partons of the incident nuclei, e.g. $qg \rightarrow q\gamma$, $q\bar{q} \rightarrow \gamma g$ or $q\bar{q} \rightarrow \ell\bar{\ell}$, or radiated from the thermally equilibrated partons and hadrons or via hadronic decays. The direct photons are defined to be all produced photons except those from hadron decays in the last stage of the collision. The high- p_T isolated photon can be used to estimate the momentum of the associated parton allowing a characterisation of the in-medium parton energy loss, see Fig. 24. The prompt photons also carry information about the initial state and its possible modifications in nuclei and should thus be one of the best probes of the gluon saturation. The thermal photons emitted from the produced matter in nuclear collisions carry information on the temperature of QGP.

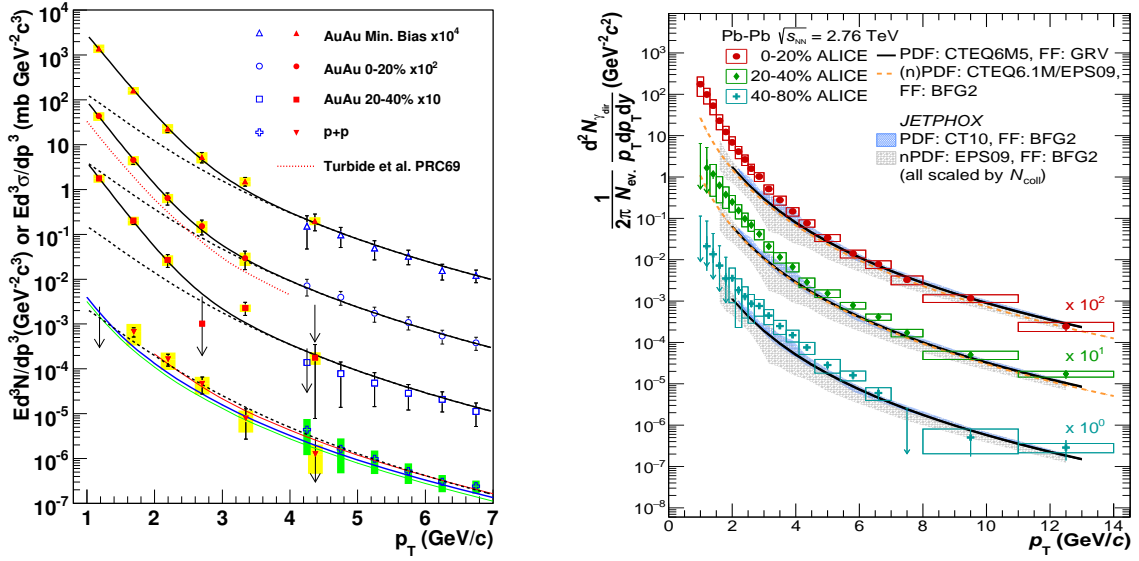


FIG. 26: Left: The invariant cross section ($p+p$) and invariant yield (Au+Au) of direct photons as functions of p_T . The three curves on the $p+p$ data represent the NLO pQCD calculations, and the dashed curves show a modified power-law fit to the $p+p$ data, scaled by $T_{AA} = \langle N_{\text{coll}} \rangle / \sigma_{NN}^{\text{in}}$. The dashed (black) curves are the same but with the exponential plus scaled $p+p$ data. The dotted (red) curve near the 0–20% centrality data is a theory calculation. Source: reproduced from Ref. [287]. Right: The direct photon spectra in Pb+Pb collisions at $\sqrt{s_{NN}} = 2.76$ TeV for the 0-20% (scaled by a factor of 100), the 20-40% (scaled by a factor of 10) and the 40-80% centrality classes compared to the NLO pQCD predictions for the direct photon yield in pp collisions at the same energy scaled by a number of binary nucleon collisions for each centrality class. Source: reproduced from Ref. [288].

The first observation of direct photons in ultra-relativistic heavy-ion collisions has been made by the CERN SPS experiment WA98 [294]. In 10% most central Pb+Pb collisions at $\sqrt{s_{NN}} = 17.2$ GeV they observed a clear excess of direct photons in the range of $p_T > 1.5 \text{ GeV}/c$ which was not present in more peripheral collisions. The extraction of the direct photon signal which is extremely difficult was described in-depth in Ref. [295]. The data from RHIC and the LHC are presented in Fig. 26 on the left and right panels, respectively.

VI. NEW DEVELOPMENTS

A. Search for the tricritical point of QCD phase diagram

The search for the (tri)critical point (CEP) in the $T-\mu_B$ phase diagram, where the phase transition between the QGP and hadron matter changes from the first to the second order one, represents one of the most active field of contemporary ultra-relativistic heavy-ion physics, both experimentally [59, 298–300] and in the theory [58, 301]. In order to gain more insight into the CEP location the quite advanced techniques from condensed matter physics like a Finite-Size Scaling (FSS) analysis of data [302] or thermal fluctuations characterized by the appropriate cumulants of the partition function [301, 303] are being exploited.

The search for the CEP exploiting the potential of the RHIC accelerator complex was

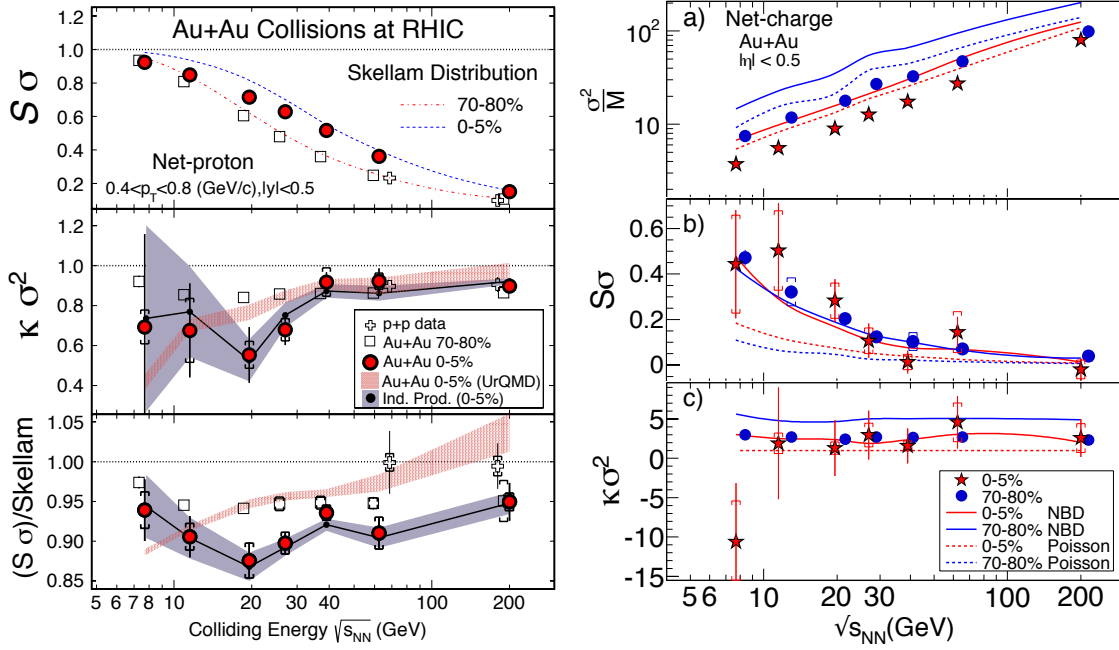


FIG. 27: The energy dependence of appropriate combinations of the moments – mean (M), variance (σ^2), skewness (S) and kurtosis (κ) of the multiplicity of conserved charges at mid-rapidity in Au+Au collisions for seven energies ranging from $\sqrt{s_{NN}} = 7.7$ to 200 GeV and for two centralities, the most central (0-5%) and peripheral (70-80%) bins. Left: The collision energy and centrality dependence of the net-proton $S\sigma$ and $\kappa\sigma^2$ from Au+Au and $p+p$ collisions at RHIC (adapted from Ref. [296]). Right: The beam-energy dependence of the net-charge multiplicity distributions moments (a) σ^2/M , (b) $S\sigma$, and (c) $\kappa\sigma^2$, after all corrections. Source: reproduced from Ref. [297]. The results from the Poisson and the Negative Binomial Distribution (NBD) baselines are superimposed. The values of $\kappa\sigma^2$ for the Poisson baseline are always unity.

mounted by the STAR and PENIX collaborations in 2010 within the *Beam Energy Scan* (BES) program [59]. Going down from the RHIC maximum energy $\sqrt{s_{NN}} = 200$ GeV they have scanned the available phase space down to $\sqrt{s_{NN}} = 7.7$ GeV. Some of the results from that scan were already mentioned in previous sections and can be found in Figs. 8, 10, 17, 19, 20. In the following we therefore restrict ourselves to the measurements which provide a direct link to the lattice results discussed in section III D. As already mentioned there, the study of ratios of the Taylor expansion coefficients given by Eq. 3.31, which are also known also as susceptibilities, seems to be very attractive since both the temperature and volume dependences drop out. In particular, the ratio χ_4^B/χ_2^B calculated from the moments of the net-baryon multiplicity N_B has different values for the hadronic and partonic phases [303]. For HRG it equals unity but is expected to deviate from unity near the CEP. Other interesting ratios of the net-baryon charge moments which can be expressed using mean (M_B), variance (σ_B^2), skewness (S_B) and kurtosis (k_B) of the net baryon number distributions read

$$R_{ij}^B \equiv \frac{\chi_i^B}{\chi_j^B}, \quad R_{12}^B = \frac{M_B}{\sigma_B^2}, \quad R_{31}^B = \frac{S_B \sigma_B^3}{M_B}, \quad R_{42}^B = k_B \sigma_B^2. \quad (6.1)$$

Experimentally, the net-baryon number N_B fluctuations and their cumulants are not accessible and so one has to resort to measurements of the cumulants of the net-proton number N_P fluctuations [296, 304]. On the other hand, the electric charge fluctuations are experimentally accessible [297]. This is illustrated in Fig. 27 where the measurements from the STAR experiment at RHIC are shown.

B. Collectivity in small systems

Recent years have witnessed a surprising development in multiparticle dynamics of high multiplicity $p+p$ [305–307] and $p+A$ [308–313] collisions. It has all started in 2010 with the observation of *ridge-like* structures in $p+p$ collisions by the CMS experiment at the LHC [305]. The surprise was due to the fact that a very similar effect has been found just few years before in heavy-ion collisions: first in Au+Au collisions at $\sqrt{s_{NN}} = 200$ GeV at RHIC [314, 315] and later on also in Pb+Pb collisions at the LHC [316] and in Cu+Cu collisions at $\sqrt{s_{NN}} = 62.4$ GeV and 200 GeV at RHIC [317].

In heavy-ion collisions it was found that pairs of particles are preferentially emitted with small relative azimuthal angles ($\Delta\phi = \phi_1 - \phi_2 \approx 0$). Surprisingly, this preference persists even when the particles are separated by large pseudo-rapidity (η) gaps ($-4 < |\Delta\eta| < 2$). These long-range correlations, known as the ridge, have been traced to the conversion of density anisotropies in the initial overlap of the two nuclei into momentum space correlations through subsequent interactions in the expansion [318].

In $p+p$ minimum bias collisions at the LHC, the peak in the correlation function of particles with $p_T > 0.1$ GeV/c observed at small angular differences ($\Delta\eta, \Delta\phi \approx 0$), see Fig. 28(a), is due to several effects: resonance decays, Bose-Einstein correlations and near-side jet fragmentation. The fragmentation due to back-to-back jets is visible as a broad elongated ridge around $\Delta\phi \approx \pi$. The pattern does not change much even when selecting the events with very high multiplicity $N \geq 110$, see Fig. 28(c). The cut on the multiplicity enhances the relative contribution of high p_T jets which fragment into a large number of particles and, therefore, has a qualitatively similar effect on the shape as the particle cut $1 < p_T < 3$ GeV/c on minimum bias events, see Fig. 28(b). However, using now the particle cut $1 < p_T < 3$ GeV/c in conjunction with a high multiplicity cut changes the picture dramatically, see Fig. 28(d). A novel feature never seen before in $p+p$ collisions at lower energies shows up – a clear and significant ridge-like structure at $\Delta\phi \approx 0$ extending to $|\Delta\eta|$ of at least 4 units [305].

Let us note that for two particles with approximately the same energy $E_1 \approx E_2 \approx E$ the correlations at $\Delta\eta \approx \Delta y$ are by the uncertainty relation $\Delta x \approx 1/\Delta p = 1/(E\Delta y)$ connected to the correlations in coordinate space. While for pions with $\Delta\eta \approx 1$ and $p_T \approx 0.1$ GeV/c we have $\Delta x \approx 1$ fm, for $\Delta\eta \approx 4$ and $p_T \approx 1$ GeV/c one gets $\Delta x \approx 0.02$ fm. It is obvious that at such small inter-parton distances one enters the realm of initial state description of nuclear collisions when the density of matter even inside the proton fluctuates, see section IV D 2. The CGC scenario was recently exploited in Ref. [319] to predict long-range photon-jet correlations in $p+p$ and $p+A$ collisions at near-side for low transverse momenta of the produced photon and jet in high-multiplicity events.

The relevance of the saturation approach is further supported by the observation of the same ridge-like structure in $p+p$ collisions at $\sqrt{s} = 13$ TeV [306, 307], see Fig. 29. The associated yield of long-range near-side correlations for high-multiplicity events ($N > 110$) peaks in the region $1 < p_T < 2$ GeV/c, see Fig. 29 (a). The yield reaches a maximum around

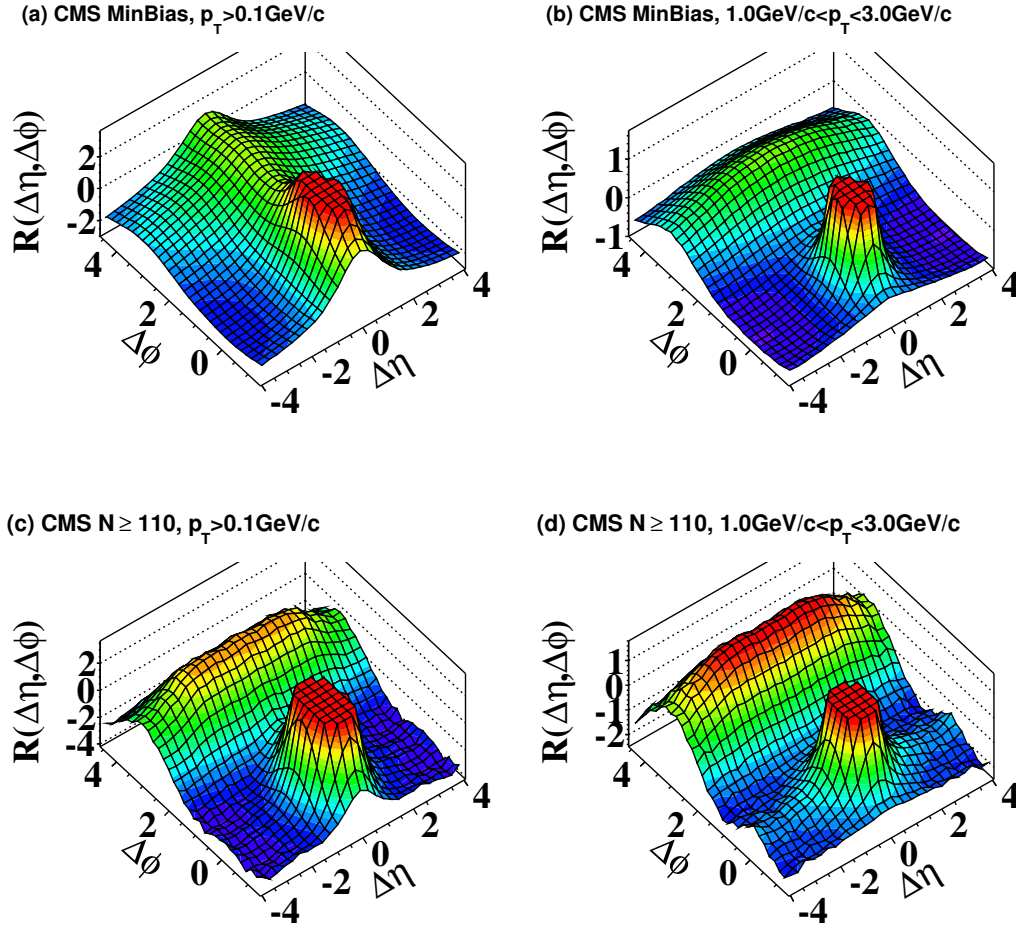


FIG. 28: The 2-D two-particle correlation functions for $p+p$ at $\sqrt{s} = 7$ TeV: (a) minimum bias events with $p_T > 0.1$ GeV/c, (b) minimum bias events with $1 < p_T < 3$ GeV/c, (c) high multiplicity ($N_{\text{trk}}^{\text{offline}} \geq 110$) events with $p_T > 0.1$ GeV/c and (d) high multiplicity ($N_{\text{trk}}^{\text{offline}} \geq 110$) events with $1 < p_T < 3$ GeV/c. The sharp near-side peak from jet correlations is cut off in order to better illustrate the structure outside that region. Source: reproduced from Ref. [305].

$p_T \approx 1$ GeV/c and decreases with increasing p_T . No center-of-mass energy dependence is visible. The multiplicity dependence of the associated yield for $1 < p_T < 2$ GeV/c particle pairs is shown in Fig. 29 (b). For low-multiplicity events, the associated yield is consistent with zero. At higher multiplicity the ridge-like correlation emerges, with an approximately linear rise of the associated yield with multiplicity for $N \geq 40$. Let us note that within the CGC models the observation that the integrated near-side yield as a function of multiplicity is independent of collision energy is a natural consequence of the fact that multiparticle production is driven by a single semi-hard saturation scale [320].

Another interesting phenomenon observed during recent years is a flow-like pattern in super-central $p+p$ and $p+\text{Pb}$ collisions at the LHC [309] and in $d+\text{Au}$, $^3\text{He}+\text{Au}$ and $p(d)+\text{Au}$ collisions at RHIC [312, 313]. Not only that these collisions reveal a similar elliptic flow v_2 but in some cases also v_3 anisotropy observed previously only in collisions of large nuclei. The measurement of higher-order cumulants of the azimuthal distributions has strengthened

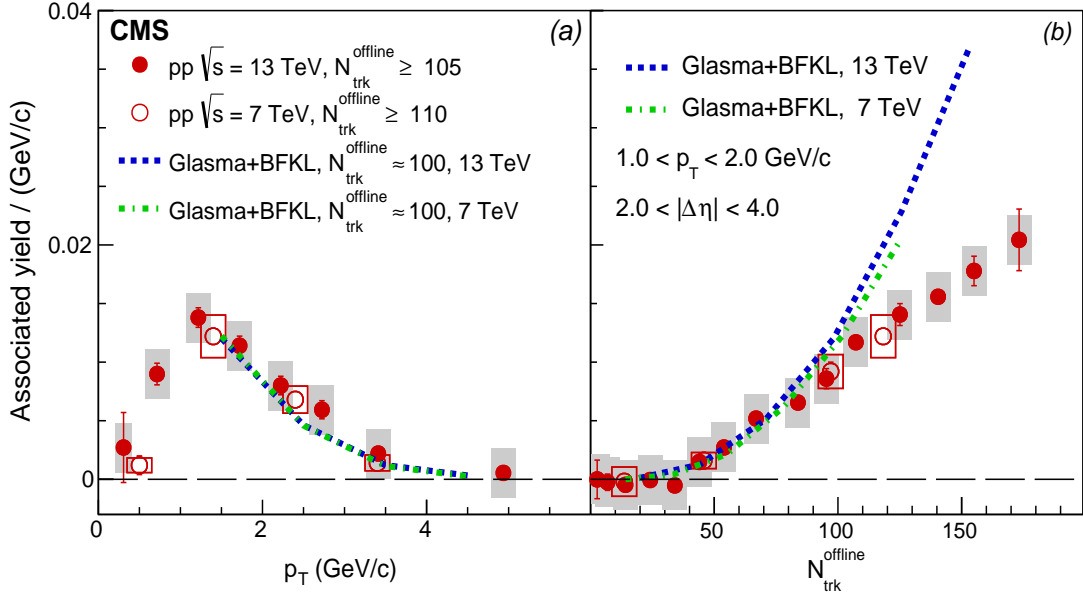


FIG. 29: The associated yield for the near-side of the correlation function averaged over $2 < |\Delta\eta| < 4$ for $p+p$ data at $\sqrt{s} = 13$ TeV (filled circles) and 7 TeV (open circles) [306]. Panel (a) shows the associated yield as a function of p_T for events with $N_{\text{trk}}^{\text{offline}} \geq 105$. In the panel (b) the associated yield for $1 < p_T < 2$ GeV/c is shown as a function of multiplicity, $N_{\text{trk}}^{\text{offline}}$. The p_T selection applies to both particles in each pair. Curves represent the predictions of the gluon saturation model [320].

the collective nature interpretation of the anisotropy seen in $p+Pb$ collisions. Moreover, the collective radial flow analysis of $p+p$ data enabled authors of Ref. [321] to claim that in this case the fireball explosions start with a very small initial size, well below 1 fm. This rises questions about whether the perfect liquid sQGP is also formed in these much smaller systems [322–324]. Are these flow-like structures only similar in appearance to what one observes in heavy-ion collisions, or do they have the same physical origin? Obviously, answering these question may help us to understand the emergence of collective phenomena in strongly-interacting systems in general. To make a further progress on these fundamental questions, more analyses, both experimental and theoretical are really needed [325].

VII. CONCLUSIONS

In this review, we have tried to present an up-to-date phenomenological summary of a relatively new and rapidly developing field of contemporary physics – the physics of Quark Gluon Plasma. We have also explored its broader ramification when discussing matter under extreme conditions, strongly interacting plasmas, physics of strong electromagnetic fields, history of ultra-relativistic heavy-ion collisions, relativistic hydrodynamics, role of the QCD ground state and QCD saturation phenomena. In the experimental part, we were overwhelmed by a huge amount of results and so, in order to keep this review of tolerable length, we have to skip several quite important topics. Just to name a few – flow and suppression of identified particles [30, 326], femtoscopy [327, 328] or identified particle yields and chemical freeze-out conditions [29, 30, 254]. We hope that the interested reader will find

in given references enough information to pursue a deeper study of these important subjects. However, in skipping these topics, we hope that we have not given up our main goal – to give the reader a possibility to see the QGP landscape at large. At last, we would like to say that it is never enough to stress how important this field is also for other branches of physics and so we finish with yet another argument. The study of ultra-relativistic heavy-ion collisions appears so far our only way of studying the phase transitions in non-Abelian gauge theories (most likely taken place in early universe) under laboratory conditions.

Acknowledgements

This work was supported in part by the Swedish Research Council, contract number 621-2013-428, the grant LG 13031 of the Ministry of Education of the Czech Republic and by the grant 13-20841S of the Czech Science Foundation (GACR).

-
- [1] J. C. Collins and M. J. Perry, Phys. Rev. Lett. **34**, 1353 (1975).
 - [2] N. Cabibbo and G. Parisi, Phys. Lett. B **59** (1975) 67.
 - [3] M. Gell-Mann, Phys. Lett. **8**, 214 (1964).
 - [4] G. Zweig, CERN-TH-401, <http://inspirehep.net/record/11881/files/CM-P00042883.pdf>.
 - [5] H. Fritzsch, M. Gell-Mann and H. Leutwyler, Phys. Lett. B **47**, 365 (1973).
 - [6] D. J. Gross and F. Wilczek, Phys. Rev. Lett. **30**, 1343 (1973).
 - [7] H. D. Politzer, Phys. Rev. Lett. **30**, 1346 (1973).
 - [8] Y. Nambu, Sci. Am. **235N5**, 48 (1976).
 - [9] K. Yagi, T. Hatsuda and Y. Miake, *Quark-gluon plasma: From big bang to little bang*, Camb. Monogr. Part. Phys. Nucl. Phys. Cosmol. **23**, (2005).
 - [10] H. R. Schmidt and J. Schukraft, J. Phys. G **19**, 1705 (1993).
 - [11] R. Stock, Nucleus-Nucleus Collisions and the QCD Matter Phase Diagram, in Landolt-Börnstein - Group I Elementary Particles, Nuclei and Atoms, Vol.**21A**, Chapter 7, Springer Berlin Heidelberg, 2009. arXiv:0807.1610 [nucl-ex].
 - [12] J. Schukraft and R. Stock, arXiv:1505.06853 [nucl-ex].
 - [13] U. W. Heinz and M. Jacob, nucl-th/0002042.
 - [14] I. Arsene *et al.* [BRAHMS Collaboration], Nucl. Phys. A **757**, 1 (2005).
 - [15] B. B. Back *et al.* [PHOBOS Collaboration], Nucl. Phys. A **757**, 28 (2005).
 - [16] J. Adams *et al.* [STAR Collaboration], Nucl. Phys. A **757**, 102 (2005).
 - [17] K. Adcox *et al.* [PHENIX Collaboration], Nucl. Phys. A **757**, 184 (2005).
 - [18] M. Gyulassy and L. McLerran, Nucl. Phys. A **750**, 30 (2005).
 - [19] J. Kapusta, B. Müller and J. Rafelski (eds), *Quark-Gluon Plasma: Theoretical Foundations. An annotated reprint collection.*, ISBN: 0-444-511110-5, Elsevier (2003), 817p.
 - [20] L. P. Csernai, *Introduction to relativistic heavy ion collisions*, Chichester, UK: Wiley (1994) 310 p.,
http://th.physik.uni-frankfurt.de/~svogel/lecture_ss_2014/paper_5.pdf.
 - [21] J. Letessier and J. Rafelski, *Hadrons and quark - gluon plasma*, Camb. Monogr. Part. Phys. Nucl. Phys. Cosmol. **18** (2002).

- [22] R. Vogt, *Ultrarelativistic heavy-ion collisions*, Elsevier Science (2007), ISBN:9780444521965.
- [23] W. Florkowski, *Phenomenology of Ultra-Relativistic Heavy-Ion Collisions*, Singapore, Singapore: World Scientific (2010) 416 p.
- [24] J. Rak and M. J. Tannenbaum, *High p_T physics in the heavy ion era*, Camb. Monogr. Part. Phys. Nucl. Phys. Cosmol. **34**, (2013).
- [25] P. Braun-Munzinger and J. Stachel, Nature **448**, 302 (2007).
- [26] E. Shuryak, Prog. Part. Nucl. Phys. **62**, 48 (2009).
- [27] S. Sarkar, H. Satz and B. Sinha, *The physics of the quark-gluon plasma*, Lect. Notes Phys. **785**, pp. 369 (2010).
- [28] W. Florkowski, Acta Phys. Polon. B **45**, no. 12, 2329 (2014).
- [29] G. Roland, K. Safarik and P. Steinberg, Prog. Part. Nucl. Phys. **77**, 70 (2014).
- [30] R. Nouicer, Eur. Phys. J. Plus **131**, no. 3, 70 (2016).
- [31] Y. I. B. Zeldovich, Yu. P. Raizer *Physics of Shock Waves and High-Temperature Hydrodynamics Phenomena*, Academic Press, New York and London, 1966, Dover, Mineola, NY (2002), ISBN-13: 978-0486420028.
- [32] V. I. Fortov *Extreme States of Matter on Earth and in the Cosmos*, Springer 2011, ISBN: 978-3-642-16463-7 (Print) 978-3-642-16464-4 (Online).
- [33] J. R. Oppenheimer and G. M. Volkoff, Phys. Rev. **55**, 374 (1939).
- [34] L. D. Landau, Physik. Zeits. Sowjetunion **1**, 285 (1932).
- [35] Y. B. Zeldovich, Sov. Phys. JETP **14**, 1143 (1962).
- [36] G. Baym and S. A. Chin, Phys. Lett. B **62**, 241 (1976).
- [37] G. Gamow, Phys. Rev. **70**, 572 (1946).
- [38] A. A. Penzias and R. W. Wilson, Astrophys. J. **142**, 419 (1965).
- [39] A. D. Sakharov, Pisma Zh. Eksp. Teor. Fiz. **3**, no. 11, 439 (1966) [JETP Lett. **3**, 288 (1966)].
- [40] K. Huang and S. Weinberg, Phys. Rev. Lett. **25**, 895 (1970).
- [41] R. Hagedorn, Nuovo Cim. Suppl. **3**, 147 (1965).
- [42] J. Rafelski (ed.), *Melting Hadrons, Boiling Quarks - From Hagedorn Temperature to Ultra-Relativistic Heavy-Ion Collisions at CERN: With a Tribute to Rolf Hagedorn*, ISBN: 978-3-319-17544-7 (Print) 978-3-319-17545-4 (Online), <http://link.springer.com/content/pdf/10.1007%2F978-3-319-17545-4.pdf>.
- [43] A. Majumder and B. Muller, Phys. Rev. Lett. **105**, 252002 (2010).
- [44] Y. B. Zeldovich, Acta Phys. Hung. **22**, 51 (1967).
- [45] Y. B. Zeldovich, Sov. Phys. Uspechi **9**, 602 (1967).
- [46] A. D. Linde, Rept. Prog. Phys. **42**, 389 (1979).
- [47] D. Bailin and A. Love, *Cosmology in gauge field theory and string theory*, ISBN: 0 7503 0492 8 Bristol, UK: IOP (2004) 313 p.
- [48] D. Boyanovsky, H. J. de Vega and D. J. Schwarz, Ann. Rev. Nucl. Part. Sci. **56**, 441 (2006).
- [49] M. Trodden, Rev. Mod. Phys. **71**, 1463 (1999).
- [50] K. Kajantie, M. Laine, K. Rummukainen and M. E. Shaposhnikov, Phys. Rev. Lett. **77**, 2887 (1996).
- [51] L. Susskind, Phys. Rev. D **20**, 2610 (1979).
- [52] P. Petreczky, J. Phys. G **39**, 093002 (2012).
- [53] Y. Aoki, G. Endrodi, Z. Fodor, S. D. Katz and K. K. Szabo, Nature **443**, 675 (2006).
- [54] T. Bhattacharya *et al.*, Phys. Rev. Lett. **113**, no. 8, 082001 (2014).
- [55] M. Cheng *et al.*, Phys. Rev. D **77**, 014511 (2008).
- [56] D. Rischke, Prog. Part. Nucl. Phys. **52** (2004)197.

- [57] L. McLerran and R. D. Pisarski, Nucl. Phys. A **796**, 83 (2007).
- [58] M. Buballa, Phys. Rept. **407** (2005) 205.
- [59] M. M. Aggarwal *et al.* [STAR Collaboration], arXiv:1007.2613 [nucl-ex].
- [60] N. Itoh, Prog. Theor. Phys. **44** 291 (1970).
- [61] E. V. Shuryak, Sov. Phys. JETP **47**, 212 (1978) [Zh. Eksp. Teor. Fiz. **74**, 408 (1978)].
- [62] S. Ichimaru, Rev. Mod. Phys. **54**, 1017 (1982).
- [63] P. Braun-Munzinger, V. Koch, T. Schäfer and J. Stachel, Phys. Rept. **621**, 76 (2016).
- [64] P. Braun-Munzinger and J. Wambach, Rev. Mod. Phys. **81**, 1031 (2009).
- [65] K. Fukushima and T. Hatsuda, Rept. Prog. Phys. **74**, 014001 (2011).
- [66] D. Bailin and A. Love, Phys. Rept. **107**, 325 (1984).
- [67] M. Buballa, J. Hosek and M. Oertel, Phys. Rev. Lett. **90**, 182002 (2003).
- [68] M. G. Alford, K. Rajagopal and F. Wilczek, Nucl. Phys. B **537**, 443 (1999).
- [69] W. Becker (ed.), *Neutron Stars and Pulsars*, Springer Berlin 2009, ISBN 978-3-540-76965-1.
- [70] A. B. Migdal, Rev. Mod. Phys. **50**, 107 (1978).
- [71] D. G. d'Enterria *et al.* [CMS Collaboration], J. Phys. G **34**, 2307 (2007).
- [72] Water structure and science, http://www1.lsbu.ac.uk/water/water_phase_diagram.html.
- [73] M. A. Shifman, A. I. Vainshtein and V. I. Zakharov, Nucl. Phys. B **147**, 385 (1979); Nucl. Phys. B **147**, 448 (1979).
- [74] T. Schäfer and E. V. Shuryak, Rev. Mod. Phys. **70**, 323 (1998).
- [75] D. Diakonov, Prog. Part. Nucl. Phys. **51**, 173 (2003).
- [76] D. Diakonov, Nucl. Phys. Proc. Suppl. **195**, 5 (2009).
- [77] A. A. Belavin, A. M. Polyakov, A. S. Schwartz and Y. S. Tyupkin, Phys. Lett. B **59**, 85 (1975).
- [78] A. I. Vainshtein, V. I. Zakharov, V. A. Novikov and M. A. Shifman, Sov. Phys. Usp. **25**, 195 (1982) [Usp. Fiz. Nauk **136**, 553 (1982)].
- [79] S. G. Matinyan and G. K. Savvidy, Nucl. Phys. B **134**, 539 (1978).
- [80] R. Pasechnik, Universe **2**, no. 1, 4 (2016) [arXiv:1605.07610 [gr-qc]].
- [81] R. Pasechnik, V. Beylin and G. Vereshkov, JCAP **1306**, 011 (2013).
- [82] R. Pasechnik, V. Beylin and G. Vereshkov, Phys. Rev. D **88** (2013) 2, 023509.
- [83] R. Pasechnik, G. Prokhorov and O. Teryaev, arXiv:1609.09249 [hep-ph].
- [84] H. Pagels and E. Tomboulis, Nucl. Phys. B **143**, 485 (1978).
- [85] G. Prokhorov, R. Pasechnik and G. Vereshkov, JHEP **1407**, 003 (2014).
- [86] B. Abelev *et al.* [ALICE Collaboration], Phys. Rev. C **88**, 044910 (2013).
- [87] B. B. Abelev *et al.* [ALICE Collaboration], Phys. Rev. C **89**, no. 2, 024911 (2014).
- [88] J. Adam *et al.* [ALICE Collaboration], Phys. Rev. C **93**, no. 5, 054908 (2016).
- [89] M. Petráň, J. Letessier, V. Petráček and J. Rafelski, Phys. Rev. C **88**, no. 3, 034907 (2013).
- [90] T. Csorgo and L. P. Csernai, Phys. Lett. B **333**, 494 (1994).
- [91] E. Shuryak, arXiv:1412.8393 [hep-ph].
- [92] J. P. Blaizot, F. Gelis, J. F. Liao, L. McLerran and R. Venugopalan, Nucl. Phys. A **873**, 68 (2012).
- [93] V. Begun, W. Florkowski and M. Rybczynski, Phys. Rev. C **90**, no. 1, 014906 (2014).
- [94] V. Begun, W. Florkowski and M. Rybczynski, Phys. Rev. C **90**, no. 5, 054912 (2014).
- [95] V. Begun and W. Florkowski, Phys. Rev. C **91**, 054909 (2015).
- [96] V. Begun, Phys. Rev. C **94**, no. 5, 054904 (2016).
- [97] M. Plumer, S. Raha and R. M. Weiner, Nucl. Phys. A **418**, 549C (1984).
- [98] D. H. Rischke, M. I. Gorenstein, A. Schafer, H. Stoecker and W. Greiner, Phys. Lett. B **278**,

- 19 (1992).
- [99] V. M. Bannur, Phys. Lett. B **362**, 7 (1995).
 - [100] M. H. Thoma, J. Phys. G **31**, L7 (2005) Erratum: [J. Phys. G **31**, 539 (2005)].
 - [101] V. M. Bannur, J. Phys. G **32**, 993 (2006).
 - [102] T. Schafer and D. Teaney, Rept. Prog. Phys. **72**, 126001 (2009).
 - [103] M. Bonitz, C. Henning and D. Block, Rep. Prog. Phys. **73**, 066501 (2010).
 - [104] S. Giorgini, L. P. Pitaevskii and S. Stringari, Rev. Mod. Phys. **80**, 1215 (2008).
 - [105] C. Cao, E. Elliott, J. Joseph, H. Wu, J. Petricka, T. Schäfer and J. E. Thomas, Science **331**, 58 (2011).
 - [106] C. V. Johnson, P. Steinberg, Phys. Today **63N5**, 29 (2010).
 - [107] P. Kovtun, D. T. Son, A. O. Starinets, Phys. Rev. Lett. **94**, 111601 (2005).
 - [108] J. E. Thomas, Phys. Today **63N5**, 34 (2010).
 - [109] S. Gupta, Phys. Lett. B **588**, 136 (2004).
 - [110] A. Bazavov *et al.* [HotQCD Collaboration], Phys. Rev. D **90**, 094503 (2014).
 - [111] L. D. Landau and E. M. Lifshitz, *Statistical Physics, Part 1*, Pergamon Press, London 1980.
 - [112] E. V. Shuryak and O. V. Zhirov, Phys. Lett. B **171**, 99 (1986).
 - [113] C. M. Hung and E. V. Shuryak, Phys. Rev. Lett. **75**, 4003 (1995).
 - [114] T. Matsui and H. Satz, Phys. Lett. B **178**, 416 (1986).
 - [115] N. Brambilla *et al.*, Eur. Phys. J. C **71**, 1534 (2011).
 - [116] S. Borsányi, Z. Fodor, S. D. Katz, A. Pásztor, K. K. Szabó and C. Török, JHEP **1504**, 138 (2015).
 - [117] A. Bazavov, P. Petreczky and A. Velytsky, arXiv:0904.1748 [hep-ph].
 - [118] A. Bazavov *et al.*, Phys. Rev. D **85**, 054503 (2012).
 - [119] H. T. Ding, F. Karsch and S. Mukherjee, Int. J. Mod. Phys. E **24**, no. 10, 1530007 (2015).
 - [120] W. Scheid, H. Muller and W. Greiner, Phys. Rev. Lett. **32**, 741 (1974).
 - [121] M. I. Sobel, H. A. Bethe, P. J. Siemens and J. P. Bondorf, Nucl. Phys. A **251**, 502 (1975).
 - [122] G. F. Chapline, M. H. Johnson, E. Teller and M. S. Weiss, Phys. Rev. D **8**, 4302 (1973).
 - [123] S. Nagamiya and M. Gyulassy, Adv. Nucl. Phys. **13**, 201 (1984).
 - [124] R. Stock, Phys. Rept. **135** (1986) 259.
 - [125] T. D. Lee and G. C. Wick, Phys. Rev. D **9**, 2291 (1974).
 - [126] M. Harrison, S. G. Peggs and T. Roser, Ann. Rev. Nucl. Part. Sci. **52**, 425 (2002).
 - [127] L. Evans and P. Bryant, JINST **3**, S08001 (2008).
 - [128] A. Adare *et al.* [PHENIX Collaboration], Phys. Rev. C **93**, no. 2, 024901 (2016).
 - [129] S. Chatrchyan *et al.* [CMS Collaboration], Phys. Rev. Lett. **109**, 152303 (2012).
 - [130] J. T. Mitchell [PHENIX Collaboration], Nucl. Phys. A **956**, 842 (2016).
 - [131] J. D. Bjorken, Phys. Rev. D **27**, 140 (1983).
 - [132] W. Fischer *et al.*, Phys. Rev. C **89**, no. 1, 014906 (2014).
 - [133] E. Fermi, Z. Phys. **29**, 315 (1924).
 - [134] C. F. von Weizsacker, Z. Phys. **88**, 612 (1934).
 - [135] E. J. Williams, Phys. Rev. **45**, 729 (1934).
 - [136] J. D. Jackson, *Classical Electrodynamics*, ISBN-9780471309321.
 - [137] G. Baur, K. Hencken, D. Trautmann, S. Sadovskiy and Y. Kharlov, Phys. Rept. **364**, 359 (2002).
 - [138] C. A. Bertulani, S. R. Klein and J. Nystrand, Ann. Rev. Nucl. Part. Sci. **55**, 271 (2005).
 - [139] A. J. Baltz *et al.*, Phys. Rept. **458**, 1 (2008).
 - [140] S. R. Klein, arXiv:1502.06662 [nucl-ex].

- [141] K. Tuchin, *Adv. High Energy Phys.* **2013**, 490495 (2013).
- [142] C. Kouveliotou, R. C. Duncan and C. Thompson, *Sci. Am.* **288N2**, 24 (2003).
- [143] D. E. Kharzeev, L. D. McLerran and H. J. Warringa, *Nucl. Phys. A* **803**, 227 (2008).
- [144] H.-T. Ding, A. Francis, O. Kaczmarek, F. Karsch, E. Laermann and W. Soeldner, *Phys. Rev. D* **83**, 034504 (2011).
- [145] A. Amato, G. Aarts, C. Allton, P. Giudice, S. Hands and J. I. Skullerud, *Phys. Rev. Lett.* **111**, no. 17, 172001 (2013).
- [146] G. Aarts, C. Allton, A. Amato, P. Giudice, S. Hands and J. I. Skullerud, *JHEP* **1502**, 186 (2015).
- [147] P. Filip, *J. Phys. Conf. Ser.* **636**, no. 1, 012013 (2015).
- [148] D. E. Kharzeev, J. Liao, S. A. Voloshin and G. Wang, *Prog. Part. Nucl. Phys.* **88**, 1 (2016).
- [149] U. Gürsoy, D. Kharzeev and K. Rajagopal, *Phys. Rev. C* **89**, no. 5, 054905 (2014).
- [150] D. Kharzeev, R. D. Pisarski and M. H. G. Tytgat, *Phys. Rev. Lett.* **81**, 512 (1998).
- [151] B. I. Abelev *et al.* [STAR Collaboration], *Phys. Rev. Lett.* **103**, 251601 (2009).
- [152] L. Adamczyk *et al.* [STAR Collaboration], *Phys. Rev. Lett.* **114**, no. 25, 252302 (2015).
- [153] L. Adamczyk *et al.* [STAR Collaboration], *Phys. Rev. Lett.* **113**, 052302 (2014).
- [154] B. Abelev *et al.* [ALICE Collaboration], *Phys. Rev. Lett.* **110**, no. 1, 012301 (2013).
- [155] V. Khachatryan *et al.* [CMS Collaboration], arXiv:1610.00263 [nucl-ex].
- [156] S. Schlichting and S. Pratt, *Phys. Rev. C* **83**, 014913 (2011).
- [157] V. Skokov, P. Sorensen, V. Koch, S. Schlichting, J. Thomas, S. Voloshin, G. Wang and H. U. Yee, arXiv:1608.00982 [nucl-th].
- [158] F. Becattini, I. Karpenko, M. Lisa, I. Uppsala and S. Voloshin, arXiv:1610.02506 [nucl-th].
- [159] J. Aichelin, *Phys. Rept.* **202**, 233 (1991).
- [160] K. Werner, *Phys. Rept.* **232**, 87 (1993).
- [161] M. Gyulassy and X. N. Wang, *Comput. Phys. Commun.* **83**, 307 (1994).
- [162] S. A. Bass *et al.*, *Prog. Part. Nucl. Phys.* **41**, 255 (1998).
- [163] T. J. Humanic, *Phys. Rev. C* **57**, 866 (1998).
- [164] Z. W. Lin, C. M. Ko, B. A. Li, B. Zhang and S. Pal, *Phys. Rev. C* **72**, 064901 (2005).
- [165] S. Roesler, R. Engel and J. Ranft, hep-ph/0012252.
- [166] T. Pierog, I. Karpenko, J. M. Katzy, E. Yatsenko and K. Werner, *Phys. Rev. C* **92**, no. 3, 034906 (2015).
- [167] Y. Akamatsu, S. i. Inutsuka, C. Nonaka and M. Takamoto, *J. Comput. Phys.* **256**, 34 (2014).
- [168] P. Bozek and I. Wyskiel-Piekarska, *Phys. Rev. C* **85**, 064915 (2012).
- [169] R. Derradi de Souza, T. Koide and T. Kodama, *Prog. Part. Nucl. Phys.* **86**, 35 (2016).
- [170] P. F. Kolb, J. Sollfrank and U. W. Heinz, *Phys. Rev. C* **62**, 054909 (2000).
- [171] I. P. Lokhtin, L. V. Malinina, S. V. Petrushanko, A. M. Snigirev, I. Arsene and K. Tywoniuk, *Comput. Phys. Commun.* **180**, 779 (2009).
- [172] T. Hirano, P. Huovinen, K. Murase and Y. Nara, *Prog. Part. Nucl. Phys.* **70**, 108 (2013).
- [173] C. Shen, Z. Qiu, H. Song, J. Bernhard, S. Bass and U. Heinz, *Comput. Phys. Commun.* **199**, 61 (2016).
- [174] B. B. Abelev *et al.* [ALICE Collaboration], *Phys. Lett. B* **728**, 25 (2014).
- [175] S. S. Adler *et al.* [PHENIX Collaboration], *Phys. Rev. C* **69**, 034909 (2004).
- [176] C. Nonaka and S. A. Bass, *Phys. Rev. C* **75**, 014902 (2007)
- [177] B. Muller, *Nucl. Phys. A* **661**, 272 (1999).
- [178] W. Kittel, E. A. De Wolf, *Soft multihadron dynamics*. World Scientific (2005).
- [179] L. D. Landau, *Izv. Akad. Nauk Ser. Fiz.* **17**, 51 (1953).

- [180] R. M. Weiner, *Int. J. Mod. Phys. E* **15**, 37 (2006).
- [181] U. W. Heinz, *Landolt-Bornstein* **23**, 240 (2010), [arXiv:0901.4355 [nucl-th]].
- [182] H. Stöcker and W. Greiner, *Phys. Rept.* **137**, 277 (1986).
- [183] T. Hirano, N. van der Kolk and A. Bilandzic, *Lect. Notes Phys.* **785**, 139 (2010), [arXiv:0808.2684 [nucl-th]].
- [184] C. Eckart, *Phys. Rev.* **58**, 919 (1940).
- [185] A. Nakamura and S. Sakai, *Phys. Rev. Lett.* **94**, 072305 (2005).
- [186] F. Karsch, D. Kharzeev and K. Tuchin, *Phys. Lett. B* **663**, 217 (2008).
- [187] B. I. Abelev *et al.* [STAR Collaboration], *Phys. Rev. C* **79**, 034909 (2009).
- [188] P. J. Siemens and J. O. Rasmussen, *Phys. Rev. Lett.* **42**, 880 (1979).
- [189] E. Schnedermann, J. Sollfrank and U. W. Heinz, *Phys. Rev. C* **48**, 2462 (1993).
- [190] F. Retiere and M. A. Lisa, *Phys. Rev. C* **70**, 044907 (2004).
- [191] F. Cooper and G. Frye, *Phys. Rev. D* **10**, 186 (1974).
- [192] L. Kumar [STAR Collaboration], *Nucl. Phys. A* **931**, 1114 (2014).
- [193] T. Sjostrand, S. Mrenna and P. Z. Skands, *Comput. Phys. Commun.* **178**, 852 (2008).
- [194] R. Baier, A. H. Mueller, D. Schiff and D. T. Son, *Phys. Lett. B* **502**, 51 (2001).
- [195] Z. Xu and C. Greiner, *Phys. Rev. C* **71**, 064901 (2005).
- [196] A. Kurkela and G. D. Moore, *JHEP* **1112**, 044 (2011).
- [197] P. Romatschke, arXiv:1609.02820 [nucl-th].
- [198] W. Broniowski, M. Chojnacki, W. Florkowski and A. Kisiel, *Phys. Rev. Lett.* **101**, 022301 (2008).
- [199] H. Petersen, C. Coleman-Smith, S. A. Bass and R. Wolpert, *J. Phys. G* **38**, 045102 (2011).
- [200] U. Heinz and J. S. Moreland, *Phys. Rev. C* **84**, 054905 (2011).
- [201] J. Noronha-Hostler, B. Betz, J. Noronha and M. Gyulassy, *Phys. Rev. Lett.* **116**, no. 25, 252301 (2016).
- [202] M. L. Miller, K. Reygers, S. J. Sanders and P. Steinberg, *Ann. Rev. Nucl. Part. Sci.* **57**, 205 (2007).
- [203] R. J. Glauber, *Phys. Rev.* **100**, 242 (1955).
- [204] W. Czyz and L. C. Maximon, *Annals Phys.* **52**, 59 (1969).
- [205] R. J. Glauber and G. Matthiae, *Nucl. Phys. B* **21**, 135 (1970).
- [206] R. J. Glauber, *Nucl. Phys. A* **774**, 3 (2006).
- [207] C. J. Joachain and C. Quigg, *Rev. Mod. Phys.* **46**, 279 (1974).
- [208] V. Franco and G. K. Varma, *Phys. Rev. C* **18**, 349 (1978).
- [209] M. C. Abreu *et al.* [NA50 Collaboration], *Phys. Lett. B* **521**, 195 (2001).
- [210] W. Broniowski, M. Rybczynski and P. Bozek, *Comput. Phys. Commun.* **180**, 69 (2009).
- [211] C. Loizides, J. Nagle and P. Steinberg, *SoftwareX* **1-2**, 13 (2015) [arXiv:1408.2549 [nucl-ex]].
- [212] G. Aad *et al.* [ATLAS Collaboration], *Phys. Rev. Lett.* **110**, no. 2, 022301 (2013).
- [213] V. N. Gribov, *Sov. Phys. JETP* **26**, 414 (1968) [*Zh. Eksp. Teor. Fiz.* **53**, 654 (1967)].
- [214] V. N. Gribov, *Sov. Phys. JETP* **29**, 483 (1969) [*Zh. Eksp. Teor. Fiz.* **56**, 892 (1969)].
- [215] V. A. Abramovsky, V. N. Gribov and O. V. Kancheli, *Yad. Fiz.* **18**, 595 (1973) [*Sov. J. Nucl. Phys.* **18**, 308 (1974)].
- [216] V. M. Braun and Y. M. Shabelski, *Int. J. Mod. Phys. A* **3**, 2417 (1988).
- [217] H. J. Drescher, M. Hladik, S. Ostapchenko, T. Pierog and K. Werner, *Phys. Rept.* **350**, 93 (2001).
- [218] S. Ostapchenko, *Phys. Rev. D* **83**, 014018 (2011).
- [219] R. Pasechnik, R. Enberg and G. Ingelman, *Phys. Rev. D* **82**, 054036 (2010).

- [220] R. Pasechnik, R. Enberg and G. Ingelman, Phys. Lett. B **695**, 189 (2011).
- [221] J. Nemchik, V. Petracek, I. K. Potashnikova and M. Sumbera, Phys. Rev. C **78**, 025213 (2008).
- [222] C. Loizides, Phys. Rev. C **94**, no. 2, 024914 (2016).
- [223] L. V. Gribov, E. M. Levin and M. G. Ryskin, Phys. Rept. **100**, 1 (1983).
- [224] Y. L. Dokshitzer, Sov. Phys. JETP **46**, 641 (1977) [Zh. Eksp. Teor. Fiz. **73**, 1216 (1977)].
- [225] V. N. Gribov and L. N. Lipatov, Sov. J. Nucl. Phys. **15**, 438 (1972) [Yad. Fiz. **15**, 781 (1972)].
- [226] G. Altarelli and G. Parisi, Nucl. Phys. B **126**, 298 (1977).
- [227] L. D. McLerran and R. Venugopalan, Phys. Rev. D **49**, 3352 (1994).
- [228] J. Jalilian-Marian and Y. V. Kovchegov, Prog. Part. Nucl. Phys. **56**, 104 (2006).
- [229] F. Gelis, E. Iancu, J. Jalilian-Marian and R. Venugopalan, Ann. Rev. Nucl. Part. Sci. **60**, 463 (2010).
- [230] D. Kharzeev, E. Levin and M. Nardi, Nucl. Phys. A **747**, 609 (2005).
- [231] J. Jalilian-Marian, A. Kovner, A. Leonidov and H. Weigert, Nucl. Phys. B **504**, 415 (1997).
- [232] J. Jalilian-Marian, A. Kovner, A. Leonidov and H. Weigert, Phys. Rev. D **59**, 014014 (1998).
- [233] A. Kovner, J. G. Milhano and H. Weigert, Phys. Rev. D **62**, 114005 (2000).
- [234] H. Weigert, Nucl. Phys. A **703**, 823 (2002).
- [235] E. Iancu, A. Leonidov and L. D. McLerran, Nucl. Phys. A **692**, 583 (2001).
- [236] E. Ferreira, E. Iancu, A. Leonidov and L. McLerran, Nucl. Phys. A **703**, 489 (2002).
- [237] K. J. Golec-Biernat and M. Wusthoff, Phys. Rev. D **60**, 114023 (1999).
- [238] F. Caola and S. Forte, Phys. Rev. Lett. **101**, 022001 (2008).
- [239] E. Basso, V. P. Goncalves, M. Krelina, J. Nemchik and R. Pasechnik, Phys. Rev. D **93**, no. 9, 094027 (2016).
- [240] E. Basso, V. P. Goncalves, J. Nemchik, R. Pasechnik and M. Sumbera, Phys. Rev. D **93**, no. 3, 034023 (2016).
- [241] B. Schenke, P. Tribedy and R. Venugopalan, Phys. Rev. Lett. **108**, 252301 (2012).
- [242] D. Kharzeev, E. Levin and M. Nardi, Phys. Rev. C **71**, 054903 (2005).
- [243] H.-J. Drescher and Y. Nara, Phys. Rev. C **75**, 034905 (2007).
- [244] K. J. Golec-Biernat and M. Wusthoff, Phys. Rev. D **59**, 014017 (1998).
- [245] J. Bartels, K. J. Golec-Biernat and H. Kowalski, Phys. Rev. D **66**, 014001 (2002).
- [246] H. Kowalski and D. Teaney, Phys. Rev. D **68**, 114005 (2003).
- [247] T. Hirano, P. Huovinen and Y. Nara, Phys. Rev. C **84**, 011901 (2011).
- [248] K. Aamodt *et al.* [ALICE Collaboration], Phys. Rev. Lett. **105**, 252302 (2010).
- [249] <https://www.phy.duke.edu/modeling-relativistic-heavy-ion-collisions>
- [250] J. Bielcikova, PoS EPS -**HEP2015**, 022 (2015).
- [251] A. Andronic *et al.*, Eur. Phys. J. C **76**, no. 3, 107 (2016).
- [252] J. Rafelski and B. Muller, Phys. Rev. Lett. **48**, 1066 (1982) Erratum: [Phys. Rev. Lett. **56**, 2334 (1986)].
- [253] P. Koch, B. Muller and J. Rafelski, Phys. Rept. **142**, 167 (1986).
- [254] A. Andronic, P. Braun-Munzinger and J. Stachel, Phys. Lett. B **673**, 142 (2009).
- [255] D. Teaney, J. Lauret and E. V. Shuryak, Phys. Rev. Lett. **86**, 4783 (2001).
- [256] P. Tribedy and R. Venugopalan, Phys. Lett. B **710**, 125 (2012) Erratum: [Phys. Lett. B **718**, 1154 (2013)].
- [257] G. Aad *et al.* [ATLAS Collaboration], Phys. Lett. B **710**, 363 (2012).
- [258] J. Y. Ollitrault, Phys. Rev. D **46**, 229 (1992).
- [259] A. M. Poskanzer and S. A. Voloshin, Phys. Rev. C **58**, 1671 (1998).

- [260] S. Manly *et al.* [PHOBOS Collaboration], Nucl. Phys. A **774**, 523 (2006).
- [261] K. Aamodt *et al.* [ALICE Collaboration], Phys. Rev. Lett. **107**, 032301 (2011).
- [262] U. Heinz and R. Snellings, Ann. Rev. Nucl. Part. Sci. **63**, 123 (2013).
- [263] L. B. Venema *et al.*, Phys. Rev. Lett. **71**, 835 (1993).
- [264] L. Adamczyk *et al.* [STAR Collaboration], Phys. Rev. Lett. **116**, no. 11, 112302 (2016).
- [265] S. Wheaton and J. Cleymans, Comput. Phys. Commun. **180**, 84 (2009).
- [266] B. B. Abelev *et al.* [ALICE Collaboration], Phys. Lett. B **728**, 216 (2014) Erratum: [Phys. Lett. B **734**, 409 (2014)].
- [267] J. Adam *et al.* [ALICE Collaboration], Phys. Lett. B **758**, 389 (2016).
- [268] J. D. Bjorken, FERMILAB-PUB-82-059-THY, FERMILAB-PUB-82-059-T.
- [269] D. A. Appel, Phys. Rev. D **33**, 717 (1986).
- [270] M. Gyulassy and M. Plumer, Phys. Lett. B **243**, 432 (1990).
- [271] V. Khachatryan *et al.* [CMS Collaboration], arXiv:1611.01664 [nucl-ex].
- [272] J. Adams *et al.* [STAR Collaboration], Phys. Rev. Lett. **97**, 162301 (2006).
- [273] D. d’Enterria, PoS QNP **2012**, 018 (2012) [arXiv:1207.4362 [nucl-ex]].
- [274] S. Chatrchyan *et al.* [CMS Collaboration], Phys. Lett. B **718**, 773 (2013).
- [275] R. Baier, Y. L. Dokshitzer, A. H. Mueller, S. Peigne and D. Schiff, Nucl. Phys. B **484**, 265 (1997).
- [276] S. Caron-Huot, Phys. Rev. D **79**, 065039 (2009).
- [277] M. Laine, Eur. Phys. J. C **72**, 2233 (2012).
- [278] J. P. Blaizot and Y. Mehtar-Tani, Nucl. Phys. A **929**, 202 (2014).
- [279] M. Panero, K. Rummukainen and A. Sch’fer, Phys. Rev. Lett. **112**, no. 16, 162001 (2014).
- [280] H. Liu, K. Rajagopal and U. A. Wiedemann, Phys. Rev. Lett. **97**, 182301 (2006).
- [281] S. Chatrchyan *et al.* [CMS Collaboration], Phys. Rev. Lett. **109**, 222301 (2012).
- [282] B. Svetitsky, Phys. Rev. D **37**, 2484 (1988).
- [283] C. Young and E. Shuryak, Phys. Rev. C **79**, 034907 (2009).
- [284] P. Petreczky and C. Young, arXiv:1606.08421 [nucl-th].
- [285] S. Digal, P. Petreczky and H. Satz, Phys. Rev. D **64**, 094015 (2001).
- [286] CMS Collaboration, CMS-PAS-HIN-16-008.
- [287] A. Adare *et al.* [PHENIX Collaboration], Phys. Rev. Lett. **104**, 132301 (2010).
- [288] J. Adam *et al.* [ALICE Collaboration], Phys. Lett. B **754**, 235 (2016).
- [289] E. V. Shuryak, Phys. Lett. B **78**, 150 (1978) [Sov. J. Nucl. Phys. **28**, 408 (1978)] [Yad. Fiz. **28**, 796 (1978)].
- [290] E. L. Feinberg, Nuovo Cim. A **34**, 391 (1976).
- [291] G. Domokos and J. I. Goldman, Phys. Rev. D **23**, 203 (1981).
- [292] V. P. Goncalves, M. Krelina, J. Nemchik and R. Pasechnik, arXiv:1608.02892 [hep-ph].
- [293] P. Stankus, Ann. Rev. Nucl. Part. Sci. **55**, 517 (2005).
- [294] M. M. Aggarwal *et al.* [WA98 Collaboration], Phys. Rev. Lett. **85**, 3595 (2000).
- [295] M. M. Aggarwal *et al.* [WA98 Collaboration], nucl-ex/0006007.
- [296] L. Adamczyk *et al.* [STAR Collaboration], Phys. Rev. Lett. **112**, 032302 (2014).
- [297] L. Adamczyk *et al.* [STAR Collaboration], Phys. Rev. Lett. **113**, 092301 (2014).
- [298] M. Sumbera, EPJ Web Conf. **28**, 03006 (2012), [arXiv:1201.6163 [nucl-ex]].
- [299] M. Sumbera [STAR Collaboration], Acta Phys. Polon. Supp. **6**, 429 (2013).
- [300] A. Adare *et al.* [PHENIX Collaboration], Phys. Rev. C **93**, no. 1, 011901 (2016).
- [301] M. A. Stephanov, K. Rajagopal and E. V. Shuryak, Phys. Rev. Lett. **81**, 4816 (1998).
- [302] R. A. Lacey, Phys. Rev. Lett. **114**, no. 14, 142301 (2015).

- [303] R. V. Gavai and S. Gupta, Phys. Lett. B **696**, 459 (2011).
- [304] M. M. Aggarwal *et al.* [STAR Collaboration], Phys. Rev. Lett. **105**, 022302 (2010).
- [305] V. Khachatryan *et al.* [CMS Collaboration], JHEP **1009**, 091 (2010).
- [306] V. Khachatryan *et al.* [CMS Collaboration], Phys. Rev. Lett. **116**, no. 17, 172302 (2016).
- [307] G. Aad *et al.* [ATLAS Collaboration], Phys. Rev. Lett. **116**, no. 17, 172301 (2016).
- [308] G. Aad *et al.* [ATLAS Collaboration], Phys. Rev. Lett. **110**, no. 18, 182302 (2013).
- [309] S. Chatrchyan *et al.* [CMS Collaboration], Phys. Lett. B **718**, 795 (2013).
- [310] B. Abelev *et al.* [ALICE Collaboration], Phys. Lett. B **719**, 29 (2013).
- [311] V. Khachatryan *et al.* [CMS Collaboration], Phys. Rev. Lett. **115**, no. 1, 012301 (2015).
- [312] A. Adare *et al.* [PHENIX Collaboration], Phys. Rev. Lett. **115**, no. 14, 142301 (2015).
- [313] J. D. Orjuela Koop, A. Adare, D. McGlinchey and J. L. Nagle, Phys. Rev. C **92**, no. 5, 054903 (2015).
- [314] B. I. Abelev *et al.* [STAR Collaboration], Phys. Rev. C **80**, 064912 (2009).
- [315] B. Alver *et al.* [PHOBOS Collaboration], Phys. Rev. Lett. **104**, 062301 (2010).
- [316] K. Aamodt *et al.* [ALICE Collaboration], Phys. Lett. B **708**, 249 (2012).
- [317] G. Agakishiev *et al.* [STAR Collaboration], Phys. Rev. C **85**, 014903 (2012).
- [318] S. A. Voloshin, Nucl. Phys. A **749**, 287 (2005).
- [319] A. H. Rezaeian, Phys. Rev. D **93**, no. 9, 094030 (2016).
- [320] K. Dusling, P. Tribedy and R. Venugopalan, Phys. Rev. D **93**, no. 1, 014034 (2016).
- [321] Y. Hirono and E. Shuryak, Phys. Rev. C **91**, no. 5, 054915 (2015).
- [322] P. Romatschke, Eur. Phys. J. C **75**, no. 7, 305 (2015).
- [323] H. Niemi, PoS EPS **-HEP2015**, 220 (2015).
- [324] T. Koblesky, arXiv:1510.00435 [nucl-ex].
- [325] F. Antinori *et al.*, arXiv:1604.03310 [hep-ph].
- [326] R. Bala, I. Bautista, J. Bielcikova and A. Ortiz, Int. J. Mod. Phys. E **25**, no. 07, 1642006 (2016).
- [327] Y. M. Sinyukov, S. V. Akkelin, I. A. Karpenko and V. M. Shapoval, Adv. High Energy Phys. **2013**, 198928 (2013).
- [328] M. Lisa, Acta Phys. Polon. B **47**, no. 7, 1847 (2016). arXiv:1607.06188 [nucl-th].